Multimodal approach to the evaluation of diffuse neuroinflammation in multiple sclerosis using positron emission tomography and diffusion tensor imaging

Svetlana Bezukladova 41319

sbezukla@abo.fi

Master's thesis
Åbo Akademi University
Turku PET centre
11.09.2018

Master's degree of Biomedical Imaging
In vivo & Clinical Imaging

Credits: 45 ECTS

Supervisors:
1: Eero Rissanen, MD, PhD
2: Laura Airas, MD, PhD, Professor of Neuroimmunology

Dedicated to my mother

ÅBO AKADEMI UNIVERSITY

Faculty of Science and Engineering
Biomedical Imaging

SVETLANA BEZUKLADOVA:

Multimodal approach to the evaluation of diffuse neuroinflammation in multiple sclerosis using positron emission tomography and diffusion tensor imaging

Master's thesis, 73 pp.
In Vivo & Clinical Imaging
September 2018

Neuroinflammation, neurodegeneration and demyelination of brain, spinal cord and optic nerves are attributed to multiple sclerosis (MS) pathogenesis. Conventional magnetic resonance imaging (MRI) is mainly used for evaluation of inflammatory activity and diffuse atrophy in diagnosis and follow-up in MS. Diffusion tensor imaging (DTI) implementation makes it possible to reveal microstructural alterations in normal appearing white matter tracts, undetectable in conventional MRI. Positron emission tomography (PET) *in vivo* molecular imaging of activated microglia with translocator protein (TSPO) binding radioligand, provide additional information on the inflammatory activity in normal appearing white matter (NAWM) as well as in the differentiation between the chronic active and inactive MS lesion type. Combination of both imaging modalities will enable a better understanding of MS pathology and can possibly contribute to the prediction of a progressive course of the disease.

The aim of this research was to evaluate structural and molecular brain changes using combined MR and PET *in vivo* imaging techniques in MS patients compared to healthy controls (HC), with correlational analyses of DTI data to TSPO-PET radioligand binding. The data of 55 MS patients with both RRMS (n = 40) and SPMS (n = 15) disease types and 15 healthy subjects were acquired from previously performed MS imaging studies in Turku PET Centre.

KEYWORDS: Multiple sclerosis, diffusion tensor imaging, PET, MRI, disease progression

TABLE OF CONTENTS

REVIEW OF LITERATURE

1.1 Multiple sclerosis

Multiple sclerosis (MS) is a common progressive inflammatory and neurodegenerative disease of the central nervous system (CNS), affecting approximately 2.3 million people worldwide (Browne et al., 2014). Typically, MS starts between the second and fourth life decade, progressing over time. Autoimmune in its nature, it begins with inflammatory chain reaction, when peripheral autoreactive immune cells migrate into the CNS and attack the myelin structures, forming focal inflammatory lesions. Development of sclerotic lesions in brain, spinal cord, optic nerves, and attributed to it chronic neuroinflammation and neurodegeneration, therefore leading to the accumulation of physical and cognitive impairment.

1.1.1 Epidemiology

The aetiology of MS is not yet fully understood, but multiple genetic (Baranzini and Oksenberg, 2017) and environmental risk factors (O'Gorman et al., 2012) i.e. hereditary predisposition, immunological and hormonal changes and their interactions are believed to contribute to the disease development. Geographical location and incidence rate also display a link: regions farther from the equator are in a high-risk group for disease onset. Low sun exposure at higher latitudes is likely to cause vitamin D deficiency, that is a one of the risk factors for MS (Kočovská et al., 2017). Other risk factors include smoking, viral infections (EBV, human herpes virus) and microbiome composition (Olsson et al., 2016; Tremlett and Waubant, 2017).

1.1.2 Diagnosis and course of the disease

There is no single diagnostic test for MS today, therefore clinical assessment, including magnetic resonance imaging (MRI) and spinal fluid analysis used to support the diagnosis. MRI visualize brain white matter abnormalities and mainly employed for diagnosis and follow-up of the disease. Cerebral fluid analysis investigates the immunoglobulin (IgG) level and is an additional diagnostic test used to support the demyelinating nature of the neurological condition. Nevertheless, clinical symptoms and course of the disease are heterogeneous among the MS patients, thus standardized

guideline for diagnosis have been proposed. The gold standard for MS is the revised McDonald criteria (Thompson et al., 2018), based on the concept that lesions appear in different CNS parts, i.e. disseminate in space (DIS), and accumulate within years i.e. disseminate in time (DIT). The first clinical episode with neurological symptoms and sign of demyelination referred to as clinically isolated syndrome (CIS). It is usually isolated in time and space (i.e. monophasic and monofocal). Long-term risk of transition from CIS to clinically definite MS (CDMS) is very high, with 60-80% for subjects with abnormal MRI onset, and about 20% for subjects without present lesions (Miller et al., 2012). Several prognostic factors were named that predict the transition: number, volume and site of lesions, notably contrast-enhancing, brain atrophy, serum anti-MOG and anti-MBP antibodies and evoked potential test findings (Bergamaschi, 2007).

As the disease progresses, patient with more than two relapses and clinical evidence of newly formed lesions meet diagnostic criteria for relapsing-remitting MS form. RRMS form is the most common among the patients and associated with repeating attacks or periodic neurological symptoms with partial or complete recovery. Symptoms may include weakness of the lower or upper limbs, numbness or tingling, bowel and urinary disturbance, loss of coordination, blurred vision. Most of the RRMS patients (50-60%) eventually enter a secondary progressive phase (SPMS), when worsening of clinical condition of the patient, independent of relapses, lead to permanent disability.

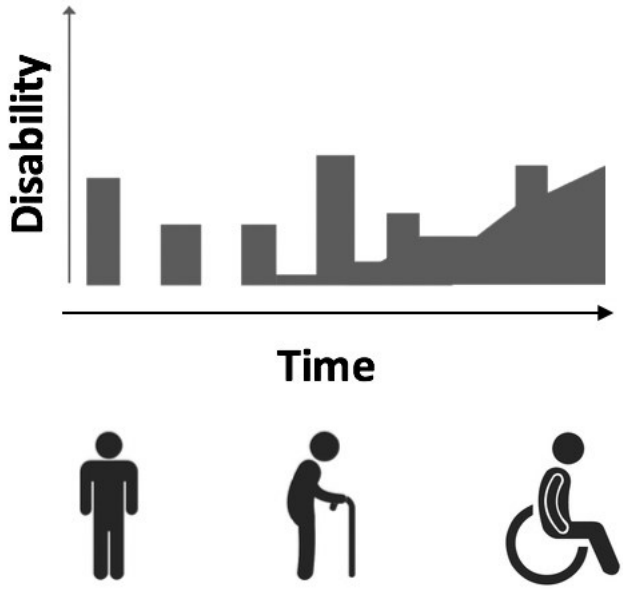

Figure 1. Schematic representation of MS progression.

It has been shown that disease advance associates with age: median age of MS patients with risk of converting to the secondary progressive phase of the disease is at 40-55 years, with median time to a secondary progression of 20 years (Koch et al., 2010).

The SPMS diagnosis cannot be defined at once, as the accumulation of neurological deficit is often slow and ambiguous. Therefore, evaluation of the neurological impairment of the patient is done according Kurtzke Expanded Disability Status Scale (EDSS) (John F.Kurtzke, 1983). This method provides a scale from 0 to 10 with 0.5 steps, where 0 correspond to no disability and 10 - to death of the patient due to MS. EDSS include Functional Systems (FS), graded separately (Table 1).

Table 1. Expanded disability status scale in the evaluation of clinical disability in MS (modified from Kurtzke et al 1983).

EDSS	**Definition**
0.0	Normal neurologic exam (all grade 0 in FS)
1.0	No disability, minimal signs in one FS (one FS grade 1)
1.5	No disability, minimal signs in more than one FS (more than one FS grade 1)
2.0	Minimal disability in one FS (one FS grade 2, others 0 or 1)
2.5	Minimal disability in two FS (two FS grade 2, others 0 or 1)
3.0	Moderate disability in one FS (one FS grade 3, others 0 or 1), or mild disability in three or four FS (three/four FS grade 2, others 0 or 1) though fully ambulatory
3.5	Fully ambulatory but with moderate disability in one FS (one grade 3) and one or two FS grade 2; or two FS grade 3; or five FS grade 2 (others 0 or 1)
4.0	Fully ambulatory without aid or rest for walk ≥ 500 meters; self-sufficient, up and about some 12 hours a day despite relatively severe disability consisting of one FS grade 4 (others 0 or l), or combinations of lesser grades exceeding limits of previous steps
4.5	Fully ambulatory without aid or rest for walk ≥ 300 meters; up and about much of the day, able to work a full day, may otherwise have some limitation of full activity or require minimal assistance; characterized by relatively severe disability, usually consisting of one FS grade 4 (others 0 or 1) or combinations of lesser grades exceeding limits of previous steps
5.0	Ambulatory without aid or rest for walk ≥ 200 meters; disability severe enough to impair full daily activities. Usual FS equivalents are one grade 5 alone, others 0 or 1; or combinations of lesser grades usually exceeding specifications for step 4.0.)
5.5	Ambulatory without aid or rest for walk ≥ 100 meters; disability severe enough to preclude full daily activities
6.0	Intermittent or unilateral constant assistance (cane, crutch, or brace) required to walk about 100 meters with or without resting

6.5	Constant bilateral assistance (canes, crutches, or braces) required to walk about 20 meters without resting
7.0	Unable to walk beyond about 5 meters even with aid, essentially restricted to wheelchair; wheels self in standard wheelchair and transfers alone; up and about in w/c some 12 hours a day
7.5	Unable to take more than a few steps; restricted to wheelchair; may need aid in transfer; wheels self but cannot carry on in standard wheelchair a full day; may require motorized wheelchair
8.0	Essentially restricted to bed or chair or perambulated in wheelchair but may be out of bed itself much of the day; retains many self-care functions
8.5	Essentially restricted to bed much of the day; has some effective use of arm(s); retains some self-care functions
9.0	Helpless bed patient; can communicate and eat
9.5	Totally helpless bed patient; unable to communicate effectively or eat/swallow
10.0	Death due to MS

1.1.3 Disease mechanisms

Neuroinflammation and neurodegeneration are both attributed to MS pathology, but it is still remained unknown what is the driving force of the disease progression. Animal and immunological studies showed that the early stage of the disease is mainly associated with peripheral immune activity, whereas progressive stage is manifested by immune reaction within CNS (reviewed in Friese et al., 2014; Baecher-Allan et al., 2018). Chronic inflammation, myelin loss, neuronal and axonal degeneration lead to the formation of sclerotic scar or plaque, that is the hallmark of MS pathology. The consequence of myelin loss is in disruption of axon saltatory conduction and electric signal propagation, resulting in physiological symptoms as numbness, tingling, paraesthesia and dysfunction of organ systems.

Multiple sclerosis is considered as an autoimmune disease caused by a breakdown of control mechanisms, regulating self-reactive lymphocytes. Current model of disease mechanism suggests that initial activation of peripheral lymphocytes is the first step in pathological MS cascade, followed by proliferation of T-cells and their migration across the blood brain barrier (BBB) into the CNS. By secretion of pro-inflammatory cytokines (TNFα, IFNγ) and chemokines, activated T-cells contribute to BBB disruption and entering into CNS. Invading across the barrier, they auto-react on presented in the CNS self-antigens e.g. myelin, therefore promoting the recruitment of other inflammatory cells: macrophages, cytotoxic T-cells and B-cells. Consequently,

accumulation of T- and B lymphocytes driving the immune response further, through recruitment of microglia and macrophages in the brain parenchyma (Hemmer et al., 2015).

Activated microglia and macrophages attribute to chronic inflammation through secretion of neurotoxins – reactive oxygen and nitrogen species, glutamate and chemotactic cytokines, that evokes an oxidative stress and leads to mitochondrial dysfunction and oligodendrocyte damage (Correale, 2014). In turn, imbalance of glutamate leads to increase of Ca^{2+} and Na^{2+} concentration, causing neuronal apoptosis and necrosis, resulting in neuroaxonal injury (Paling et al., 2013). Beside activated microglia, reactive astrocytes have been also considered to play role in a progression mechanism. Like microglia, activated astrocytes have been suspected in secretion of pro-inflammatory cytokines, chemokines, reactive oxygen and nitrogen species, therefore causing oxidative stress and contributing to neural tissue damage (Ponath et al., 2018).

B cells are another potential candidate in MS progression, playing its role by antigen representation, antibodies secretion and production of abnormal pro-inflammatory interleukin ratios (Amit et al., 2010). All aforementioned factors, together with excessive secretion of tumour necrosis factor (TNFα), unequivocally contribute to injury of neuronal structures. Lymphoid structures containing B-, T- and plasma cells are often found in the close proximity to meningeal space of majority SPMS patients (Barbara et al., 2006), forming a complex of cell population within CNS, independent from peripheral immune activity (Magliozzi et al., 2007). It has been shown that the presence of ectopic follicle-like structure associated with increased cortical atrophy and cortical demyelination, lower median age at disease onset, time to disease progression and increased clinical disability in SPMS patients (Magliozzi et al., 2007; Howell et al., 2011).

1.1.4 Role of microglia in MS

This study is focused on the event of chronic microglial activation during the CNS neuroinflammation, that is considered to be a key-factor in MS progression. Microglia are the resident immune cells of the CNS, present at a low level in a healthy brain and responsible for its homeostatic regulation. Together with macrophages, microglia have a number of functions, important for CNS maintenance, for example involvement in

synaptic plasticity in the adult brain, innate immunity, neuronal programmed cell death (Bogie et al., 2014).

Homeostatic microglia cells survey the brain parenchyma, detecting the pathogens or the signaling from the apoptotic cells. Dependent on a molecular signaling factors from injury or pathogen invasion, ramified microglia can either proliferate into reactive pro-inflammatory (M1) phagocytic phenotype, or to an alternatively activated (or M2) anti-inflammatory type (Boche et al., 2013).

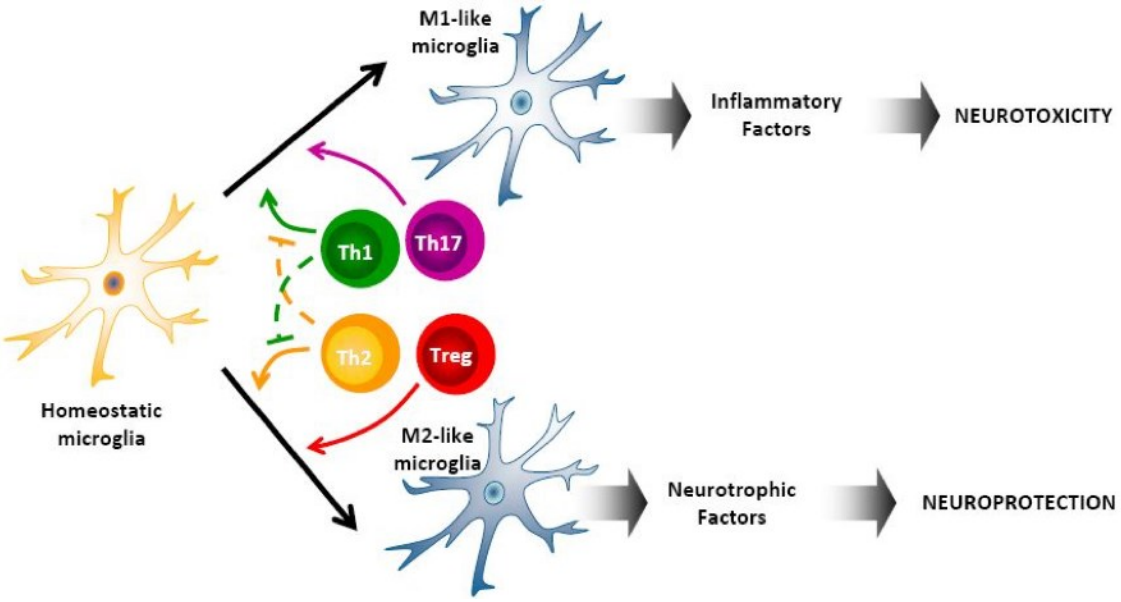

Figure 2. Microglia activation patterns. Th1/Th2/Th17 stands for the T helper cells, T reg is the regulatory T cell (Modified from Pacheco et al., 2012).

The pro-inflammatory “activated” microglia accumulate at the site of injury, phagocytosing cellular debris of the damaged cells, or killing the potential pathogens. Beside the phagocytosis, activated microglia secrete and release inflammatory factors, such as cytokines and cytotoxic substances, therefore promoting oxidative stress, that can cause the collateral damage to the adjacent cells. During the episode (or attack), the activated microglia stimulate the recruitment of monocytes from the peripheral bloodstream and their infiltration into the CNS. The inflammatory monocytes and activated microglia at the lesion site in turn reactivate the infiltration of autoagressive T-cells into the CNS, that considered to sustain the chronic inflammatory reaction in MS. On the other hand, the protective M2 cells phenotype contribute to potential tissue repair, by expressing anti-inflammatory and immune-regulatory mediators. Animal studies of experimental autoimmune encephalomyelitis (EAE) model of multiple

sclerosis showed, that imbalance towards pro-inflammatory (M1-like) macrophages and microglia activation patterns induce relapse occurrence (Mikita et al., 2011). This finding suggests that imbalance in M1/M2 macrophages/microglia equilibrium might be a key element in the chronic inflammatory process in progressive MS.

In early MS, monocyte-derived macrophages, microglia and anti-inflammatory myelin-laden foamy macrophages are often abundantly present in the active demyelinating lesions and may play a neuroprotective role by stimulating remyelination. However, in chronic active lesions the microglia and macrophages are concentrated around the sclerotic tissue, at the edge of the lesion site (Frischer et al., 2015). These lesions are called "the smoldering" plaques, and often found during the progressive MS phase (Dal-Bianco et al., 2017). Activated microglia is also found in the absence of the lesions, throughout the normal appearing white and grey matter (Seewann et al., 2009; Haider et al., 2014). The presence of diffused activated microglia in non-lesional brain matter may precede the new lesions formation and have been considered as progression predictor (Kutzelnigg et al., 2005). In fact, activated microglia can be detected with TSPO-PET imaging (Banati, 2002) or quantitative susceptibility mapping (QSM) modality (Gillen et al., 2018).

1.1.5 MS treatment

There are several defined types of MS today: 85% of people with MS has a relapsing-remitting form of the disease onset, following with transitioning to a secondary progressive form. About 10% are diagnosed with primary-progressive (PPMS) form onset, characterized with insidious worsening symptoms without relapses (Goldenberg, 2012). All forms have different underlying pathophysiology and hence need to be treated in appropriate to disease type way.

Current MS therapies only provide modulation of the immune system or immune suppression for patients in the early stage of the disease, reducing the inflammatory activity and delaying the disease progression. Disease modifying treatment (DMT) is believed to be the most effective during the early, inflammatory MS phase, when EDSS has not yet reached the score of 3. This EDSS status has been considered as the starting point of accumulation of irreversible neurodegeneration (Leray et al., 2010). Unfortunately, there is no curative treatment available for MS today and no treatment

available to slow down the disease at its secondary-progressive stage (Costello et al., 2014).

Two longitudinal sub-studies in this thesis investigated disease modifying treatment effect on MS, including fingolimod (Gilenya®) and natalizumab (Tysabri®). Fingolimod, or FTY720, is the oral immunomodulatory drug, which targets sphingosine-1-phospate (S1P) receptors, that results in suppression of T cells migration into the CNS, promotes oligodendrocyte survival, causes astrocytes migration and plays role in neurogenesis (Chun and Hartung, 2010; Dev et al., 2008). Fingolimod treatment resulted in a lower relapses rate, reduction in brain volume loss and favourable brain MRI outcome in RRMS patients in Phase III clinical trials (De Stefano et al., 2017, 2016), however only 25% of progression rate reduction was shown in FREEDOMS-II trial (Gajofatto et al., 2015).

Natalizumab is a humanized monoclonal antibody, α4-integrin antagonist, considered as a second-line treatment against highly-active RRMS form. The action mechanism of natalizumab is in the inhibition of lymphocyte migration into the CNS, by binding to α4β1-integrin and blocking vascular-cell adhesion molecules interaction. Several studies, including Phase III trials (Polman et al., 2006; McCormack, 2013) showed significantly reduced relapse rate and risk of progression in RRMS patients, compared with placebo group. Moreover, treatment resulted in reduced number of new T2-hyperintense and T1-hypointense lesions, and also reduced the volume of both T2 and T1-lesions (Miller et al., 2003; Piehl et al., 2011). Despite positive outcomes, natalizumab treatment resulted in adverse events such as headache, fatigue, urinary tract infection among the most common, and showed the risk of developing progressive multifocal leukoencephalopathy (PML), when exposure to drug lasted longer than 2 years (Bloomgren et al., 2012).

Since natalizumab prevents lymphocytes trafficking into the CNS, it has been hypothesized whether natalizumab treatment might be beneficial for progressive MS by reducing the chronic intrathecal inflammation and number of pro-inflammatory cytokines (Sellebjerg et al., 2016). According Christensen and Cadavid (Romme Christensen et al., 2014; Cadavid et al., 2013), short-term natalizumab studies showed a promising potential in SPMS treatment, with improvement in Timed 25-Foot Walk (T25FW) and magnetization transfer ratios in NAWM and cerebral cortex of progressive MS patients. Natalizumab efficacy in reduction of disability progression in

advanced SPMS had been under 2 years investigation in ASCEND trial, but controversially with previous short-term studies, it did not show delay in disease progression, but showed the improved 9-Hole Peg test (9HPT) results (Hartung et al., 2017).

1.2 Imaging of multiple sclerosis

Imaging of multiple sclerosis in the clinical setting is often restricted to a conventional MRI (cMRI) modality, that only capable to identify the sclerotic plaques and brain atrophy, allowing to monitor the disease evolution. Contrast enhancement (e.g. gadolinium) allows to detect the acute lesions in T1-weighted images (Filippi, 2000). However, the gadolinium uptake is restricted only to an active MS phase, when the BBB is not intact (Soon et al., 2007), moreover, the gadolinium itself may cause the potential adverse effects (Dillman et al., 2007). Unfortunately, cMRI not able to detect the diffuse pathological changes or the metabolic changes of the brain.

To overcome the limitations of cMRI, the combination of both PET and DTI imaging modalities may enable a better understanding of hidden MS pathology, not visible using conventional MRI. Diffusion tensor imaging is a sensitive marker for assessment of pathology related structural alterations in the brain (Alexander et al., 2007). On the other hand, quantification of microglial activation with translocator protein binding radioligand [^{11}C](R)-PK11195 positron emission tomography (PET) allows the measurement of neuroinflammation *in vivo* (Debruyne et al., 2003; Vivash and O'Brien, 2016).

1.2.1 Conventional magnetic resonance imaging (MRI)

Conventional MRI has become a powerful tool in the clinical routine of MS diagnosis and disease activity follow up (Filippi and Rocca, 2007). In the clinical setting, T1- and T2- weighted imaging with a contrast agent application and fluid-attenuated inversion recovery (FLAIR) are generally included in MR imaging protocol. T1-weighted brain imaging is mainly used to identify the pathological changes, while T2-weighted sequence has shown a better differentiation between grey matter (GM) and white matter (WM), and considerably improved structural tissue resolution. FLAIR sequence allows to detect pathological changes in the areas, affected by cerebrospinal fluid (CSF) artifacts (periventricular region), or by partial volume effects (gray/white matter

junction, brain stem) (De Coene et al., 1992). Despite being a cornerstone in detecting brain structural abnormality, conventional MRI imaging protocol is not able to access the brain's complex axonal architecture.

Several MRI-based techniques, including magnetization transfer ratio (MTR) imaging, quantitative susceptibility mapping (QSM), proton 1H-MR spectroscopy and diffusion weighted imaging (DWI) has sufficiently improved the ability to evaluate the disease burden. This study is focused on diffusion weighted imaging, and consequently diffusion tensor imaging, that is a sensitive tool for a non-invasive visualization of axonal organization of the brain.

1.2.2 Diffusion tensor imaging (DTI)

Diffusion tensor imaging has become a powerful MR imaging tool in diagnostic applications in the last decade. It has been widely used in surgical interventions of brain tumours (Pujol et al., 2015), detection of ischemia (Fragata et al., 2017) and traumatic brain injury (Hulkower et al., 2013). Pathological processes and ageing can affect the brain tissue integrity, at the same time the diffusion of water molecules is highly sensitive to changes in the cells microstructure. With implementation of DTI technique, it is possible to interpret the measured diffusivities and diffusion anisotropy, thereby revealing the brain matter alterations at the cellular level.

1.2.2.1 Physical basis and the principle of DTI

Diffusion weighted imaging is an MR based technique. Measurement of the MR signal attenuation, caused by the movement of water molecules is the principal application of DTI (Alexander et al., 2007).

DTI uses magnetic properties of the most abundant (55-75%) (Popkin and Rosenberg, 2011) in the human body water molecules, that consist of two hydrogen and oxygen atoms. The hydrogen nuclei, consisting from protons and neutrons, have a net positive charge and a characteristic motion, producing a small angular momentum. When human body is placed inside of the magnet and high magnetic field (B0) is applied, the nuclear spins are aligned parallel (low-energy state) and anti-parallel (high-energy state) to the external field, creating a net magnetic moment M. When a radio frequency (RF) is shortly applied, perpendicular to the magnetic field B0, it causes the absorption of energy by low-energy state nuclei, so the net magnetic momentum is changed. The

hydrogen nuclei best absorb energy with a specific "resonance frequency", that dependent on the magnetic field strength. The resonance frequency (or Larmor frequency ω) can be derived from the Larmor equation (1):

$$\omega = \gamma * B0, \quad (1)$$

where γ is the gyromagnetic ratio constant;

$\gamma\ (^1H) = 2.675 \times 10^8$ rad/s/T or 42.58 MHz/T

Switching off the RF signal causing the anti-parallel nuclei to realign back, parallel to B0, by the relaxation process. The energy, emitted during the relaxation, induce a voltage, that can be detected by a conductive receiver coil, placed around the object. The signal intensity is then reconstructed by Fourier transform to obtain a three-dimensional grey-scale magnetic resonance image (Guy and Ffytche, 2005).

Localizing the MR signal at the specific region of the interest require using the gradient coils, that produce the linear magnetic field inhomogeneities. Gradients can be applied in three dimensions Gx, Gy, Gz by controlling the strength and polarity. Different brain areas have various proton density, that define the slower/faster rate of the relaxation, therefore producing higher or lower MR signal intensity. To detect the movement of water molecules within the cellular structures and reconstruct this, as a signal within the voxel of diffusion-weighted images, several gradient directions have to be applied. The diffusion-encoding gradient can be represented as 3D vector q, oriented in the direction of diffusion and having a length, proportional to the gradient strength:

$$q = \gamma * \delta * G_{diff}, \quad (2)$$

where δ is the duration of the diffusion-encoding gradient, G_{diff} is the diffusion gradient strength, γ is the gyromagnetic ratio constant;

The diffusion weighting can be expressed as a b value ($b \sim q^2 * \Delta T$), that proportional to the diffusion time interval, multiplied to the squared strength of the gradient (Hagmann et al., 2006).

Mathematical model, called "tensor", which defines the shape of the 3D ellipsoid, is used to measure the diffusion anisotropy. At least 6 gradient directions of linear inhomogeneous magnetic fields are required to obtain the signal, needed for the tensor

reconstruction. The six parameters, such as the length of the longest (λ1), middle (λ2) and shortest (λ3) axes or "eigenvalues", and three-unit vectors or "eigenvectors" v1, v2, and v3, describe the axes orientation in space (Figure 3). The "diffusion ellipsoid" represents directions of the diffusivities: parallel to the white matter tracts, or axial diffusivity (AD), and perpendicular to the fibers, or radial diffusivity, RD = (λ2+λ3)/2. The mean diffusivity (MD) is an average value of all three eigenvalues, that defines the mean-squared displacement of water molecules within the voxel, reflecting the magnitude of diffusion independent of anisotropy, MD = (λ1+λ2+λ3)/3 (Le Bihan et al., 2001). Another important parameter widely used in DTI is the fractional anisotropy (FA), enable to quantify the preferential diffusion directionality along WM tracts.

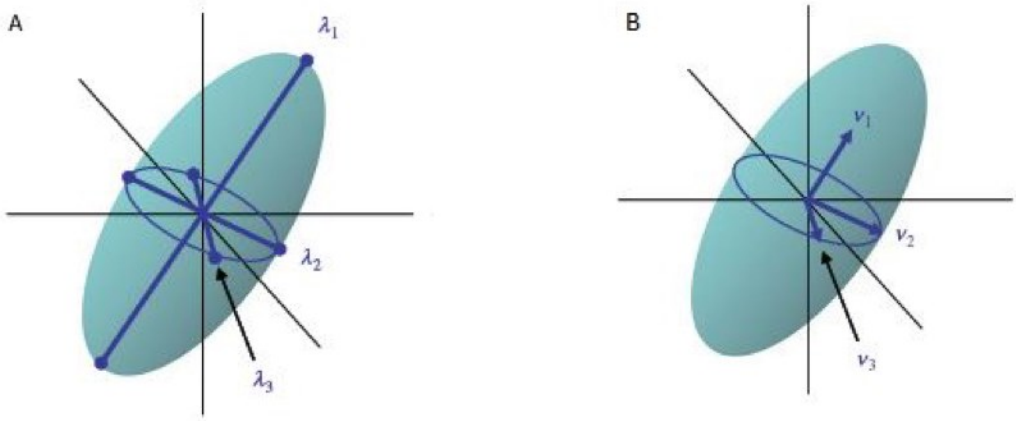

Figure 3. Parameters defining the tensor model A) eigenvalues, B) eigenvectors. (Modified from Mori, 2007).

The isotropic diffusion model represents an ideal sphere shape with FA value of 0, whilst FA value of 1 stands for anisotropic diffusion and can be visualized as an ellipsoid (Figure 4). At least 20 gradient directions are necessary for FA estimation, and minimum 30 sampling orientations are required for robust tensor reconstruction and calculation of mean diffusivity (Jones, 2004).

1.2.2.2 Biological basis of diffusion in the brain

Anatomical regions of the brain are defined by different microstructural organization, that in turn interpret the movement of water molecules. The biological sources of the anisotropy are the axonal membranes and the cytoskeleton, containing the neurofilaments and microtubules. The myelin sheath can prevent the diffusion in the direction, perpendicular to the axon (Winston, 2012). In the brain, CSF diffusion within the ventricles is not restricted by the presence of the cells, therefore it is high and

isotropic, i.e. directionally independent. On the contrary, the grey matter region, represented by the cell bodies, has slow and isotropic diffusion, while axonal organization of white matter determine the anisotropic and high diffusivity (Figure 4).

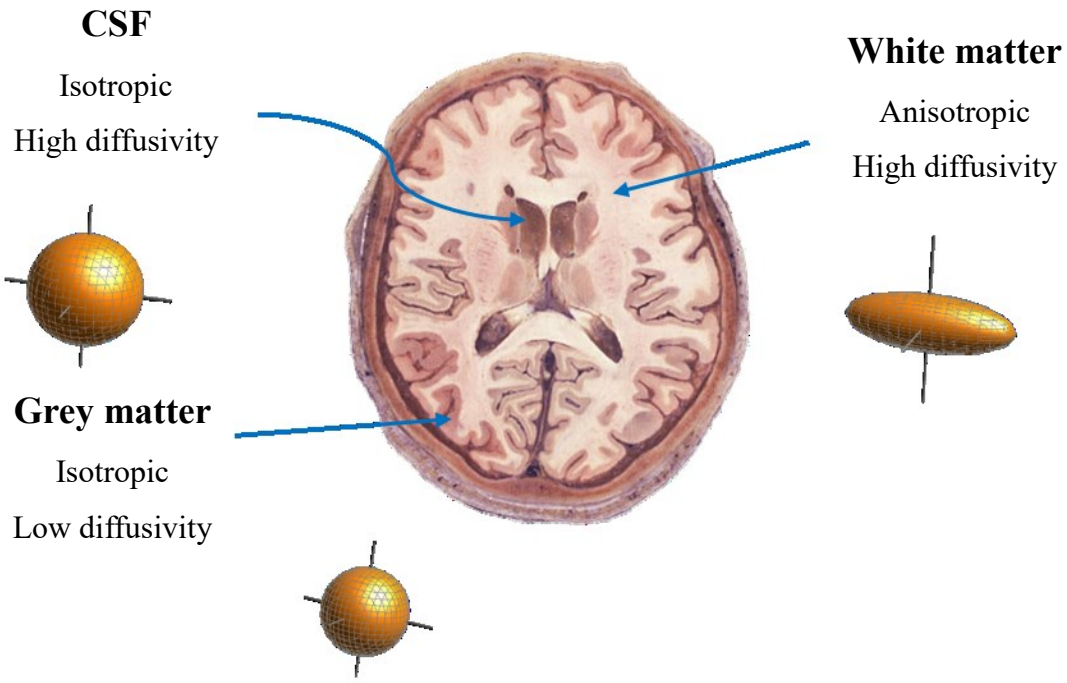

Figure 4. Water diffusion within the brain regions.

Demyelination and axonal injury are the pathological features of multiple sclerosis, resulting in loss of highly organized fibers structure and myelin integrity (Lassmann et al., 2001). As a result, water molecules diffusion in the damaged area is no more hindered in the parallel and perpendicular directions to the tracts. Several studies have demonstrated the FA reduction and increase in MD in white matter, NAWM and lesions, visible in T2-weighted MRI in MS, compared to healthy controls (Symms et al., 2004; Werring, 2000; Castriota-Scanderbeg et al., 2003; Kim et al., 2017; Roosendaal et al., 2009). The greater increase in diffusivity often indicating disorganization of the fibers, correlated with disease duration and was more prominent in the advanced phase of the disease (Scanderbeg et al., 2000). RD change suggested the demyelination patterns within the lesions and in non-lesional tissue (Klistorner et al., 2016, 2015; Roosendaal et al., 2009). Altered AD is attributed to axonal loss, that takes place in acute MS lesion and progresses over time. Associations between reduced tract integrity and EDSS have also been found (Harrison et al., 2013; Onu et al., 2012; Ciccarelli et al., 2001).

However, the interpretation of change in diffusion should be done carefully, as the diffusion tensor is an oversimplified model of the diffusion in the biological tissues. The acquisition artifacts and low SNR, issues with fiber crossing/merging, and the presence of more than one fiber in a voxel may produce the misleading results (Wheeler-Kingshott and Cercignani, 2009). To overcome the limitations of the ellipsoid diffusion tensor model, several advanced DTI techniques with complex models CHARMED (Assaf and Basser, 2005) and NODDI (Zhang et al., 2012) have been developed.

1.2.3 Positron emission tomography

Positron emission tomography is a non-invasive, specific and highly sensitive nuclear medicine imaging, that can be used for evaluation of metabolic changes within the body. PET imaging has been utilized in the preclinical research and human studies, related to oncology, cardiology, neurodegenerative and psychiatric diseases (Salata and Singh, 2017; Nandu et al., 2018; Slifstein and Abi-Dargham, 2017; Cerami et al., 2017). Subsequently, it has become an important tool in the detecting of brain neuroinflammation in the last decade (Dupont et al., 2017; Airas et al., 2018). This imaging technique is able to visualize the hidden pathological changes *in vivo*, contributing to the understanding of disease pathogenesis.

1.2.3.1 Physical basis of PET imaging

Positron emission tomography utilize the detection of radioactivity from the radiopharmaceutical, administered intravenously into the human body, where it binds and interacts with specific targets in a tissue, therefore providing quantitative measure of metabolic and cellular activity.

Principally, the PET tracer is composed of radioactive isotope, produced by the proton accelerator, or cyclotron. The radionuclides of interest (^{11}C, ^{18}F, ^{15}O, ^{13}N) are biologically presented elements, that makes them directly applicable to animal and human studies. The forementioned radioisotopes have a short half-life (Miller et al., 2008), corresponding to the timescale of the studied biological event, thus reducing the long-term risks, caused by the ionizing radiation and providing quick biodistribution from the target. The next step of the compound synthesis is the internalization of the radionuclide into a specific molecular structure (vehicle, ligand), that binds to a corresponding target within the tissue. The radiotracer is required to have a pharmaceutical quality, before being administered to a patient, thus the compound is

purified, formulated, sterilized and undergo quality assurance control. Following intravenous administration, the unstable radioisotope decays with positron (β^+) radiation, colliding with surrounded electrons in the tissue. Consequently, PET is based on detection of the annihilation coincidence (ACD) of the two opposed 511 keV γ-rays, emitted in a result of positron-electron annihilation in the medium (human body).

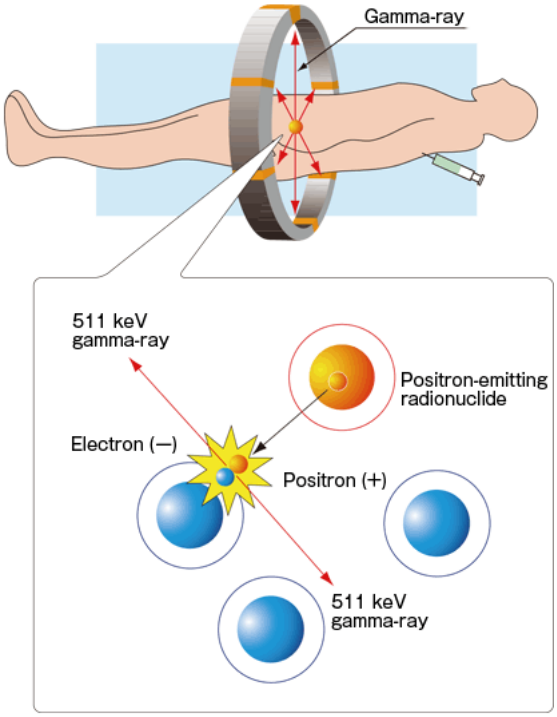

Figure 5. Schematic representation of PET signal acquisition. (https://www.hamamatsu.com/jp/en/technology/innovation/pet/index.html)

The ionizing radiation is detected and measured by the highly sensitive gamma camera, placed around the subject. Gamma camera imaging is often performed in two types - static or dynamic, with dynamic imaging involves the acquisition of series of planar images with varying distribution activity of radiopharmaceutical. Upon acquisition, the raw data is reconstructed with Fourier transform and filtered-back projection, followed by correction for scattering and attenuation (Zanzonico, 2012). The radioligand binding count per voxel is proportional to activity concentration and quantified in terms of SUV (standardized uptake value):

$$\text{SUV} = \frac{MBq\ /cm^3 of tissue}{MBq\ injected/gm\ body\ mass} \tag{3}$$

However, the SUV measurement does not allow the pharmacokinetic modelling of neuroreceptor binding, therefore the kinetic modelling, such as Logan plot, have been utilized. The Logan plot calculates the neuroreceptor binding in a target tissue as the distribution volume ratio (DVR), that is the proportion of the distribution volume (DV) in target region to the DV in a reference region (free of specific binding). Therefore, radioligand kinetics can be measured with a 2-tissue compartments model, utilizing the calculation of non-metabolized tracer in the plasma as the function of time, or time activity curve (TAC).

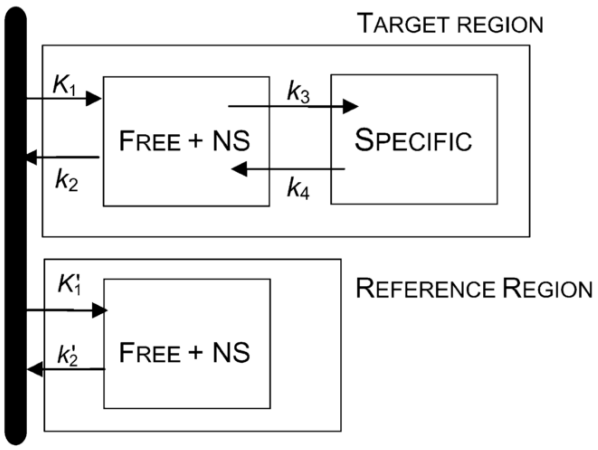

Figure 6. Two tissue compartmental model for TSPO imaging. K1 and k2 represent rate constants for radioligand transport from plasma to tissue and *vice versa*; k3 and k4 are the constant rates between the free and specific binding compartments. Modified from (Turkheimer et al., 2007)

To reconstruct the TAC, repeated arterial blood samples are taken during the dynamic PET imaging. DVR can be calculated with the equation (Logan et al., 1990):

$$\text{DVR} = \frac{\frac{K1}{k2}*\left(1+\frac{k3}{k4}\right)}{\frac{K'1}{k'2}} = 1 + \frac{k3}{k4} = 1 + \frac{Bmax}{Kd} = 1 + BP, \text{ K1/k2 = K'1/k'2} \qquad (4)$$

where BP is the binding potential , B_{max} is the receptor availability, K_d is the equilibrium dissociation constant, K1, k2, k3, k4, K'1, k'2 are the rate constants between the compartments of target and reference tissues.

In order to avoid the unpleasant for the patient blood sampling during the imaging, the reference-based Logan plot methodology have been developed (Logan et al., 1996). In

reference region modelling, the curve is derived from the ROI (region of interest) with a low radioligand binding (e.g. HC gray matter). The supervised clustering algorithm (Turkheimer et al., 2007) have been implemented for automated creation of the reference region and combined with a reference region modelling for robust quantitative assessment of PET imaging.

1.2.3.2 Imaging microglia with PET

PET represents a unique tool for molecular imaging of neuroinflammation, contributing to *in vivo* investigation of the brain pathological processes. Microglia activation have been linked to a several neurodegenerative diseases, including multiple sclerosis (Bogie et al., 2014), Alzheimer's disease (AD) (Mosher and Wyss-Coray, 2014) and Parkinson's disease (PD) (Moehle and West, 2015). Consequently, PET imaging allows for *in vivo* detection of microglial and macrophages activation (Banati et al., 2002), reactive astrocytosis (Gulyás et al., 2011; Tronel et al., 2017) and can potentially be translated from animal to human studies for myelin content detection (Stankoff et al., 2006; Wang et al., 2009).

Various radioligands have been developed for the imaging of neuroinflammation in humans, but translocator protein binding radioactive tracers have been stated as the most prominent ones (Vivash and OBrien, 2016). [^{11}C](R)-PK11195 or ([N-methyl-^{11}C]-1-(2-chlorophenyl)-N-(1-methylpropyl)-3-isoquinolinecarboxamide is the most used highly selective TSPO radioligand up to date (Liu et al., 2014), although numerous 2nd generation TSPO radioligands have been developed and studied (Colasanti et al., 2014; Takano et al., 2013; Poutiainen et al., 2016). TSPO is the 18 kDa translocator protein, formerly called as the peripheral benzodiazepine receptor (BPR) (Papadopoulos et al., 2006), located primarily in the outer mitochondrial membrane and present in a low level of glial cells of the heathy brain. In response to neuronal injury, TSPO is over-expressed in microglia and astrocytes (Chen and Guilarte, 2006; Lavisse et al., 2012), thus being a sensitive probe to target neuroinflammation (Rupprecht et al., 2010).

In vivo and post-mortem immunohistochemical human studies showed that TSPO is upregulated in brain pathological conditions in MS, AD, PD and ALS (amyotrophic lateral sclerosis), Huntington disease (HD), frontotemporal dementia, ischemic stroke and encephalitis (reviewed in Cerami et al., 2017; Cosenza-nashat et al., 2009; Kannan et al., 2009). Increased specific [^{11}C]PK11195 binding, quantitatively evaluated as

binding potential (BP) or distribution volume ratio (DVR), has been detected in NAWM and perilesional WM areas in SPMS patients, compared to RRMS or HC, and was associated with a high concentration of activated microglia at the lesions periphery (Politis et al., 2012; Rissanen et al., 2014; Debruyne et al., 2003).

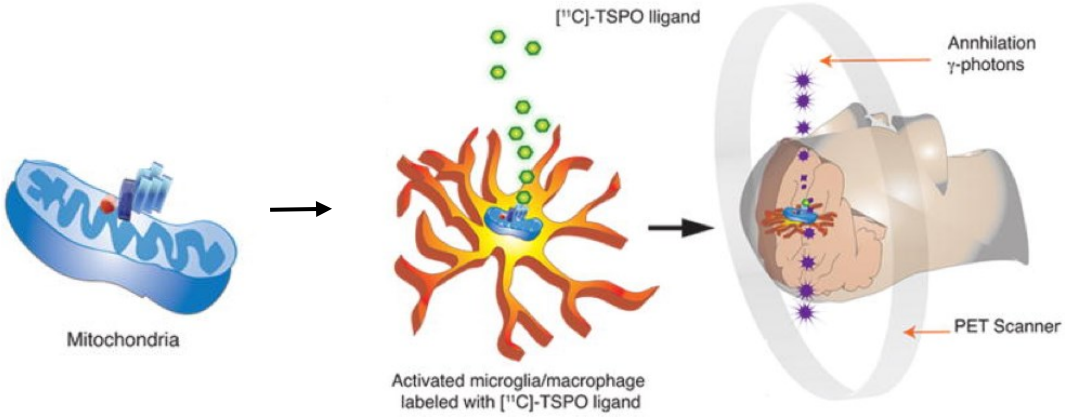

Figure 7. Imaging microglia with [^{11}C]PK11195 PET radioligand. (Modified from Venneti et al., 2013).

Despite being considered as a gold standard among TSPO-ligands, [^{11}C]PK11195 have several limitations: high lipophilicity causing a non-specific binding (Shah et al., 1994), low signal-to-noise ratio (Kobayashi et al., 2018), low bioavailability and binding to blood cells and plasma proteins (Turkheimer et al., 2015).

A previous study in our research group was performed on MS patients in early RRMS (n = 10) and late SPMS disease stage (n = 10), with comparison to a healthy control group (n = 17). The MS cohort showed a significant association of reduced FA in NAWM with disability and age. Also, increased [^{11}C]PK11195 binding in NAWM showed a correlation with brain atrophy, reduced FA in NAWM and increased lesion volume (Rissanen et al., 2018).

2 AIMS OF THE STUDY

To further substantiate previously acquired results, a larger group size was studied (n = 55), covering the full spectrum of disease progression (RRMS: n = 15, RRMS close to progressive stage conversion: n = 25, SPMS: n = 15), with comparison to a sex and age-matched control group. In addition, four DTI parameters were investigated in the whole and segmented NAWM, compared to PET findings.

Hypothesis: Microglial activation associates with normal appearing white matter structural damage in multiple sclerosis.

The main aim of the study was to evaluate structural and molecular brain changes in the pooled MS patients' cohort, using combined DT-MR and PET imaging with comparison to healthy controls, and:

1) Perform DTI analysis in the whole NAWM and segmented NAWM of MS cohort, to evaluate differences in DTI abnormalities between MS subtypes compared to HC;
2) Evaluate the possible correlations of [^{11}C]PK11195 PET binding to white matter tracts integrity in MS;
3) Evaluate the possibility of treatment response assessment with DTI analysis in MS.

3 METHODS

3.1 Participants

The imaging data was acquired from the "KADEPET-RRMS" and "KADEPET-SPMS" substudies, already carried out as part of the "Imaging CNS adenosine receptor expression in patients with Multiple sclerosis, Huntington's disease and Parkinson's disease using positron emission tomography (KADEPET) research project. In addition, baseline data from the ongoing study named "Role of microglia in the pathogenesis of progressive multiple sclerosis (PROMS)" was utilised. All of the forementioned studies have previously been approved by the Ethics Committee of the Hospital District of Southwest Finland. All study subjects had given their written, informed consent before entering the study.

The KADEPET-RRMS project has provided data for 10 RRMS patients, 28-53 years old. DTI with 64 gradient directions have been acquired at baseline, 2 and 6 months from the initiation of fingolimod treatment. The TSPO-PET imaging results of this cohort have already been reported earlier (Sucksdorff et al., 2017).

KADEPET-SPMS study included 20 patients, 29-64 years old, with both SPMS (n = 15) and RRMS (n = 5) types of MS. 6 SPMS patients and 4 RRMS patients were initiated on natalizumab treatment after the baseline imaging, whereas 10 patients (9 SPMS and 1 RRMS) without any disease modifying treatment served as a negative control group. [^{11}C]PK11195 PET and 33 directions DTI imaging were performed at baseline and after one year for all patients. A separate manuscript describing the TSPO-PET imaging data in this project is being prepared.

PROMS is an ongoing project evaluating disease progression, that include baseline imaging with TSPO-PET, MRI with DTI and clinical evaluation, and yearly follow-up with MR-imaging and clinical evaluation up to 5 years. All patients have been on different DMTs at the baseline imaging. Three patients were taking Tecfidera (dimethyl fumarate), 5 patients were on Gilenya treatment (fingolimod), 4 patients had Rebif 44 mikrog treatment (interferon beta 1-a s.c.), 4 patients received Copaxone (glatiramer acetate), 2 were on Aubagio (teriflunomide) and other 2 on Avonex (interferon beta 1-a, i.m.) treatment, while the rest of the patients (n = 5) had no treatment. PROMS study

imaging protocol included [^{11}C]PK11195 imaging and 64 gradient directions DTI for 25 RRMS patients, aged 40-60 years and 10 healthy controls, 21-52 years old. It is worth noting that MS patients in this age group are in the risk of converting to the secondary progressive phase of the disease, since the average age for the onset of the disease progression is at the age of 50 years (Koch et al., 2010).

In addition, to complement the age matching of the control group to the fore mentioned MS subgroups, four healthy controls, 48-58 years old were also included from NIMS-PET project and one healthy subject, 52 years old, from VAMI project.

Pooled treated cohort (total n = 45) i.e. KADEPET-RRMS (n = 10) at 6 months, KADEPET-SPMS (n = 10) at 1 year, PROMS (n = 25) at baseline (immunomodulatory treatment in use at the time of imaging) and pooled untreated cohort (total n = 30) e.g. KADEPET-RRMS (n = 10) at baseline, KADEPET-SPMS (n = 20) at baseline (immunomodulatory treatment not in use at the time of imaging), were used to evaluate potential DTI parameter changes in the normal appearing white matter, in comparison to healthy controls, and in comparison to microglial activation evaluated with TSPO-PET.

Pooled cohort, including 55 MS patients, i.e. KADEPET-RRMS (n = 10) and KADEPET-SPMS (n = 20) at baseline imaging, plus PROMS (n = 25), was used to evaluate association between structural integrity and microglial activation in NAWM.

3.2 MRI/DTI data acquisition

Magnetic resonance imaging in all substudies was performed with 3T MRI Phillips Ingenuity (Philips Healthcare, Cleveland, OH) scanner using a SENSE head coil. Acquisition parameters of all substudies are shown in Table 2.

Table 2. MRI acquisition parameters used in KADEPET-RRMS, KADEPET-SPMS, PROMS, NIMS and VAMI substudies.

Substudy / **MRI parameters**	3D T1-weighted sequence	Axial T2-weighted sequence	3D FLAIR VISTA	DTI sequence
KADEPET-RRMS PROMS NIMS VAMI	TR = 8.1ms TE = 3.7 ms FOV = 256 mm x 256 mm Spatial resolution = 1x1x1 mm Acquisition matrix 256 x 256mm Flip angle = 7°	TR/TE = 3756/80 ms	TE/TR/TI= 337/8000/2400 ms	63 gradient directions, b0 = 1 (b0 = 4 for VAMI substudy) b-value = 1000 s mm^{-2} TR/TE = 9500/120 ms FOV = 256 x 256 mm Spatial resolution 2x2x2 mm Acquisition matrix 128x128 mm Flip angle = 90° Acceleration factor 2
KADEPET-SPMS	TR = 8.2 ms TE = 3.7 ms FOV = 240 x 260 x 180 mm Spatial resolution = 1x1x1 mm Acquisition matrix 240 x 240mm Flip angle = 7°	TR/TE = 3000/80 ms	TE/TR/TI = 125/10000/2800 ms	33 gradient directions, b0 =1 b-value = 1000 s mm^{-2} TR/TE = 9500/120 ms FOV = 256 x 256 mm Spatial resolution 2x2x2 mm Acquisition matrix 128x128 mm Flip angle = 90° Acceleration factor 2

3.2.1 Pre-processing of the data

The raw MRI and DWI data was downloaded in DICOM format and converted to NIFTI format with dcm2nii converter tool (Li et al., 2016). The lesions at the each time point were identified with Lesion Segmentation Toolbox in SPM8 (The Wellcome Trust Centre for Neuroimaging, Institute of Neurology, University College London) (Schmidt et al., 2012), and then manually corrected slice by slice in FLAIR and T1-weighted images. The T1 image was filled with the resulting lesion masks, following with segmentation of grey and white matter with Freesurfer 6.0 software (http://surfer.nmr.mgh.harvard.edu/). The segmentation processing consisted of intensity normalization, skull-stripping, transformation into Talairach space and cortical/subcortical structure segmentation. T1 and segmented WM and GM volumes were then co-registered to MNI (Montreal Neurologic Institute) ICBM152_T1 stereotaxic space template (Mazziotta et al., 2001). To create a NAWM mask, T2 hyperintense lesions were excluded from WM mask by segmentation with Lesion Segmentation Tool (Figure 8). The binary NAWM mask also excluded the deep GM, temporomedial regions, and cerebellum.

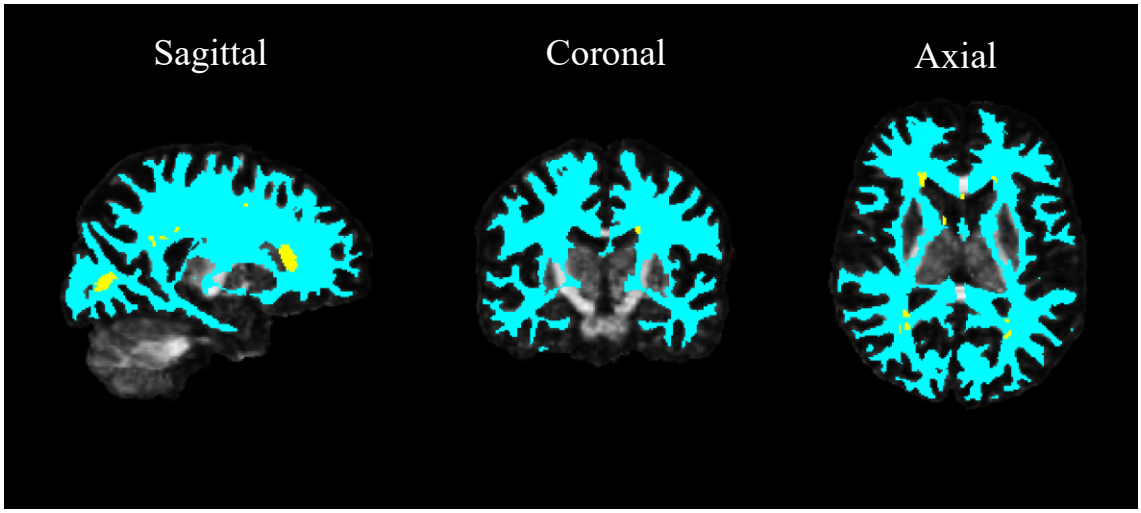

Figure 8. NAWM mask (blue) with excluded T2 lesions (yellow) overlapped with T1-weighted image (slice coordinates X = 77, Y = 109, Z = 77).

Six NAWM regions (deep WM, cingulate, frontal, temporal, occipital, parietal) were derived with Freesurfer atlas-based method, by parcellation of the subcortical WM (Salat et al., 2009) and excluded corresponding T2 hyperintense lesions (Figure 9).

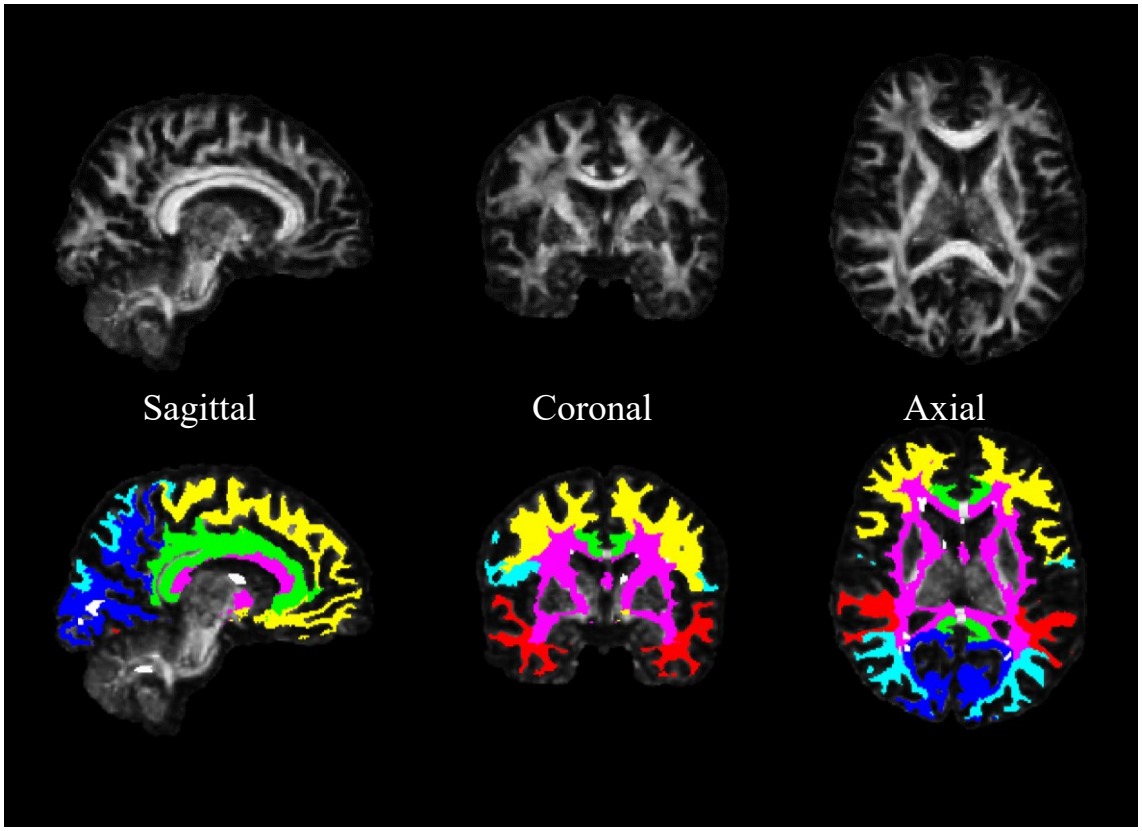

Figure 9. WM parcellation identified six ROIs: frontal WM (yellow), parietal WM (blue), temporal WM (red), occipital WM (dark blue), cingulate WM (green), deep WM (purple). Segmented lesions are shown in white.

The T2 lesion load was measured in the whole NAWM and segmented NAWM of the three study groups. It was investigated whether the lesion burden affects the diffusion in the white matter. Normalized lesion burden was calculated in each of the segmented WM region by dividing the lesion volume in each segmented WM to the volume of the associated region i.e. *normalized lesion burden in segmented WM = lesion volume within ROI / volume of ROI.*

3.2.2 DTI analysis

The raw data was checked for artefacts with ExploreDTI v4.8.6 software (http://www.exploredti.com) quality assessment tool and DTIPrep 1.2.7 software (https://www.nitrc.org/projects/dtiprep/) (Oguz et al., 2014). Subjects with a large number of artefacts (Figure 10) were excluded from further DTI analysis.

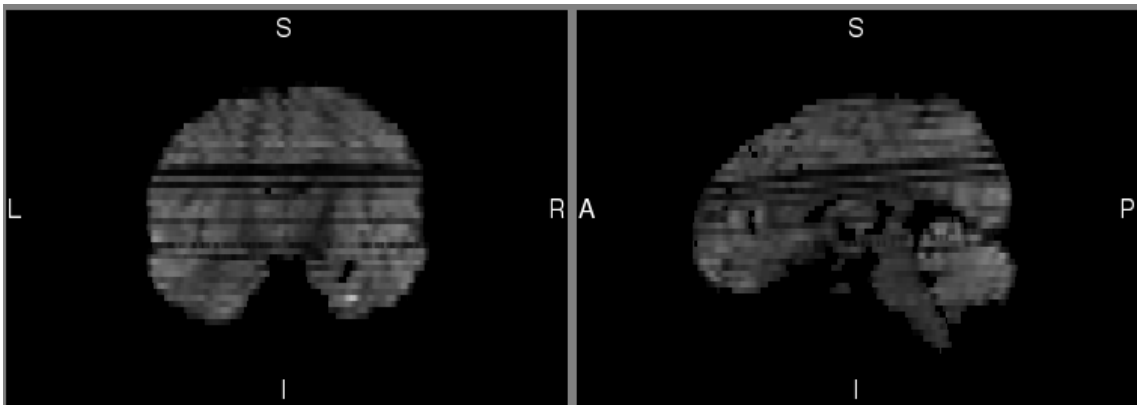

Figure 10. Inter-slice and intra-slice intensity artefact in sagittal and coronal planes of DWI data. LR (left-right), SI (superior-inferior), AP (anterior-posterior).

DWI data was pre-processed with ExploreDTI for motion, eddy current (EC) and EPI/susceptibility induced distortion correction (Leemans and Jones, 2009). First, the headers of T1 and DWI files were adjusted with "Flip/permute dimensions of *nii files" plugin, then T1 image was masked with plugin "Mask 3D *nii files" with kernel size 3 and threshold of 0.02. To run the non-rigid EPI correction, diffusion tensor tensor estimation method was set to RESTORE (robust estimation of tensors by outlier rejection) approach (Chang et al., 2005), for both native and transformed data (T1-weighted image was specified as a transformation space). The image type for registration was specified as FA. The number of resolutions was set to 4 and deformation axes were constrained to the anterior-posterior direction.

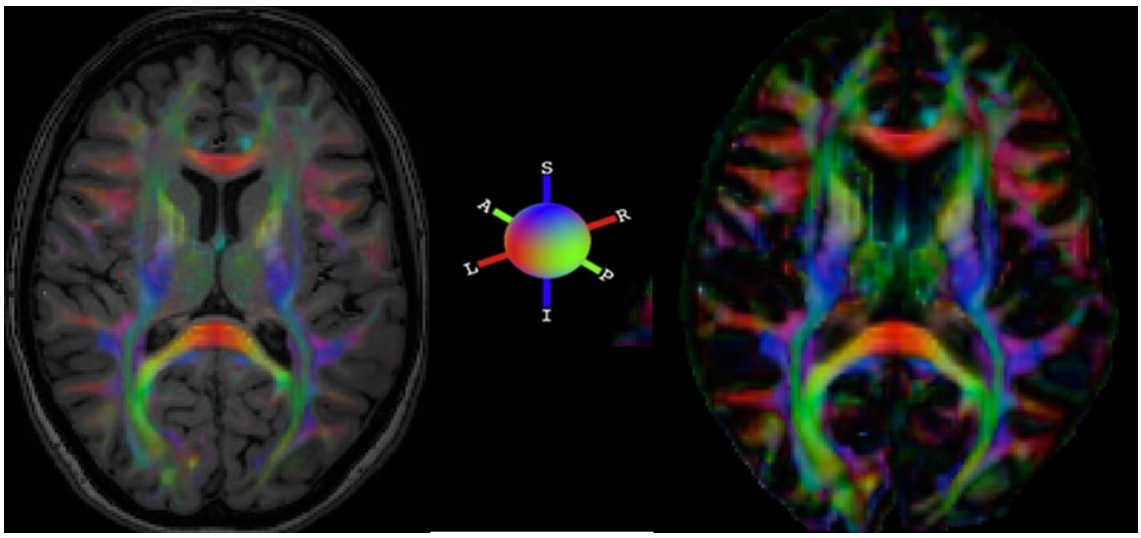

Figure 11. Diffusion tensor map with color-coded diffusion directions (right), fused with T1 sagittal image (left). LR (left-right), SI (superior-inferior), AP (anterior-posterior).

After pre-processing, four maps of interest (FA, MD, AD, RD) were reconstructed from the diffusion tensor map and co-registered in statistical parametric mapping (SPM8) to corresponding T1-weighted image in MNI152 space.

3.3 PET radioligand production and image acquisition

[^{11}C]CO_2 radioisotope with 20.4 minutes half-life was in-house (PET centre) produced with 18MeV proton bombardment of ^{14}N in cyclotron. The ^{11}C was produced *in-situ* into $^{11}CO_2$ via hot atom processes. [^{11}C]CO_2 was first converted to [^{11}C]CH_4, directed through iodine reactor, and then further converted to [^{11}C]CH_3I through the gas phase method. [^{11}C]CH_3I, released by heat and sweep gas, delivered into the reaction solution, containing precursor for PK11195, and then underwent HPLC (high performance liquid chromatography) purification and reformulated into ready-to-inject dose. Dynamic 60 minutes [^{11}C]PK11195-PET imaging was performed with ECAT HRRT scanner (CTI, Siemens Medical Solutions, Knoxville, TN, USA) with an intrinsic spatial resolution of 2.5 mm. Restriction of head movements during the scan was achieved by using individual thermoplastic head mask. Previous to the radioligand injection, the attenuation correction scan was performed with single photon transmission scanning using ^{137}Cs point source. The radioligand was administered intravenously, the target dose being 500 MBq. The injected doses were not significantly different between study groups (data not shown).

3.3.1 Modelling of [^{11}C](R)-PK11195 image data

All of the data from three study cohorts and healthy control group was processed in the following way. PET images were reconstructed using 17 time frames (total of 3600 seconds) as described previously (Rissanen, 2015). The head movement between the frames were corrected by realigning the dynamic PET images in SPM8 software, after which the PET sum images were calculated from the dynamic PET images. Individual PET sum images were co-registered to 3D T1 MR images and then all data was resliced to 1 mm voxel size. Finally, for each patient, the PET sum images from the subsequent sessions were co-registered to the first session's (baseline) PET image.

For evaluating [^{11}C]PK11195 binding, seven regions of interest (ROI) were defined using Freesurfer software in global NAWM and six WM subregions: deep WM,

cingulate, frontal, temporal, occipital and parietal WM, excluding lesional WM (i.e. MS plaques visible in FLAIR and T1 MRI sequences), segmented with LST.

Specific TSPO-PET radioligand binding was quantified as the distribution volume ratio (DVR), using Logan plot with reference tissue input. The gray matter reference region devoid of specific binding was extracted with the supervised cluster algorithm (SVCA) (SuperPK software, King's College, London, UK) with four predefined kinetic tissue classes for normal GM, normal WM, vasculature and high specific binding.

The reference tissue–input Logan method, with a 20- to 60-min time interval, was applied to the regional TACs using the SVCA gray reference input. Additionally, the modelling was performed in voxel level, where parametric maps of specific binding (measured as DVR) were calculated from the dynamic PET images, by using simplified reference tissue model (Gunn et al., 1997) with the clustered reference tissue input.

3.4 Statistical methods

The statistical analyses of DT-MR, PET imaging and clinical parameters were performed with RStudio software (version 1.1.419). The normality distribution of the data was evaluated with the Shapiro-Wilk test and checked visually with density and Q-Q plots. The nonparametric Mann–Whitney U test was chosen to evaluate the group differences of non-normally distributed data and in groups with low number of the subjects. Student's t-test was chosen to test for age difference between groups. Pairwise repeated measurements (e.g. baseline – follow up) were performed with Wilcoxon signed-rank test. The correlational analyses between variables of interest were analysed with Spearman nonparametric correlation test. P value of less than 0.05 was considered statistically significant for all analyses.

3.4.1 Tract-Based Spatial Statistics

Tract-Based Spatial Statistics (TBSS) analysis was performed using standard TBSS pipeline (Smith et al., 2006). First, FA/MD/AD/RD maps, generated in ExploreDTI, were reoriented to the FSL's standard space using an FSL command "fslreorient2std".

The TBSS pipeline consisted of 4 steps, including the data pre-processing (e.g. removing brain-edge artefacts and zeroing the end slices), registering all the data to a common 1x1x1 mm FMRIB58_FA template using nonlinear registration. The next step

involved the affine transformation of all subjects' data to the 1x1x1mm MNI152 standard space, followed by merging all the images to a single 4D image file. Thereafter, the average of all registered individual maps generated the mean cross-subject image (e.g. mean_FA), and this was then fed into skeletonization program to create a mean skeleton (e.g. mean_FA_skeleton), that represents main fiber tracts. The mean FA skeleton was thresholded with value of 0.2 to exclude the areas with high inter-subject variability. The last step in the pipeline included the alignment of each subject's FA map onto the mean skeleton, by creating a skeleton "distance map". This was done by searching the highest local FA value in the area perpendicular to the skeleton tract, and then assigning this value to the corresponding skeleton point. As a result, the pipeline creates a 4D image file, ready for voxel wise statistics analysis.

The same transformations were applied to the MD, AD and RD diffusivity maps.

To identify the DTI parameters differences between the patients and controls at the voxel level, the voxel wise statistical analysis was performed on skeletonized FA (MD/AD/RD) data. For all TBSS analyses, permutations-based statistics with 2^{10} (for group size n = 10) random permutations, performed by FSL randomize program (Winkler et al., 2014), and threshold-free cluster enhancement (TFCE) (Smith and Nichols, 2009) were used to obtain the significant differences between two groups. TFCE score was thresholded at the value of $p < 0.05$, correcting for multiple comparisons by controlling over family-wise error (FWE) rate.

3.4.2 Voxel-wise image analysis

Voxelwise Pearson's correlations were calculated in MATLAB between normalized FA and DVR images of 54 MS patients (1 subject was excluded from analysis due to large number of artifacts in raw DWI image). Parametric images were smoothed with 8mm FWHM (full width at half maximum) filter for noise and normalization compensation. The resulting p values were corrected for false discovery rate (FDR) using significance level $p < 0.05$, showing statistically significant clusters of voxels in normal appearing white matter, having negative correlation between FA and TSPO-binding.

4 RESULTS

4.1 Demographical and clinical characteristics

Description of the demographical and clinical data is summarized in Table 3. The mean age of the groups at baseline and at follow up imaging sessions was not statistically significantly different from the mean age of the healthy control group. The patients in KADEPET-SPMS and PROMS groups were older than patients in KADEPET-RRMS group, that is expected for SPMS patients (n = 15, mean age 50.3 ± 9.19 years, p = 0.048) and patients who are in the risk group of progression (n = 25, mean age 47.6 ± 3.99 years, p = 0.029), as those patients have longer disease duration (15.7 ± 6.98 years, p = 0.006 and 13.6 ± 6.44 years, p = 0.022 respectively), compared to the RRMS patients (n = 10, mean age 42.4 ± 9.4 years) with disease duration of 8.4 ± 3.8 years. The sex ratio was similar for the four groups. As expected, the EDSS of SPMS patients (n =15) at the baseline imaging was higher, EDSS = 4.87 ± 1.33, than the EDSS of relapsing-remitting patients (total n = 40) at the baseline, EDSS = 2.8 ± 0.94, p = 2.285e-05 (data not shown).

The grey matter cortex volume (p = 0.028), T2 (p = 0.154) and T1 hypointense lesion load (p = 0.125) showed a trend without statistical significance to decrease after 1 year of natalizumab treatment of 10 MS patients in KADEPET-SPMS group. However, the EDSS of treated MS patients in KADEPET-SPMS group increased from 3.5 ± 1.51 to 3.8 ± 1.41, p = 0.014 (data not shown). Meanwhile, there were no significant changes in the T2 lesion, NAWM or grey matter volumes during the 6 months after initiation of fingolimod treatment in KADEPET-RRMS group. Additionally, the EDSS showed a trend to decrease after 6 months of fingolimod treatment, from EDSS 2.7 ± 0.53 to EDSS 2.6 ± 0.72, p = 0.28.

Follow-up data of PROMS group was not available at the moment of conducting this project.

Table 3. Demographical and clinical MRI parameters of three study cohorts and healthy controls, expressed as mean values with standard deviation, except stated.

	KADEPET-RRMS	*KADEPET-SPMS*	*PROMS*	*Healthy controls*
Number of subjects	10	20	25	15
Gender	9F, 1M	12F, 8M	19F, 6M	9F, 6M
Age (years)	42.4 ± 9.4	48.3 ± 9.8	47.6 ± 3.99	42.5 ± 11.83
Disease duration (years)	8.4 ± 3.8	13.75 ± 7.1	13.6 ± 6.44 ⊗	N/A
MS subtype	10 RRMS	15 SPMS + 5 RRMS	25 RRMS	N/A
EDSS baseline	2.7 ± 0.54	4.3 ± 1.59	2.9 ± 1.04	N/A
follow up	2.6 ± 0.72	4.5 ± 1.64	N/A	N/A
NAWM (cm^3)				
baseline	447.2 ± 56.4	435.6 ± 63.8	453.8 ± 66.3	497.3 ± 35.5 *
follow up	444.8 ± 56.6	434 ± 65.1	N/A	N/A
GM ctx (cm^3)				
baseline	423.6 ± 38.2	438.8 ± 43.1	433.6 ± 35.5	490.2 ± 58.5*
follow up	423.9 ± 39.1	429.6 ± 44.9	N/A	N/A
T2 lesion load (cm^3) **				
baseline	4.1 (2.58-46.79)	17.7 (3.91-70.12)	6.7 (0.48-35.24)	N/A
follow up	4.1 (2.57-53.26)	16.2 (2.08-63.33)	N/A	
T1 hypointense lesion load (cm^3) **				
baseline	3.2 (2.22-33.53)	16.7 (3.19-67.89)	3.3 (0.23-20.78)	N/A
follow up	3.1 (2.28-40.83)	14.8 (1.65-61.32)	N/A	

* Data available for 10 HC only

⊗ Data available for 24 patients only

** Expressed as median (IQR) values

Table 3a. Extension to table 3, with additional demographical and clinical MRI parameters of KADEPET-SPMS substudy, expressed as mean values with standard deviation.

	KADEPET-SPMS	
Number of subjects	20	
Gender	8F, 7M	4F, 1M
Age (years)	50.3 ± 9.19	42.0 ± 9.66
Disease duration (years)	15.7 ± 6.98	7.9 ± 3.15
MS subtype	15 SPMS	5 RRMS
EDSS baseline	4.87 ± 1.33	2.5 ± 0.79
follow up	5.1 ± 1.42	2.7 ± 0.67

Table 4. Demographical and clinical MRI parameters of pooled cohorts, treated (n = 45) and untreated (n = 30), expressed as mean values with standard deviation.

	Pooled treated cohort	*Pooled untreated cohort*
Number of subjects	45	30
Patients pooled from subtudies	KADEPET-RRMS (n =10) at 6 months follow up KADEPET-SPMS (n =10) at 1 year follow up PROMS (n = 25)	KADEPET-RRMS (n =10) at baseline KADEPET-SPMS (n =10) at baseline
Gender	34F, 11M	21F, 9M
Age (years)	47.1 ± 7.10	46.4 ± 9.91
Disease duration (years)	12.6 ± 6.87	11.4 ± 6.96
MS subtype	6 SPMS, 39 RRMS	15 SPMS, 15 RRMS
EDSS	3.0 ± 1.14	3.75 ± 1.52

4.2 DTI in MS patients and healthy controls

DTI analysis in the whole NAWM and segmented NAWM was done for each of the study groups and for two pooled cohorts, the pooled treated cohort (n = 45) and pooled non-treated cohort (n = 30), compared to healthy control group.

4.2.1 DTI abnormalities more pronounced in SPMS

Diffusion parameters were significantly altered in NAWM and segmented WM (temporal, occipital and cingulate WM) of SPMS patients (n = 15), compared to RRMS patients (data available only for n = 4), and healthy controls (n = 15) in KADEPET-SPMS group. Fractional anisotropy was significantly reduced (p = 0.02), while radial diffusivity had a trend to increase (p = 0.06) in NAWM of SPMS patients at baseline imaging, compared to healthy controls (Figure 12).

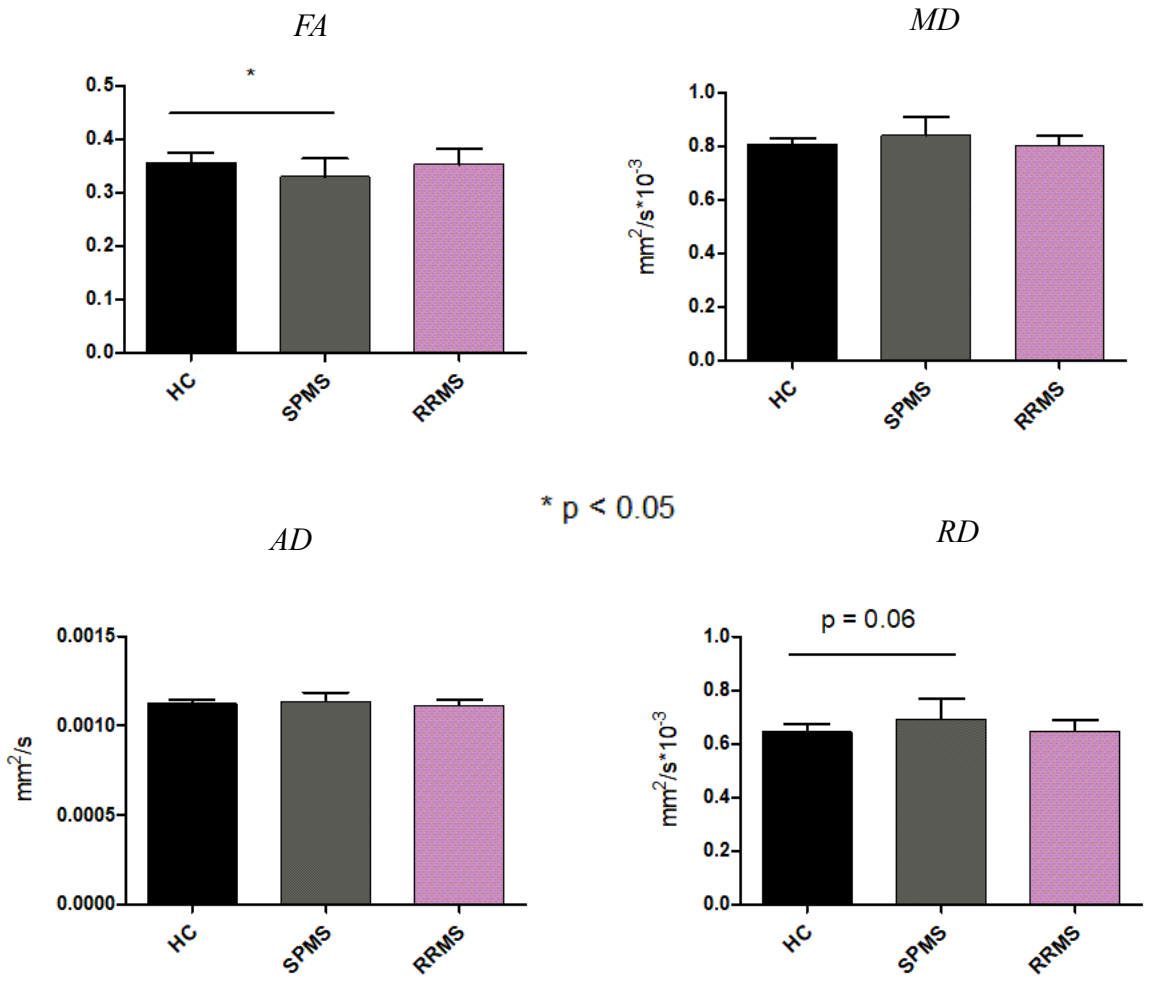

Figure 12. DTI parameters alteration in NAWM of SPMS (n =15) and RRMS (n = 4) patients at baseline imaging in the KADEPET-SPMS cohort compared to HC (n =15).

DTI analysis of segmented NAWM in KADEPET-SPMS group showed significant abnormalities in temporal, occipital and cingulate WM areas of progressive patients at baseline imaging, compared to healthy controls (Figure 13).

Fractional anisotropy was significantly decreased in temporal (p = 0.03), occipital and cingulate WM areas (p = 0.001 and p = 0.004 respectively), whereas significant increase was seen in occipital (p = 0.054) and cingulate (p = 0.002) WM for mean diffusivity (MD), in cingulate WM (p = 0.053) for diffusion along the tracts (AD), and in occipital and cingulate WM regions (p = 0.008 and p = 0.003 respectively) for radial diffusivity.

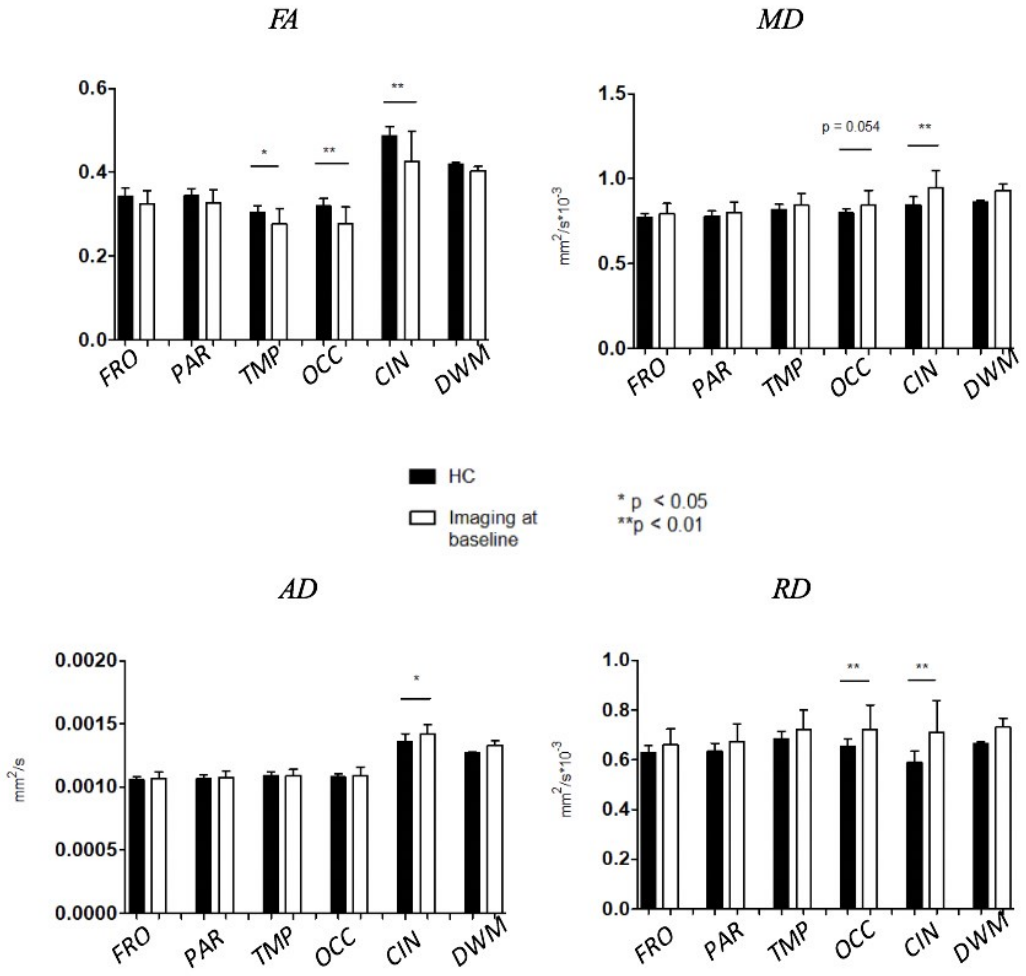

Figure 13. FA, MD, AD and RD diffusion parameters of SPMS patients (n = 15) of the KADEPET-SPMS cohort were more abnormal in temporal (TMP), occipital (OCC) and cingulate (CIN) white matter areas at baseline imaging, compared to healthy controls (n = 15). FRO = frontal, PAR = parietal, TPM = temporal, OCC = occipital, CIN = cingulate, DWM = deep white matter.

4.2.2 Diffuse abnormalities in segmented NAWM of patients at the age of risk for progression

DTI analysis in PROMS study showed significant alterations of diffusion in segmented NAWM, but not in the whole NAWM. Occipital, cingulate and deep WM areas were the most affected (Figure 14).

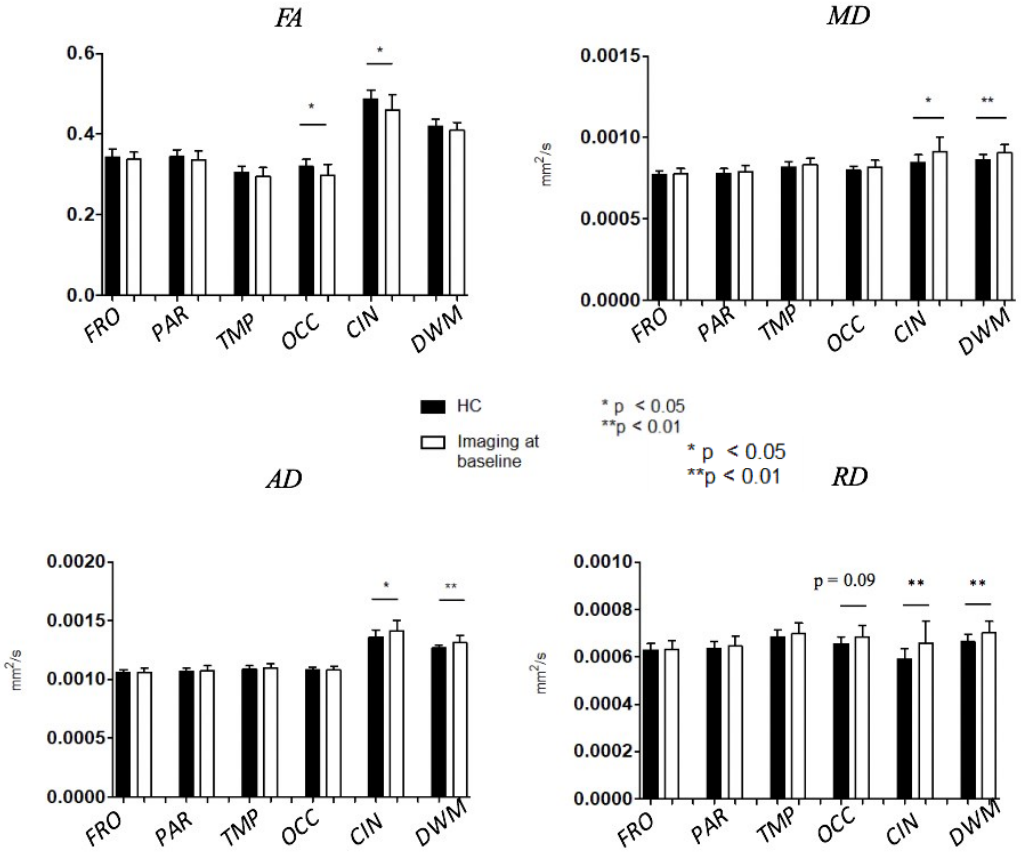

Figure 14. Diffusion parameters abnormalities in segmented NAWM of MS patients (n = 25) in PROMS study compared to healthy controls (n = 15).

All diffusivities (MD/AD/RD) were significantly higher in cingulate ($p < 0.05$ for MD/AD and $p < 0.01$ for RD) and deep WM ($p < 0.01$), while FA was significantly decreased in occipital and cingulate WM area ($p = 0.012$ and $p = 0.014$ respectively), compared to HC. Additionally, radial diffusivity showed a higher mean value close to significance ($p = 0.09$) in occipital WM, compared to HC.

Similar to PROMS, DTI analysis in KADEPET-RRMS study showed significant alterations of diffusion in segmented cingulate NAWM of 10 RRMS patients at the

baseline imaging, compared to healthy controls, but not in the whole NAWM (Figure 15).

Figure 15. Altered diffusion parameters (FA/MD/RD) in cingulate white matter of RRMS patients (n = 10) in KADEPET-RRMS substudy at baseline imaging, compared to healthy controls (n = 15).

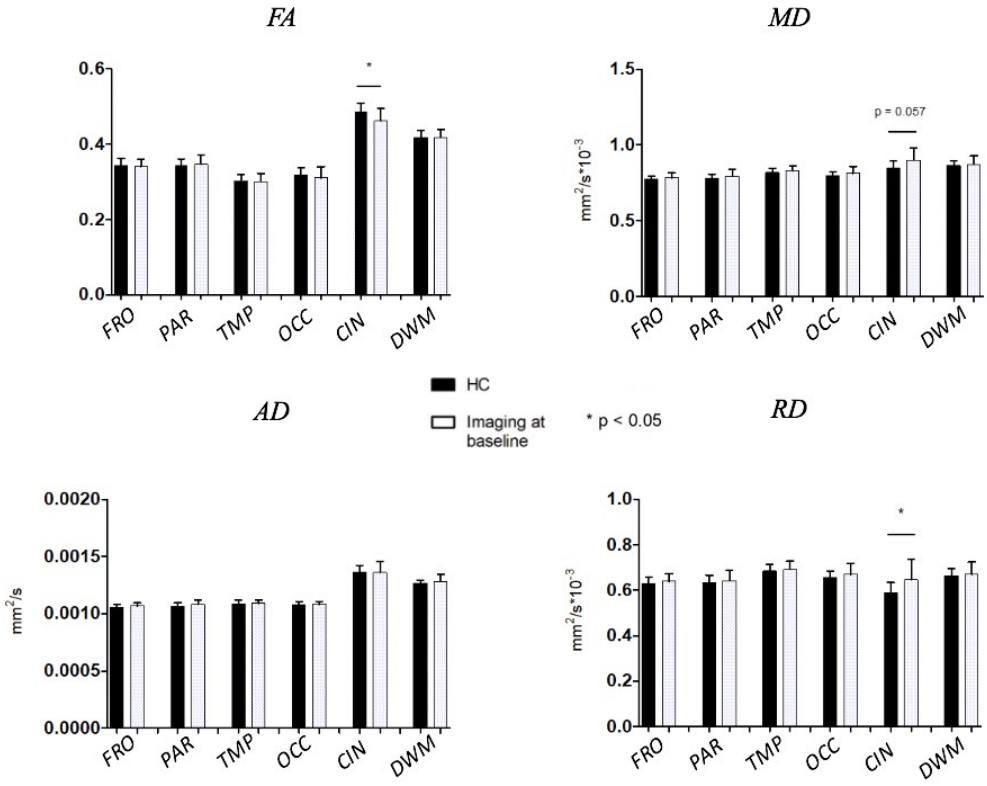

Even though the patients in this group are in the earlier disease stage with mean disease duration of 8.4 ± 3.8 years, the normal appearing cingulate white matter showed significant structural alterations. Fractional anisotropy was significantly decreased ($p = 0.03$), while mean and radial diffusivities were increased in cingulate WM ($p = 0.057$ and $p = 0.045$ respectively), compared to healthy group.

Additionally, DTI analyses were performed in the whole NAWM and in segmented NAWM of pooled cohorts, untreated (n = 30), shown in Figure 16, and treated (n = 45), compared to healthy control group (n = 15).

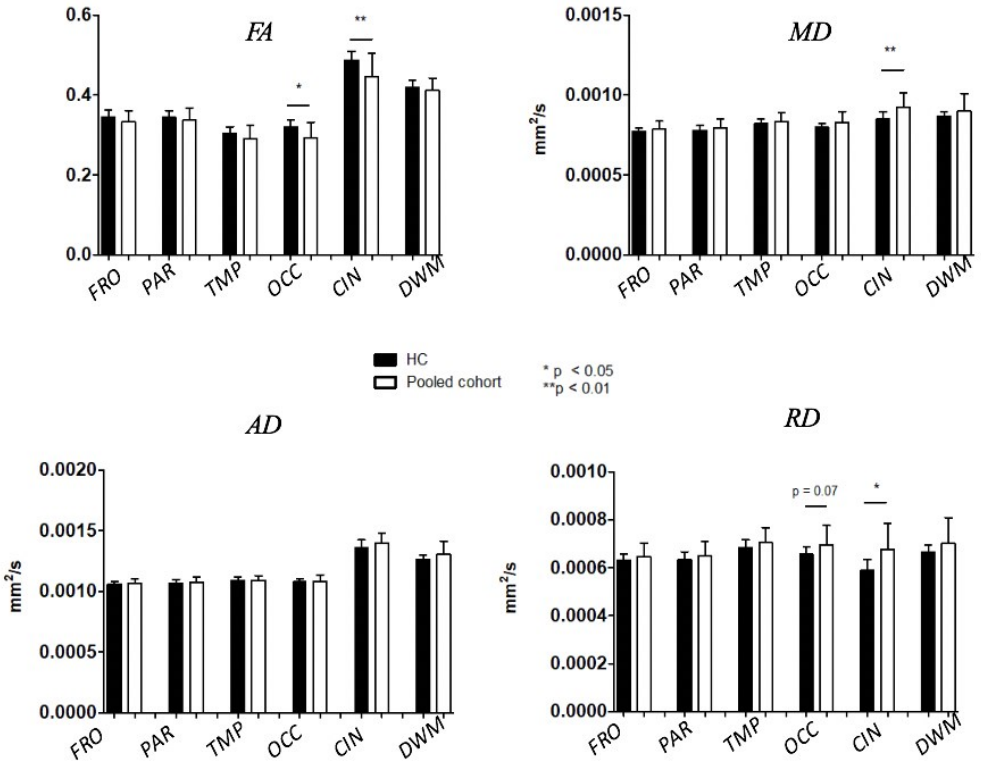

Figure 16. Diffusion parameter abnormalities in segmented NAWM of MS patients in the pooled untreated MS-cohort (n = 30) compared to healthy controls (n = 15).

No significant differences in diffusion parameters (FA/MD/AD/RD) were found in the whole NAWM of pooled untreated cohort, compared to HC. In segmented NAWM, FA was decreased in occipital and cingulate areas ($p = 0.02$ and $p = 0.006$ respectively), MD was increased in cingulate area ($p = 0.009$), while RD was increased in cingulate WM ($p = 0.01$). Additionally, radial diffusivity showed a higher mean value, close to significance in occipital WM ($p = 0.07$), compared to HC.

Similarly, to untreated cohort, treated pooled cohort (n = 45) did not show significant differences in diffusion parameters in the whole NAWM, compared to HC (n = 15), data not shown. However, in segmented NAWM, FA was significantly decreased in cingulate WM ($p = 0.03$) and in occipital WM at the level of $p = 0.057$, while MD and mean RD were significantly increased in cingulate WM ($p = 0.03$ and $p = 0.025$ respectively).

4.2.3 Diffusion tensor imaging in treatment response assessment

Diffusion analysis was performed in the longitudinal KADEPET-RRMS (n =10) study using fingolimod treatment. As shown in previous section, the diffusion parameters (FA, MD and RD) were significantly altered in cingulate WM of 10 RRMS subjects in KADEPET_RRMS study at the baseline imaging, compared to healthy controls. At follow up imaging after 6 months of fingolimod initiation no significant differences were anymore found in the cingulate WM of MS patients, compared to HC. In addition, significant increase in FA ($p = 0.02$) and decrease in RD ($p = 0.04$) were found in cingulate WM at the follow up imaging, compared to baseline among the RRMS patients. Fractional anisotropy showed a trend to increase in the deep white matter ($p = 0.08$), while the mean axial diffusivity was slightly, but not significantly, higher in temporal and deep white matter ($p = 0.08$ and $p = 0.07$ respectively) at the follow up imaging, compared to baseline.

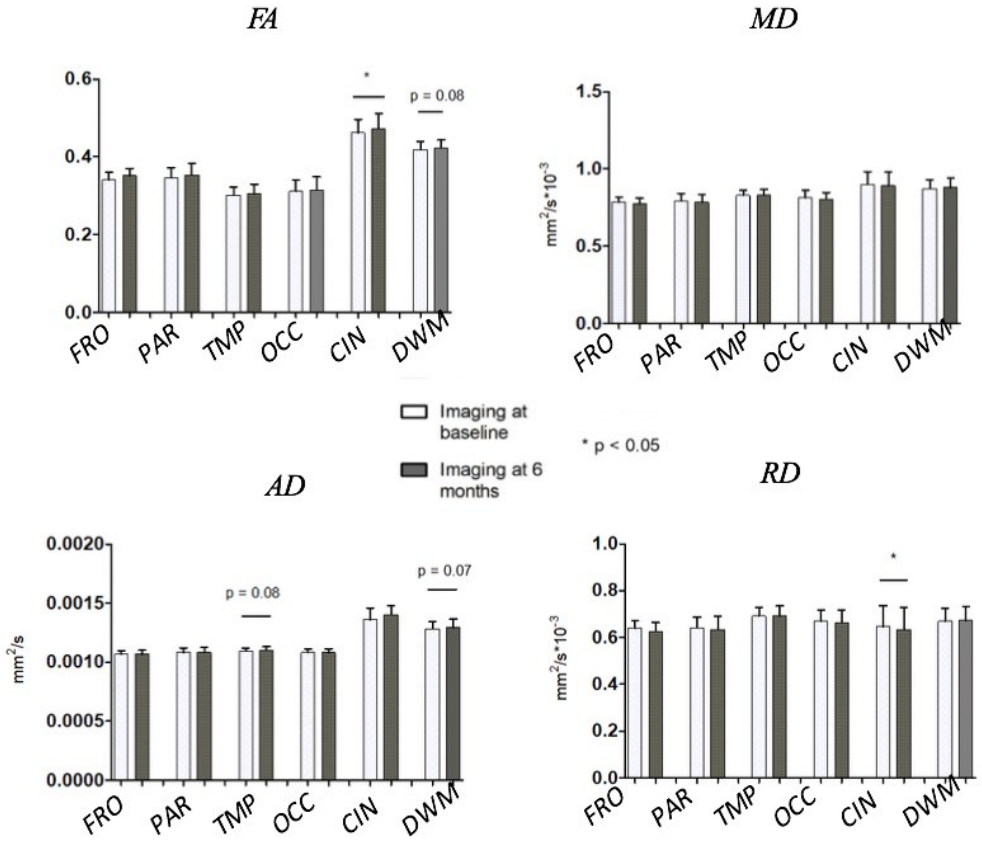

Figure 17. Diffusion parameters change in segmented NAWM of RRMS patients after 6 months fingolimod treatment.

TBSS analysis, using TFCE approach and n = 2^{10} random permutations and FWE correction, showed that 17.8 % of NAWM skeleton voxels of RRMS subjects had significantly decreased FA ($p < 0.05$) at baseline imaging, compared to HC (Figure 18 a). This number decreased to 3.15 % of voxels ($p < 0.05$) after 6 months of fingolimod treatment, compared to HC (Figure 18 b). TBSS analysis was also performed for repeated measurements BL - FU, using paired t-test with TFCE approach and n = 1024 random permutations, uncorrected for FWE. Extent of 11.7% voxels, placed mainly in cingulum, genu and splenium of corpus callosum (CC) showed increased FA ($p < 0.05$) at the follow up imaging, compared to the baseline imaging (Figure 18 c).

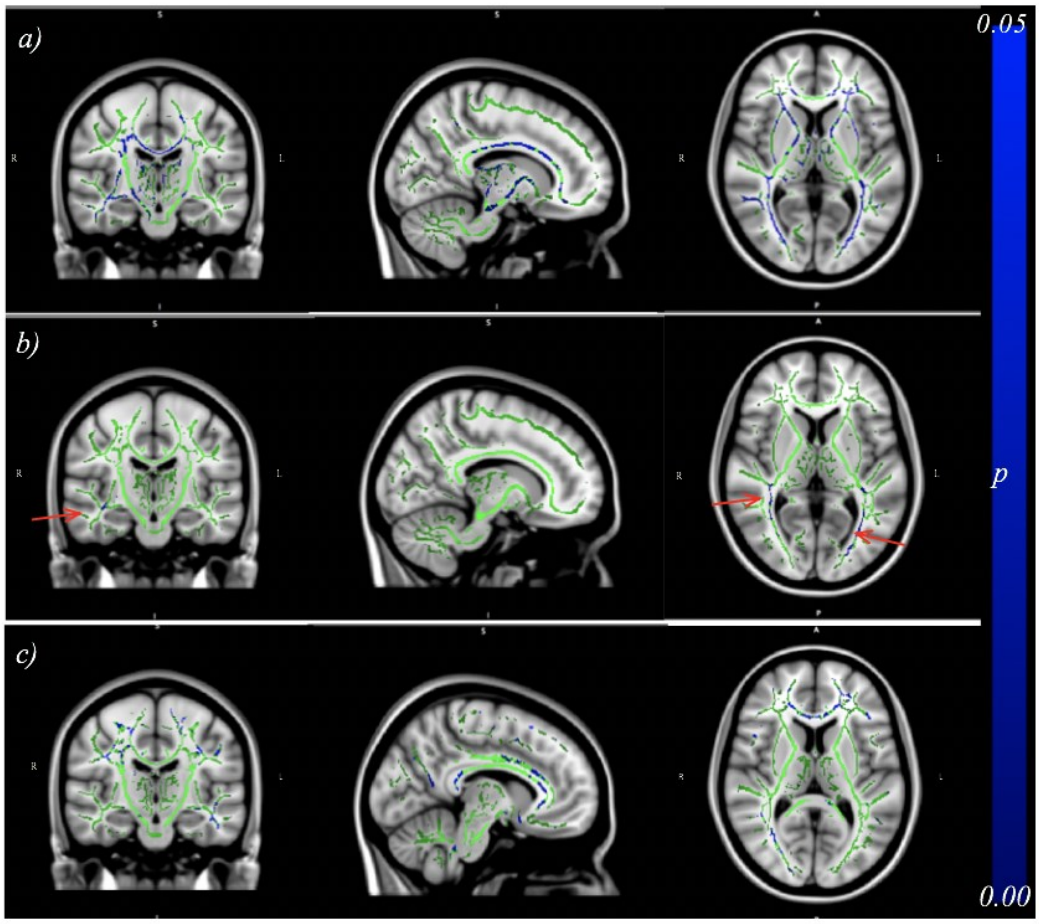

Figure 18. TBSS analysis shows a significant reduction ($p < 0.05$, FWE) in voxels extent with decreased FA after 6 months of fingolimod treatment, compared to HC, where a) baseline imaging, b) imaging at 6 months. Red arrows show voxels with significantly decreased FA at follow up imaging, compared to HC. Repeated measures (image c) show the extent of voxels with significantly increased FA ($p < 0.05$, FWE uncorrected) at follow up. The background image is a standard MNI152_T1_1mm template, the mean FA skeleton is shown in green. a, b: coronal slice is at X = 77,

sagittal slice at Y = 109, axial slice at Z = 77; c: X = 98, Y = 109, Z = 81. Abbreviations: R, right; L, left; I, inferior; S, superior; A, anterior; P, posterior.

The extent of voxels with significantly increased RD was 23.7 % at baseline and 12.9 % at 6 months imaging respectively (Figure 19 a, b). The significant voxels were placed in anterior and superior corona radiata, body and splenium of CC, anterior/posterior thalamic radiation, thalamus and superior longitudinal fasciculus.

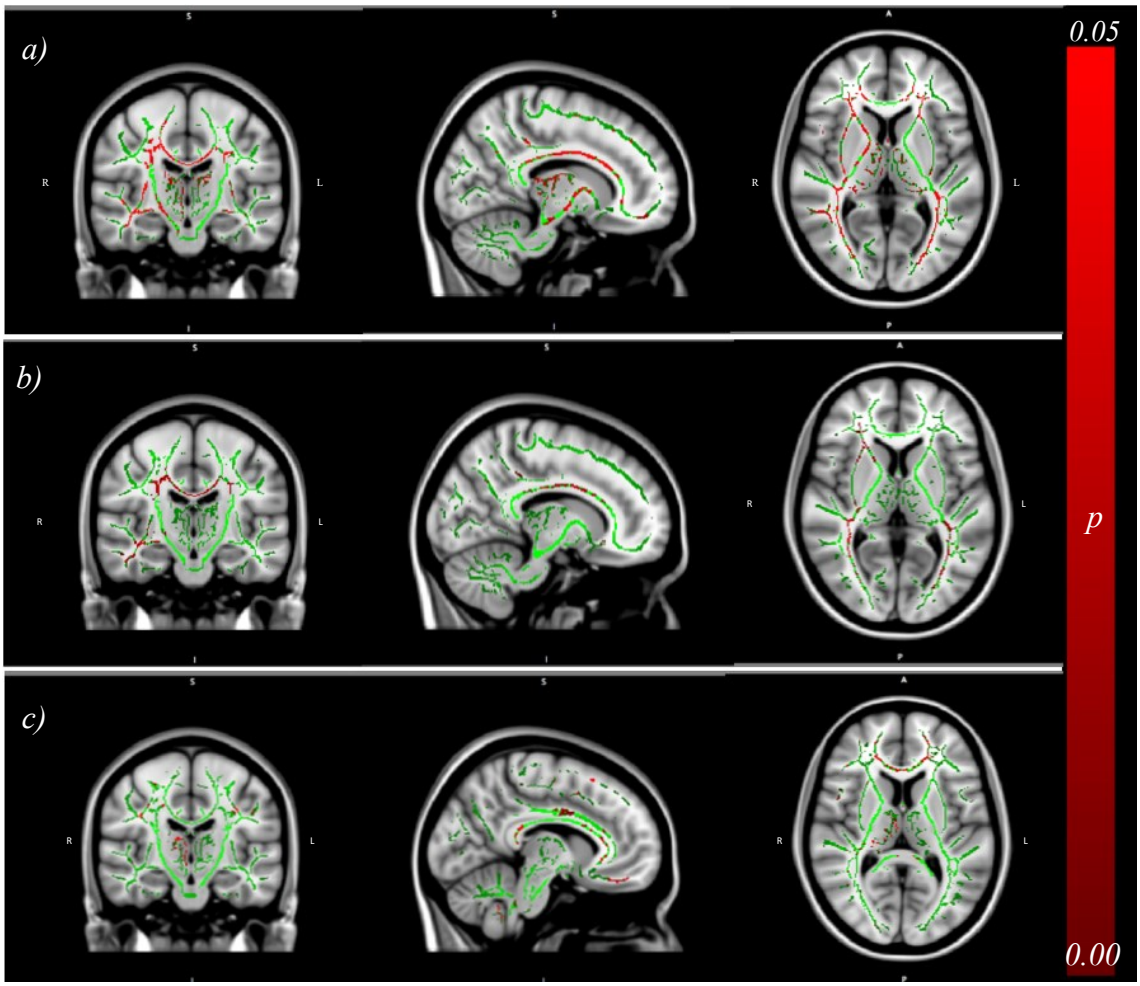

Figure 19. TBSS analysis shows a significant reduction ($p < 0.05$, FWE) in voxels extent with increased RD after 6 months of fingolimod treatment, compared to HC, where a) baseline imaging, b) imaging at 6 months. Repeated measures (image c) show the extent of voxels with significantly increased RD ($p < 0.05$, FWE uncorrected) at baseline imaging. The background image is a standard MNI152_T1_1mm template, the mean FA skeleton is shown in green. a, b: coronal slice is at X = 77, sagittal slice at Y = 109, axial slice at Z = 77; c: X = 98, Y = 109, Z = 81. Abbreviations: R, right; L, left; I, inferior; S, superior; A, anterior; P, posterior.

The repeated measures between baseline and follow up showed the 7.57 % extent of voxels with significantly increased RD ($p < 0.05$, FWE uncorrected) at baseline imaging, mainly located in cingulum, thalamus, genu and splenium of CC (Figure 19 c).

In addition, extent of voxels with increased MD lowered moderately from 24.6% to 20.7% ($p < 0.05$, FWE corrected) at baseline and follow up imaging respectively. Voxels with significantly increased MD, compared to HC were placed in splenium, genu, body of CC, superior longitudinal fasciculus, anterior and posterior thalamic radiation, superior corona radiata, corticospinal tract, thalamus, cingulum (hippocampus) and sagittal stratum (data not shown). Furthermore, axial diffusivity was increased in 16.8% of voxels ($p < 0.05$, FWE corrected) at baseline imaging, compared to healthy subjects. This number slightly increased to 19.1% at follow up imaging ($p < 0.05$, FWE corrected), with voxels placed in body, genu, splenium of CC, cingulum, anterior thalamic radiation, superior longitudinal fasciculus, sagittal stratum and all parts of corona radiata (data not shown).

Diffusion tensor imaging analysis was also performed in KADEPET-SPMS group, treated with natalizumab (n = 10). Six SPMS and four RRMS patients were imaged at the baseline and after 1 year of treatment initiation. No statistically significant differences for all DTI parameters (FA/MD/AD/RD) in the whole NAWM and segmented NAWM were found.

4.2.4 Lesion load affects DTI

Correlational analyses were performed between FA/MD/AD/RD values in each segmented WM and normalized lesion burden in corresponding WM region.

Lesion load (visible in T2 MRI sequence) in KADEPET-RRMS substudy was measured for 10 RRMS patients at baseline, normalized lesion burden was calculated according the method stated in chapter 3.2.1. Significant correlations between the normalized lesion burden and DTI parameters in the surrounding NAWM were found in three WM regions: temporal, cingulate and deep WM (Table 5).

Table 5. Correlations between lesion burden and DTI parameters in WM ROIs of 10 RRMS patients in KADEPET-RRMS group at baseline imaging, (expressed as p-values, Spearman rho). Statistically significant at the level $p < 0.05$.

	Lesion burden in segmented WM of RRMS patients (n = 10) at baseline imaging					
DTI parameter	Frontal	Parietal	Temporal	Occipital	Cingulate	Deep WM
FA	p = 0.31 rho = -0.35	p = 0.58 rho = -0.2	**p = 0.03** **rho = -0.70**	p = 0.104 rho = -0.55	**p = 0.002** **rho = -0.86**	p = 0.63 rho = -0.17
MD	p = 0.47 rho = 0.26	p = 0.279 rho = 0.38	**p = 0.01** **rho = 0.73**	p = 0.279 rho = 0.38	**p = 0.002** **rho = 0.86**	**p = 0.01** **rho = 0.75**
AD	**p = 0.01** **rho = 0.75**	p = 0.20 rho = 0.44	p = 0.6 rho = 0.18	p = 0.76 rho = 0.11	p = 0.29 rho = 0.37	**p = 0.049** **rho = 0.65**
RD	p = 0.22 rho = 0.42	p = 0.24 rho = 0.41	**p = 0.01** **rho = 0.77**	p = 0.16 rho = 0.48	**p = 0.004** **rho = 0.84**	**p = 0.01** **rho = 0.75**

T2 lesion load in KADEPET-SPMS substudy was measured at baseline imaging for 15 SPMS patients. Normalized lesion burden was correlated to corresponding DTI parameters in segmented WM regions. DTI parameters in the NAWM of all segmented WM regions showed association to lesion burden in the corresponding WM segments (Table 6).

Table 6. Correlations between lesion burden and DTI parameters in WM ROIs of SPMS patients (n = 15) in KADEPET-SPMS group at baseline imaging, (expressed as p-values, Spearman rho). Statistically significant at the level $p < 0.05$.

	Lesion burden in segmented WM of SPMS patients (n=15) at baseline imaging					
DTI parameter	Frontal	Parietal	Temporal	Occipital	Cingulate	Deep WM
FA	**p = 0.004** **rho = -0.7**	**p = 0.004** **rho = -0.71**	**p = 0.0005** **rho = -0.8**	**p = 0.001** **rho = -0.76**	**p < 2.2 e-16** **rho = -0.88**	**p = 0.01** **rho = -0.65**
MD	**p = 0.0095** **rho = 0.78**	p = 0.052 rho = 0.51	**p = 0.003** **rho = 0.72**	**p = 0.004** **rho = 0.70**	**p = 0.001** **rho = 0.77**	**p = 0.0006** **rho = 0.79**
AD	**p = 0.0001** **rho = 0.83**	p = 0.11 rho = 0.43	p = 0.052 rho = 0.51	p = 0.25 rho = 0.32	p = 0.10 rho = 0.44	**p = 0.037** **rho = 0.54**
RD	**p = 0.0005** **rho = 0.78**	**p = 0.02** **rho = 0.6**	**p = 0.002** **rho = 0.72**	**p = 0.0005** **rho = 0.78**	**p = 0.0002** **rho = 0.82**	**p = 0.0006** **rho = 0.79**

PROMS study also showed significant correlations between lesion burden in each of the segmented WM and NAWM diffusion parameters (Table 7).

Table 7. Correlations between lesion burden and DTI parameters in WM ROIs in PROMS group (n = 25) at baseline imaging, (expressed as p-values, Spearman rho). Statistically significant at the level $p < 0.05$.

	Lesion burden in segmented WM of RRMS patients, close to progression (n=25)					
DTI parameter	Frontal	Parietal	Temporal	Occipital	Cingulate	Deep WM
FA	p = 0.12 rho = -0.31	p = 0.06 rho = -0.37	**p = 0.002** **rho = -0.59**	**p = 0.02** **rho = -0.45**	**p = 0.003** **rho = -0.56**	**p = 0.01** **rho = -0.48**
MD	**p = 0.01** **rho = 0.46**	**p = 0.045** **rho = 0.40**	**p = 0.002** **rho = 0.58**	p = 0.07 rho = 0.36	**p = 0.003** **rho = 0.56**	**p = 0.003** **rho = 0.56**
AD	**p = 0.02** **rho = 0.45**	p = 0.048 rho = 0.40	**p = 0.004** **rho = 0.56**	p = 0.11 rho = 0.33	**p = 0.003** **rho = 0.57**	**p = 0.003** **rho = 0.57**
RD	**p = 0.03** **rho = 0.42**	**p = 0.026** **rho = 0.44**	**p = 0.001** **rho = 0.61**	**p = 0.04** **rho = 0.41**	**p = 0.006** **rho = 0.53**	**p = 0.006** **rho = 0.53**

4.3 PET/DTI correlational analyses

Correlational analyses of DTI parameters to TSPO radioligand binding were performed to evaluate structural and molecular brain changes and their relation to clinical disability in MS, using combined *in vivo* magnetic resonance (MR) and PET imaging in MS patients compared to healthy controls (HC).

4.3.1 Decreased tract integrity and increased microglial activation in NAWM is associated with disability

Correlational analyses of DTI parameters in NAWM to disability status, evaluated with EDSS, were done for the pooled cohort from three study groups (n = 55). The analysis showed association of decreased WM integrity to disability, more pronounced in SPMS patients (Figure 20).

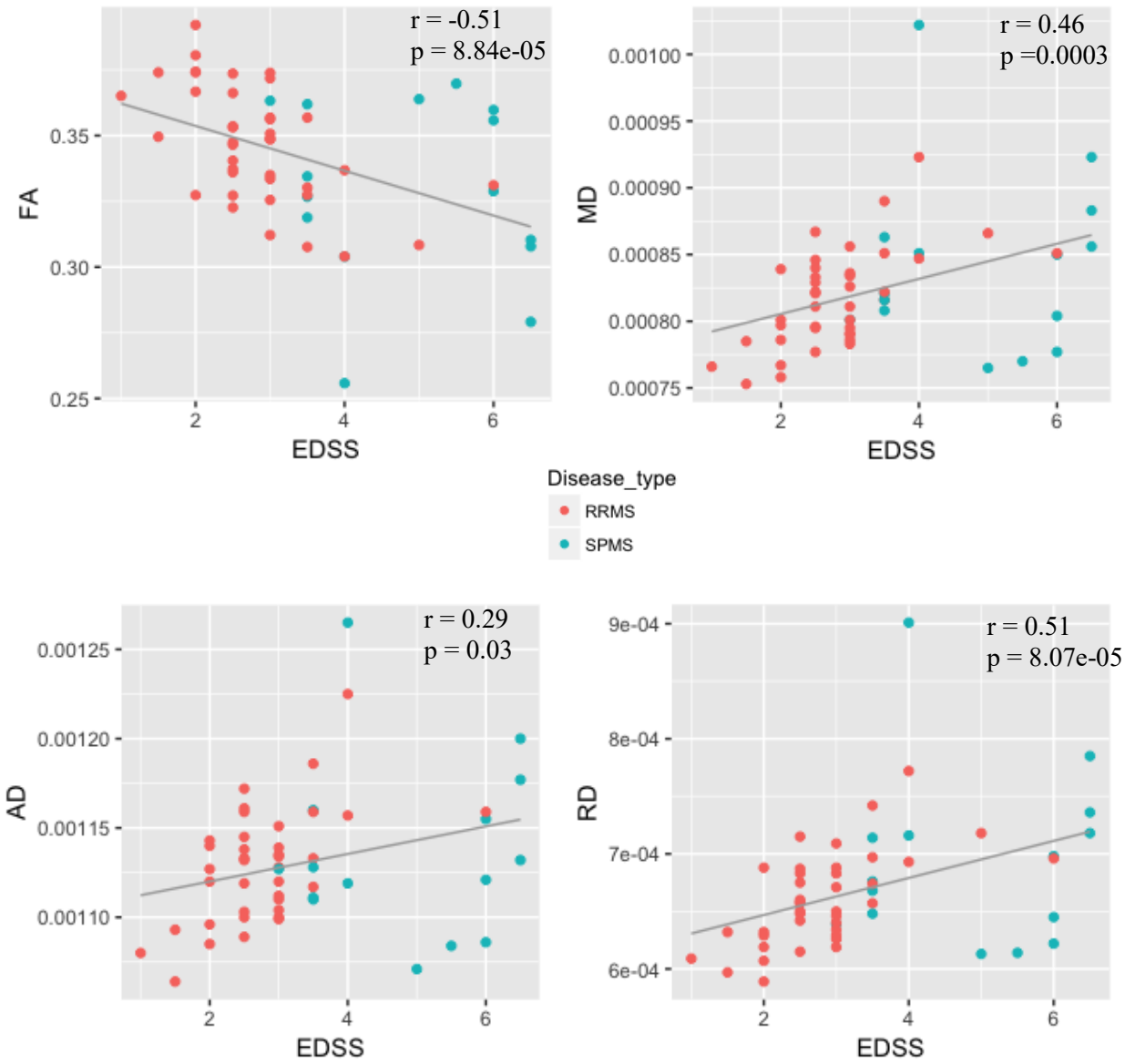

Figure 20. Correlation of diffusion parameters to disability in MS patients (n = 55). The correlations are visualized with linear regression lines and Spearman's rho. Corresponding Pearson coefficients are R = - 0.44 (p = 0.0007) for FA, R = 0.38 (p = 0.004) for MD, R = 0.28 (p = 0.03) for AD, R = 0.41 (p = 0.0002) for RD, statistically significant at the level of $p < 0.05$.

TSPO radioligand binding in NAWM was measured for 55 MS patients, with correlational analysis to evaluated with EDSS physical impairment. As a result, increased microglial activation in NAWM associated with higher clinical disability status in MS (Figure 21).

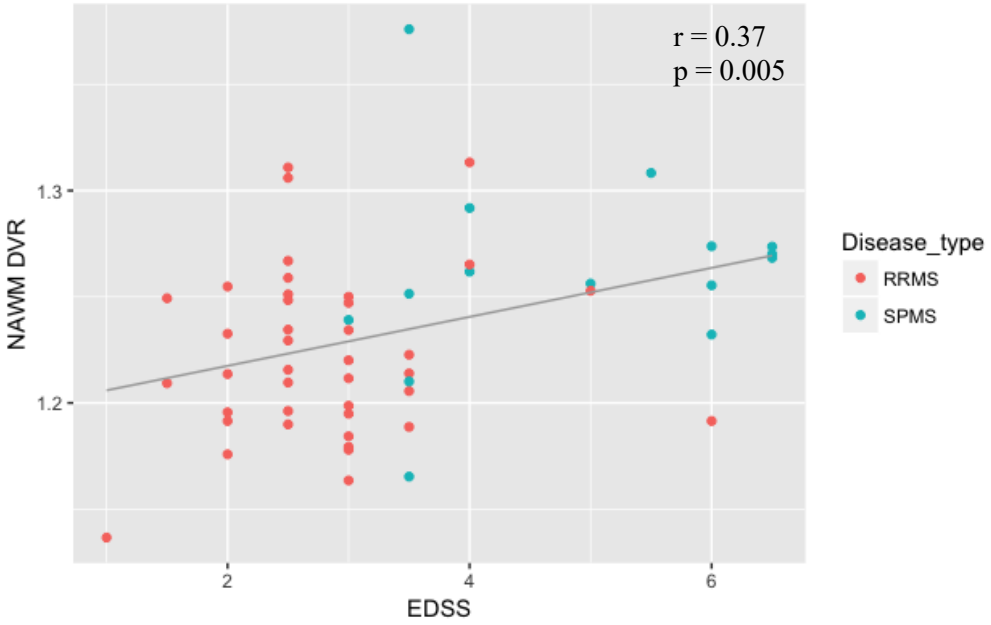

Figure 21. Correlation of TSPO radioligand binding in NAWM, expressed as DVR, to disability status scale of 55 MS patients. The correlation is visualized with linear regression line and Spearman's rho. Corresponding Pearson correlation is 0.36 ($p = 0.007$), statistically significant at the level of $p < 0.01$.

4.3.2 Increased microglial activation in NAWM is associated with structural white matter changes

Based on results from the previous section it was of interest to investigate the relation between the microglial activation and white matter integrity in MS patients. DTI analysis and TSPO-PET binding evaluation was performed in NAWM and segmented NAWM of 55 MS patients. Patients from KADEPET-RRMS and KADEPET-SPMS were included for the analysis at baseline imaging in absence of any treatment, while patients from PROMS study had different treatment at the baseline imaging.

Correlational analyses showed an association between microglial activation and structural abnormalities in NAWM of 55 MS patients (Figure 22). The correlational analyses were also performed in segmented NAWM (data not shown). The associations were found between all diffusion parameters (decreased FA and increased MD/AD/RD) and increased microglial activation in temporal WM ($p < 0.01$ for all Spearman correlations), and between decreased FA and increased TSPO-binding in deep WM ($p = 0.017$, Spearman's rho = - 0.32).

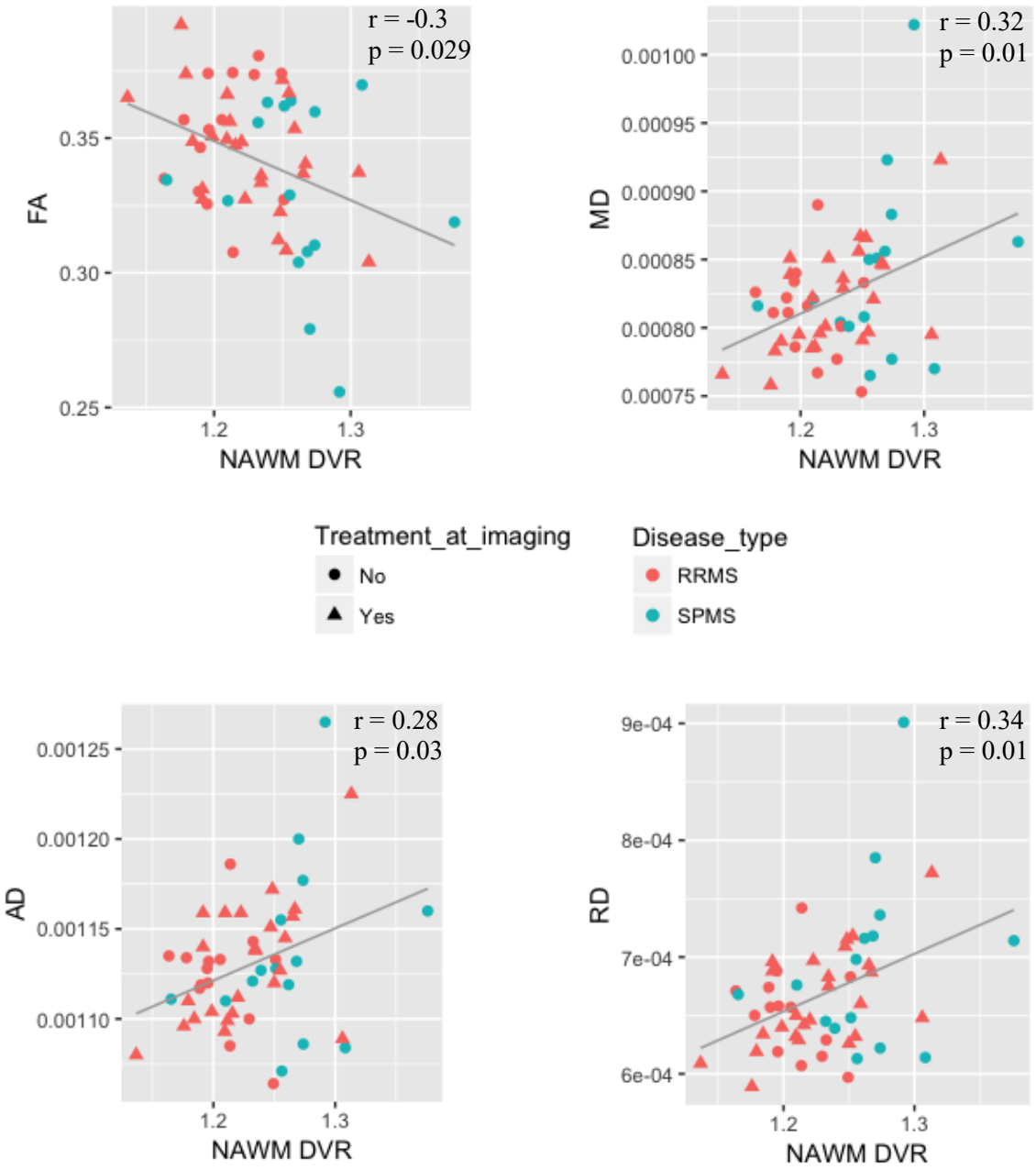

Figure 22. Reduced WM tract integrity is associated with increased TSPO binding in NAWM of 55 MS patients. TSPO radioligand binding expressed as DVR. The correlations are visualized with linear regression lines and Spearman's rho. Corresponding Pearson coefficients are R = - 0.36 (p = 0.007) for FA, R = 0.38 (p = 0.004) for MD, R = 0.34 (p = 0.01) for AD, R = 0.39 (p = 0.002) for RD, statistically significant at the level of $p < 0.05$.

The correlational analyses between DTI parameters and TSPO binding in segmented NAWM were also performed separately for groups with treatment at imaging (n = 45) and without treatment (n = 30). Correlational analyses between FA and TSPO binding in both treated and untreated pooled cohorts are shown in Figures 23, 25.

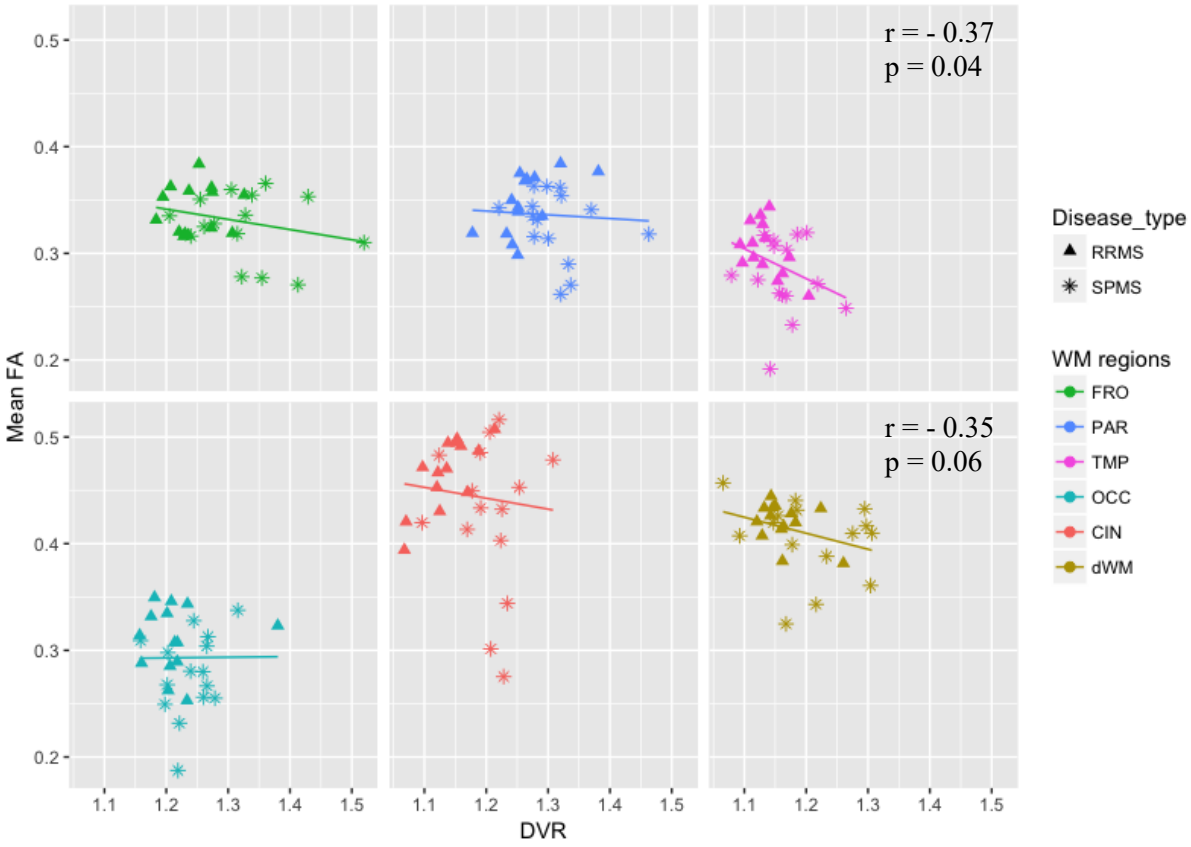

Figure 23. Increased microglial activation is associated with decreased fractional anisotropy in temporal (TMP) and deep WM (dWM) regions in MS patients without treatment at imaging (n = 30). The correlations are visualized with linear regression lines and Spearman's rho. Corresponding Pearson coefficients are R = - 0.33 (p = 0.07) for temporal WM, R = - 0.32 (p = 0.08) for deep WM.

Additionally, associations between increased mean and radial diffusivities and increased microglial activation were found in temporal WM in non-treated pooled cohort (p = 0.058, Spearman's rho = 0.35 for MD; p = 0.039, Spearman's rho = 0.38 for RD), data not shown.

SPMS patients (n = 15) showed higher microglial activation in four segmented WM regions: frontal, parietal, temporal and cingulate, compared to RRMS patients (n = 15), Figure 24.

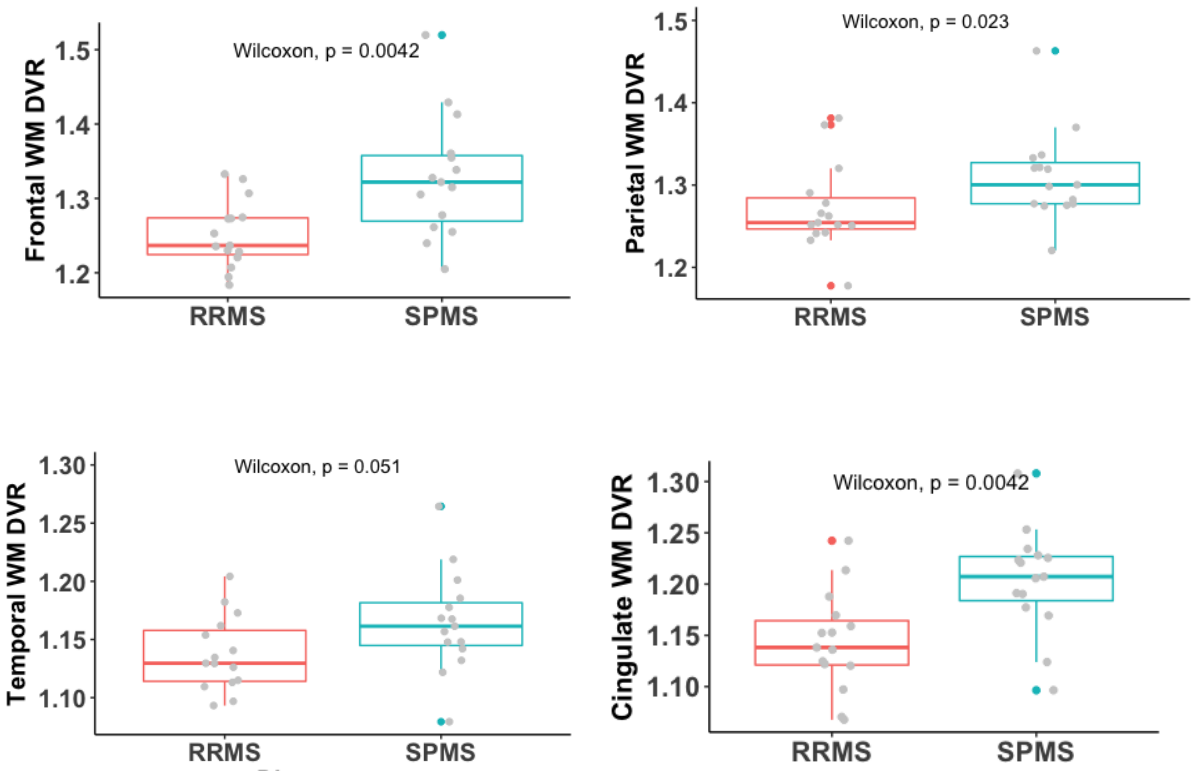

Figure 24. TSPO-binding increased in frontal, parietal, temporal and cingulate WM regions in SPMS (n = 15), compared to RRMS patients (n = 15) in pooled untreated cohort. Boxplots visualized with median values and Wilcoxon rank sum test, statistically significant at the level of $p < 0.05$.

The correlational analyses for patients with treatment at imaging showed significant negative correlation between FA and TSPO binding in parietal (PAR), temporal (TMP), occipital (OCC) and deep (dWM) WM regions (Figure 25).

In addition, positive correlations were found between increased MD/RD and TSPO binding in temporal and occipital WM regions in pooled cohort with treatment at imaging (data not shown). For mean diffusivity associations were found in temporal WM, ($p = 0.049$, $r = 0.29$), and in deep WM ($p = 0.052$, $r = 0.29$). Similarly, positive correlations were found for radial diffusivity in temporal and deep WM ($p = 0.052$, $r = 0.29$ and $p = 0.037$, $r = 0.31$ respectively). Correlations are expressed as p-values, Spearman rho and statistically significant at the level $p < 0.05$.

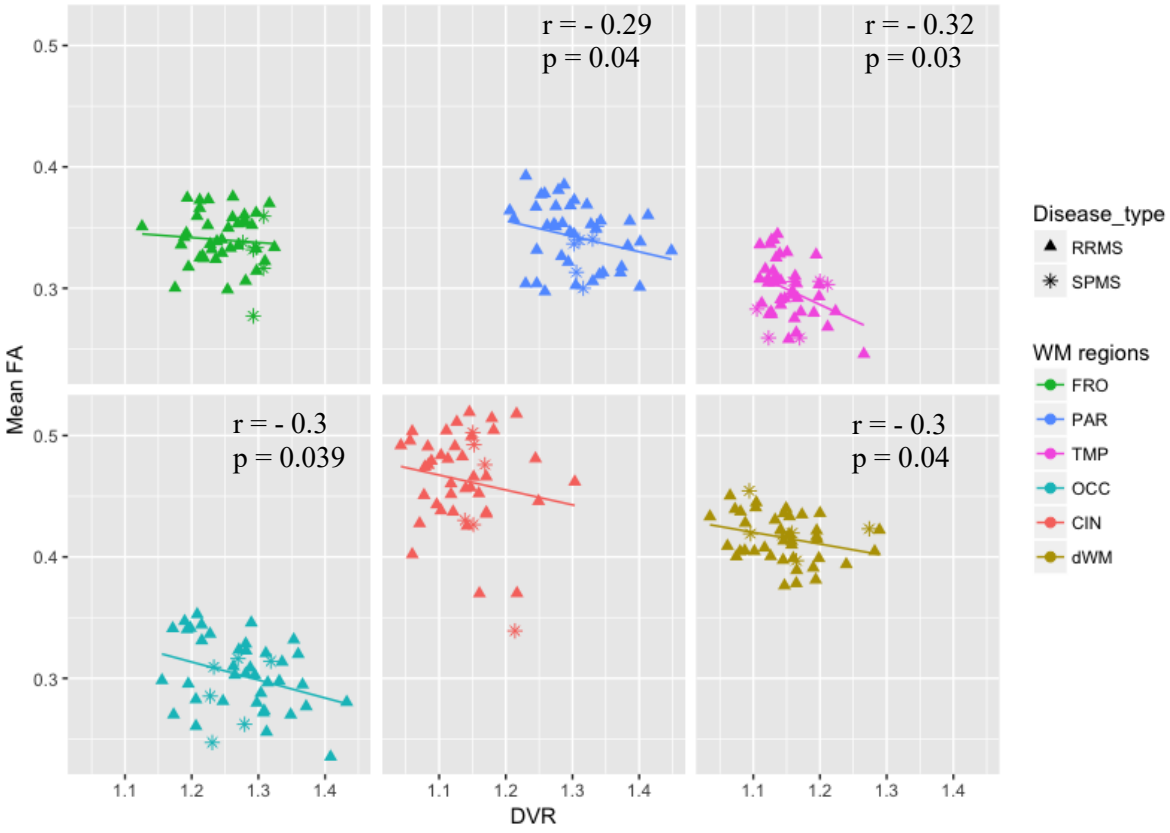

Figure 25. Increased microglial activation is associated with decreased fractional anisotropy in parietal, temporal, occipital and deep WM regions in MS patients with treatment at imaging (n = 45). The correlations are visualized with linear regression lines and Spearman's rho. Corresponding Pearson coefficients are R = - 0.27 (p = 0.07) for parietal WM, R = - 0.37 (p = 0.01) for temporal WM, R = - 0.33 (p = 0.02) for occipital WM and R = - 0.3 (p = 0.05) for deep WM.

4.3.3 Voxel-wise image analysis of PET/DTI data

Correlational groupwise analysis between FA values and TSPO binding in NAWM was performed at voxel level with FDR correction for multiple comparisons for pooled data of MS cohort (n = 54), one patient was excluded due to DTI data artifacts (Figure 26).

The voxel wise analysis showed wide spread focal areas of white matter, where decreased FA correlated significantly with increased TSPO binding as a sign of increased microglial activity. However, it was not feasible to perform corresponding correlational analyses among healthy controls for comparison due to low number of subjects in the control group (n =15).

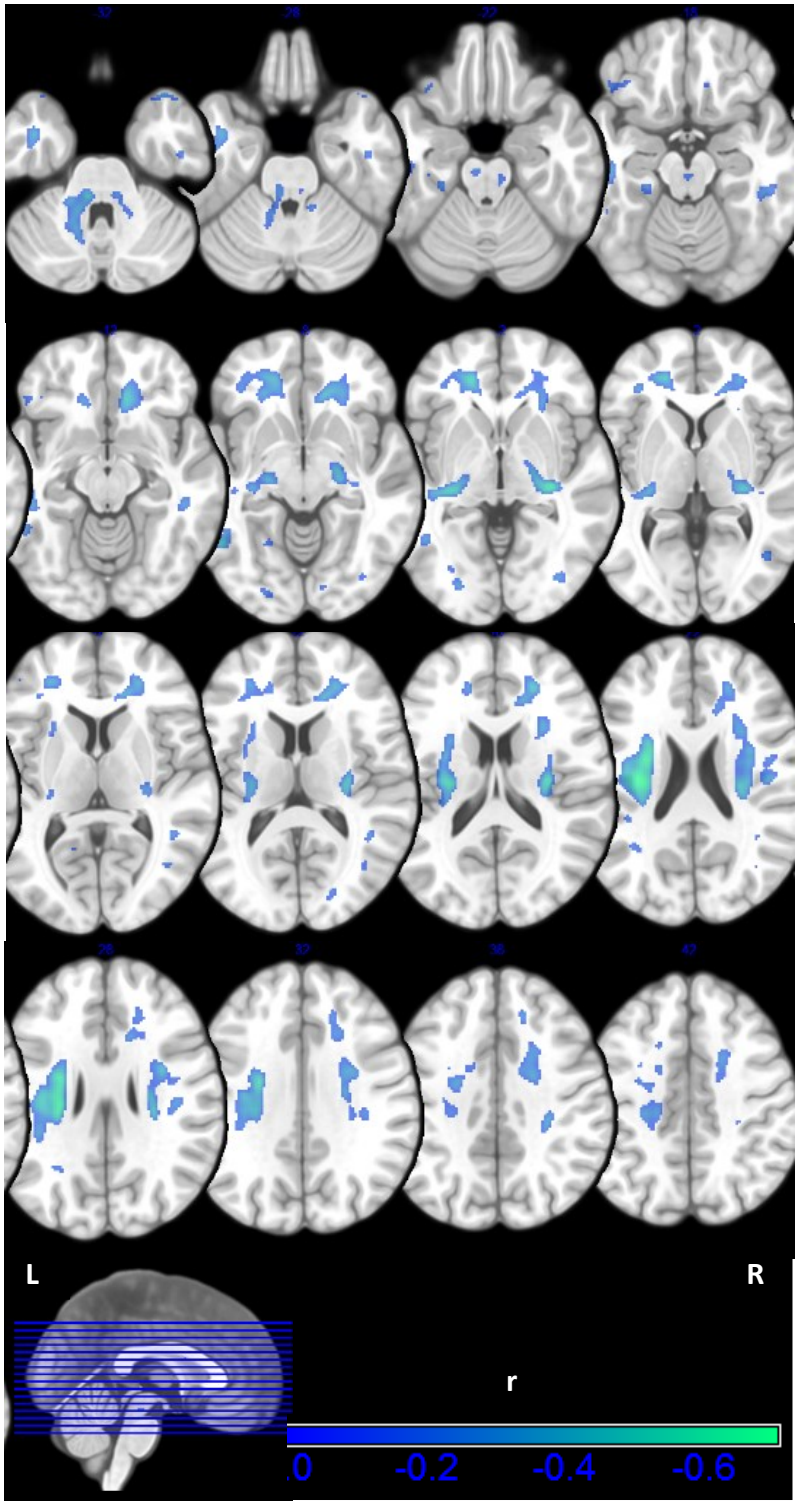

Figure 26. Decreased fractional anisotropy is associated with increased microglial activation in NAWM of pooled MS cohort (n = 54). Correlational voxel-wise analysis FDR corrected for multiple comparisons. Significant clusters were found within superior longitudinal fasciculus, corticospinal tract, cingulate gyrus, corona radiata and forceps minor, and also within thalamic radiation and thalamus, L = left, R = right.

5 DISCUSSION

5.1 Summary of the main findings

This study evaluated structural and molecular brain changes using combined MR and PET *in vivo* imaging techniques in 55 MS patients with both RRMS (n = 40) and SPMS (n = 15) disease types, compared to 15 healthy controls. Altered DTI parameters (decreased FA and increased MD, AD, RD) in NAWM and segmented NAWM (temporal, occipital, cingulate WM), with the most affected region being cingulate white matter, indicate on microstructural damage without visible changes in conventional MRI. Microstructural changes were more pronounced in SPMS than in RRMS patients. White matter disintegrity was also found in segmented WM (occipital, cingulate and deep WM) of patients at the age of risk for progression of the disease.

It was also investigated, whether the lesion load affects diffusion in regional NAWM. The cohort of SPMS patients showed the highest lesion burden with significant correlations to altered DTI parameters in all segmented WM regions. Lesion load extent was smaller in patients from PROMS study, compared to SPMS patients. RRMS patients, that are in the earlier disease stage (KADEPET-RRMS study), had the smallest lesion load extent.

Additionally, DTI showed a sensitivity to detect microstructural changes and change in diffusion within tracts after treatment initiation. The acquired diffusion parameters suggest structural improvement (increase in mean FA and decrease in mean RD values) in cingulate WM after 6 months of fingolimod treatment. TBSS voxel-wise analysis results also indicated on improvement of microstructural integrity after 6 months of Fingolimod treatment.

PET/DTI correlational analyses showed an association between decreased tract integrity and increased microglial activation in NAWM, which also associated with clinical disability.

5.2 Methodological considerations and data interpretation

The main methodological consideration for DTI analysis is in MRI sequence design, that ought to be suitable for each individual project. The MR imaging should be performed on same MRI scanner with identical protocol, with design optimization and MR imaging time does not exceed 1 hour. Short acquisition time helps to reduce possible head motion artifacts and contributes to patient's comfort. To reduce the scan and readout time, EPI and SENSE approaches can be utilized. The good compromise between acquisition time and image quality is DTI sequence with 30 - 64 gradients (Jones, 2004) and one b = 0 image acquired for each 5-10 high b-images (e.g. 1000s/mm^2). The spatial resolution is also important for DTI image quality, therefore 2-2.5 mm isotropic voxels are recommended (Soares et al., 2013).

Quality control and data preprocessing are another important steps in DTI analysis. Eddy current induced distortions and EPI susceptibility distortions, together with motion artefacts, signal dropouts and geometric deformations are potential artefacts in acquired DWI images. Thus, raw data have to be examined for potential artefacts and exclude the corrupted data or problematic gradients prior to tensor estimation. Several approaches e.g. Explore DTI RESTORE, or 3D Slicer software can be used for outliers' detection.

Diffusion tensor imaging showed sensitivity to detect microstructural changes in white matter of MS patients, appearing normal on conventional MRI. This methodology has been utilized in several MS studies (Kim et al., 2017; Roosendaal et al., 2009; Onu et al., 2012; Harrison et al., 2013; Ontaneda et al., 2017). DTI is an advantageous MRI technique: it can be a part of MRI imaging protocol, widely utilized in clinical routine, it is a non-radiative and safe imaging modality. Despite all positive aspects, DTI is rather an approximate technique, therefore the analysis results have to be interpreted carefully. DW-MRI measurements reflect the amount of water molecules diffusion within white matter tracts, that might be hindered by cell membrane, myelin sheath and cell cytoskeleton. The detection of water molecules movement is averaged over the voxel and restricted to movement along the axis of the applied gradient, therefore the interpretation of change in signal by tensor-derived measures can be ambiguous. It is known that water molecules movement along the main fiber orientation is reflected by axial diffusivity and represented by the principal eigenvalue of the tensor. Similarly, radial diffusivity describes the movement perpendicular to the fiber. The relation

between these two measures can be expressed as fractional anisotropy, therefore change in one of them e.g. decrease in myelination, that lead to increase in RD, should also reflect the change in FA (decrease in anisotropy in that case). All four parameters of the tensor are related to each other; therefore, it is inaccurate to draw conclusions about microstructural changes based only on one parameter change. All four tensor-derived parameters (FA/MD/AD/RD) should be used for precise interpretation of fiber microstructural architecture. Yet the complex axonal organization e.g. crossing fibers, fiber diameter and density might complicate the explication of DTI-derived metrics (Jones et al., 2013).

One of the diffusion tensor model drawbacks is in Gaussian assumption of anisotropic diffusion, that do not consider diffusion's directional dependence and axonal compartmentalization. To overcome the limitations of this model, other robust approaches have been proposed: high angular resolution diffusion imaging (HARDI), including diffusion kurtosis imaging (DKI) (Steven et al., 2014) and Q-ball imaging (Tuch, 2004), or previously mentioned NODDI and CHARMED models. These advanced DTI methods might improve the output of informative DTI metrics, precisely reflecting changes in axonal microstructure and underlying processes.

Methodological consideration of TBSS analysis is in failure of family-wise error correction for repeated measures. Direct comparison between baseline and follow up for all DTI parameters did not survive family-wise error correction for multiple comparisons. By applying a stringent p-value < 0.001, as recommended by (Woo et al., 2014), almost all significant voxels ($p < 0.05$, FWE uncorrected) were lost. Consequently, the repeated measures results obtained by TBSS have to be interpreted carefully.

Another main consideration of this study is in pooled cohort, included both 35 patients in absence of immunomodulatory treatment at the time of imaging (KADEPET-RRMS, n = 10, KADEPET-SPMS, n = 20, PROMS, n = 5) and also 20 patients who were on various DMTs (PROMS substudy). Because the patients from PROMS study are in the risk to SPMS conversion, disease modifying treatment at that stage of the disease can only suppress inflammatory cells migration into CNS, and reduce annualized relapse late, but likely not be able to significantly influence on WM structural integrity. Currently only three longitudinal studies, investigating fingolimod and natalizumab treatment effect on white matter structural changes with DTI analysis approach have

been published (Wiebenga et al., 2016; Senda et al., 2016; Gurevich et al., 2018). Since this study was a retrospectively performed pooling of existing data from different substudies with both DTI and TSPO imaging, carried out over the years, therefore the imaging data was a little heterogenous in DTI sequences (i.e. 33 gradient directions in KADEPET-SPMS study, compared to 64 gradient directions in other studies). However, the study by Lebel et al., 2012 did not observe statistically significant differences in FA and MD diffusion parameters in DTI data, performed with 30 and 60 gradient directions protocols. Unfortunately, it was not possible to make the study design beforehand, but this aspect would be taken into consideration for the future projects.

In addition, the main methodological consideration of TSPO-PET imaging is the inability to distinguish between M1 and M2 activated microglia phenotypes. Together with microglia, TSPO can be expressed by activated astrocytes and infiltrating mononuclear phagocytes. As an alternative to TSPO targeting radioligands, imaging with novel [^{11}C]SMW139 radioligand targeting P2X7 receptor, expressed by pro-inflammatory M1-type microglia, has been proposed (Janssen et al., 2018).

5.3 DTI in Multiple Sclerosis

The hypothesis on MS evolution states that progression results from chronic inflammation trapped within CNS, associated with spread demyelination and axonal injury, as a consequence of mitochondrial dysfunction, chronic microglial activation, extensive production of ROS and iron accumulation (Lassmann, 2018). Inflammation is seen in all stages of the disease in chronic active MS lesions and adjacent areas e.g. normal appearing white matter, with correlation between inflammation and axonal injury (Frischer et al., 2009). Therefore, it is of importance to reveal diffuse neuroinflammation and associated axonal damage in MS prior its progression phase. The technical ability of detecting hidden white matter changes will contribute to appropriate treatment planning and eventual prediction of disease progression.

Diffusion tensor imaging has been implemented in several MS studies, including *in vivo* (Natarajan et al., 2013; Harrison et al., 2011; Rashid et al., 2008; Rissanen et al., 2018; Harrison et al., 2013; Scanderbeg et al., 2000; Onu et al., 2012; Werring et al., 2001; Kim et al., 2017; Klistorner et al., 2015; Olsson et al., 2016; Ge et al., 2004), post mortem (Moll et al., 2011; Seewann et al., 2009) and longitudinal treatment studies

(Ontaneda et al., 2017; Fox et al., 2011; Wiebenga et al., 2016; Gurevich et al., 2018). It has been shown that MS patients have reduced FA in white matter appearing normal on cMRI, and increased radial diffusivity in the same regions (Roosendaal et al., 2009; Ciccarelli et al., 2001). Findings of these studies suggest structural WM damage and demyelination in several WM regions, including corpus callosum, inferior longitudinal fasciculus, left corona radiata and optic radiation, with relation to disability and cognitive impairment. This study agrees with previously reported findings, with TBSS analysis identified white matter damage (decreased FA and increased RD) in identical brain regions of MS patients.

Increased averaged water diffusion coefficient has been found in secondary-progressive lesions, compared to lesions in RRMS phase in study by Scanderbeg et al., 2000, that correlated with EDSS and disease duration. Additionally, increased ADC was found in lesions and perilesional NAWM in study by Werring, 2000, therefore supporting the hypothesis of lesions cause structural damage to adjacent normal appearing white matter. Similarly, this study showed an association between lesion load and DTI parameters alteration (increased diffusivities and decreased fractional anisotropy), that may potentially explain that lesions can produce damage and axonal disintegration to contralateral NAWM regions, that agrees with previously published literature.

Two previously published studies, involving 1 year fingolimod and natalizumab longitudinal treatment (Gurevich et al., 2018; Wiebenga et al., 2016), showed a sensitivity of DTI analysis to detect improvement in tracts' microstructural integrity. Similarly, diffusion tensor imaging analysis implemented in this study demonstrated an ability to detect the changes in diffusion within tracts after 6 months Fingolimod treatment. Despite the complexity in interpretation of TBSS repeated measures analysis, results obtained by quantitative ROI analyses and voxel-wise analysis with comparison to HC may indicate on improvement in microstructural white matter integrity in RRMS patients after 6 months of fingolimod treatment with concomitantly unchanged cMRI parameters. This indicates, that DTI could be used as a sensitive imaging biomarker in longitudinal studies to evaluate treatment response in NAWM of MS patients *in vivo.*

In addition, DTI analysis showed sensitivity in detection of white matter structural alterations in progressive MS patients and in patients with risk of progression, therefore it can be used as a sensitive tool in predicting disease progression.

5.3.1 Cingulum bundle and WM structural alteration

DTI analysis in each study group showed significant change in DTI parameters in cingulate WM region. The cingulum bundle situated in the brain midline, on the peripheral surface of the CC and runs from the frontal lobe around the rostrum and genu of the corpus callosum, envelops ventrally around the splenium, continuing to the parahippocampal gyrus (Figure 27).

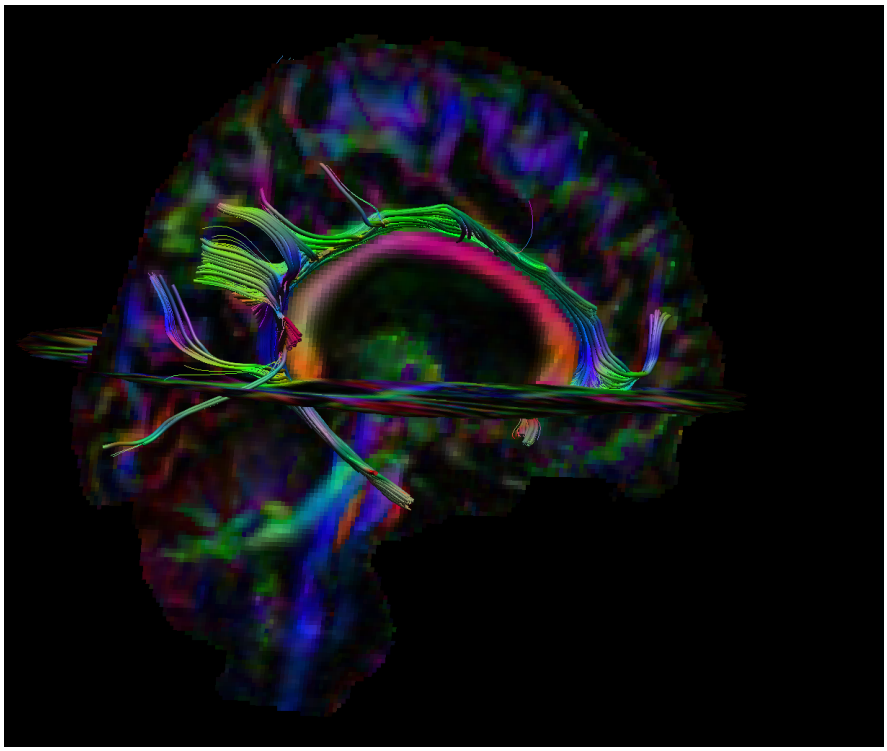

Figure 27. Tractography of the right cingulum bundle, sagittal view.

However, the parcellation method used was not very precise anatomically, as it assigned the rostral part of the corpus callosum, including rostrum, genu, splenium and isthmus of CC (Figure 28, white arrow) to cingulate WM area (Figure 28, shown in green).

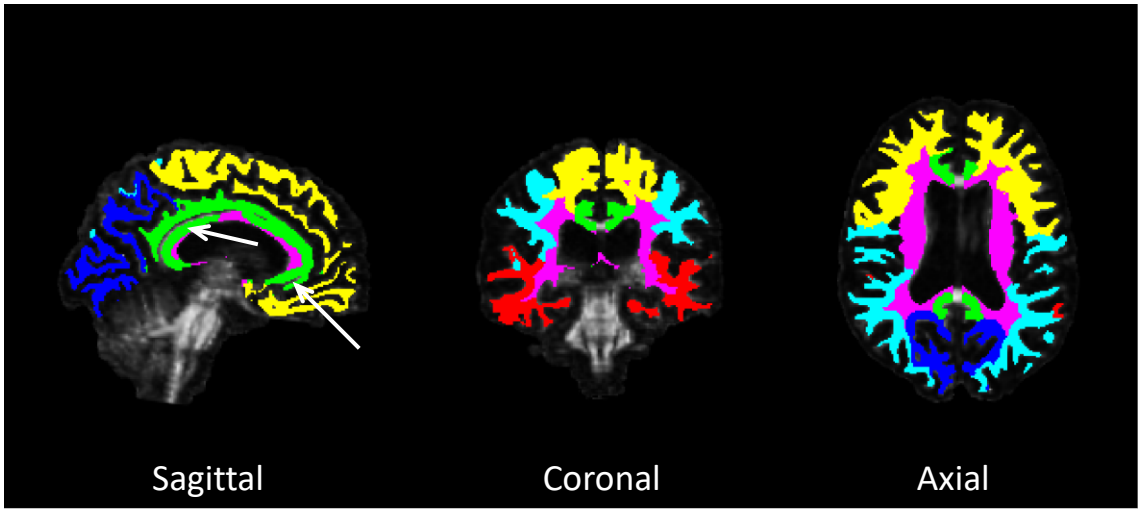

Figure 28. WM segmentation: frontal WM (yellow), parietal WM (blue), temporal WM (red), occipital WM (dark blue), cingulate WM (green), deep WM (purple).

Therefore, when interpreting mean values change in cingulate WM, we might have to consider that this area partially includes CC. It is important to note, TBSS analysis showed most of the voxels with significantly altered DTI metrics placed in callosal area.

Another reason of cingulate WM being the most affected is the high lesion burden within and around corpus callosum and adjacent to it periventricular area. The majority of the lesions in pooled MS patients' cohort located in the deep WM area (Figure 28, shown in purple), including the lateral part of the corpus callosum (Figure 28, white arrow) and periventricular area. Several studies showed correlation between regional lesion load and DTI metrics of the corresponding regions in corpus callosum (Simon et al., 2000; Ciccarelli et al., 2003). The propagation of structural changes can be potentially explained by fiber connectivity and spreading of smouldering plaques with activated microglia along the tracts. Callosal fibers connect frontal, parietal and occipital cerebral lobes, while cingulum bundle has connections with frontal, parietal and medial temporal lobe, including anterior and lateral dorsal thalamic nuclei (Bubb et al., 2018). The evidence of MS pathology involvement in the limbic system, that include the cingulum bundle, and high frequency of lesions throughout the limbic tracts has been reported previously (Sahin et al., 2016). It supports the hypothesis that focal lesions can cause the transection of axons and lead to Wallerian degeneration, resulting in axonal injury and loss in CC and adjacent WM areas.

Additionally, few studies demonstrated thalamic involvement in MS, with evidence of FA reduction in thalamus (Mesaros et al., 2011; Deppe et al., 2016) that may predict disease evolution and may contribute to cognitive decline and disability in MS. The common hypothesis is that focal lesions in thalamocortical projections can damage surrounding WM, therefore leading to thalamus atrophy and neuronal loss (Minagar et al., 2013; Vercellino et al., 2009). Results of the voxel-wise correlational analysis in this study demonstrated DTI pathology (reduced FA) in thalami and thalamic radiation of 55 MS patients, associated with increased microglial activation, and therefore support the results in previously published literature on thalamic involvement in MS.

In chapters 4.2.1- 4.2.2 we can follow the disease evolution in the different substudies, starting from the KADEPET-RRMS study patients with average disease duration of 8

years, who have been detected with structural changes in cingulate WM and callosal area, whereas RRMS patients with more advanced disease from PROMS substudy with mean disease duration of 13.6 years showed structural alterations in three WM regions: deep, cingulate and occipital WM. SPMS patients from KADEPET-SPMS study with mean time from disease onset of 15 years showed significantly decreased white matter integrity in the whole NAWM and in segmented temporal, occipital, and cingulate WM, compared to healthy controls. As expected, the lesion load in RRMS patients was smaller, than in patients at progressive stage of the disease. It has been speculated, whether the spread diffuse WM pathology, appearing normal in conventional MRI, associates with increased lesion load (Werring, 2000; Vrenken et al., 2006). The acquired results may indicate on relation between lesions extent and degree of widespread diffuse pathology, that in turn disrupt the diffusion within white matter tracts. Results in chapter 4.2.4 corroborate the hypothesis of influence of distant lesions to cause Wallerian degeneration and contribute to microstructural changes throughout MS evolution (Ciccarelli et al., 2003; Klistorner et al., 2015).

5.4 Increased microglial activation and axonal disintegrity in NAWM as a disease predictor

Previous study from our research group showed correlation between increased [^{11}C]PK11195 binding and reduced FA in NAWM and in the perilesional area of gadolinium-negative black holes of MS cohort included 9 SPMS and 10 RRMS patients (Rissanen, 2015). This study showed positive correlation between increased microglial activation and reduced FA in non-lesional WM, and negative correlations between high TSPO-binding and increased diffusivities in NAWM of MS cohort, included 40 RRMS and 15 SPMS subjects. This finding supports the hypothesis of association between chronic microglial activation and diffuse axonal inflammation and damage of brain white matter, appearing normal on cMRI.

In 4.3.2 the correlational analyses showed association between increased microglial activation and decreased FA in segmented NAWM in pooled cohorts with and without treatment at imaging. Analysis in the treated group showed four WM regions with significant negative correlations between FA and NAWM DVR, that can be explained by the bigger group size (n = 45), compared to the size of untreated group (n = 30). Moreover, there was only 6 SPMS patients in the first group, therefore less variability in

FA and DVR values, compared to quite heterogenous FA/DVR values in untreated group, included 15 SPMS patients.

Several studies, performed with *in vivo* TSPO-PET imaging, have revealed significantly increased TSPO uptake in NAWM of SPMS patients, compared to HC. RRMS patients have demonstrated moderate TSPO radioligand binding, compared to patients who are in progressive disease stage (Rissanen et al., 2014; Debruyne et al., 2003; Giannetti et al., 2015). TSPO-binding was significantly increased (results are shown in chapter 4.3.2) in segmented NAWM of SPMS patients (n = 15), compared to RRMS patients (n = 15), that supports the hypothesis of widespread microglial activation in NAWM during progressive MS phase, and agrees with the previously published literature.

Additionally, TSPO-PET imaging has been proposed as a prognostic marker for MS progression, with several studies demonstrated an association between high TSPO-uptake and faster disease progression, brain atrophy and disability (Rissanen et al., 2018; Politis et al., 2012; reviewed in Airas et al., 2018). Similarly, this study found the correlation between microglial activation and axonal disintegrity in NAWM of MS patients, with association to disability. This finding supports the potential of PET imaging to visualize hidden neuroinflammation in MS patients *in vivo* to monitor disease progression.

5.5 Combination of complementary techniques in MS imaging

To my best knowledge, this is the first study evaluating diffuse structural and biological (or pathological) changes in MS, utilizing DTI and PET complimentary imaging modalities, and performed in a large pooled cohort (n = 55) with comparison to healthy subjects (n = 15).

Multimodal brain imaging from the same individual has recently become a prospective candidate in the neuroimaging field, and certainly has a great potential in the future. Combination of complementary neuroimaging modalities allows a comprehensive examination of brain structure and its function *in vivo*. Application of DTI and PET imaging modalities for imaging of hidden neuroinflammation has revealed new insights on the complexity of the MS disease.

The consolidation of advanced multimodal imaging techniques and increasing understanding of the MS mechanism allows to follow-up thoroughly the disease

evolution and outcome of treatment methods, as well as to discover novel therapeutic targets and imaging probes. In addition to PET molecular probes targeting mitochondrial translocator protein for detection and monitoring of microglial and astrocyte activation, novel PET imaging probes targeting myelin, nitric oxide synthase (iNOS), cannabinoid (CB2), adenosine 2A and P2X7 receptors have been proposed (reviewed in Högel et al., 2018). As an additional example of novel molecular probe, detection of excessive iron accumulation in MS brain tissue, as a direct sign of neurodegeneration is possible with application of MRI and quantitative susceptibility mapping (Stüber et al., 2016), while biomarkers associated with neuroinflammation, neurofilament light (Nfl) and glial fibrillary acidic protein (GFAP) can be detected in blood serum of MS patients using the single molecule array (Simoa) technology (Housley et al., 2015). Novel drug validation tool as a "disease-in-a-dish" using iPSC (induced pluripotent stem cells) of MS patients will contribute to development of personalised medicine therapeutic approach (Sayed et al., 2016). By accelerating the neuroimaging solutions and application of multimodal imaging probes, researchers can find a full concept of brain in disease and pave the path to effective MS treatment.

6 CONCLUSIONS

This study provides data on associations of DTI findings and measurement of microglia activation in the NAWM of MS patients, and their dependence on the disease subtype. These results help to gain access to further investigations of WM diffuse pathological patterns revealing more accurate MS pathogenesis. It was evaluated whether diffusion tensor imaging can be an extension to conventional MRI protocol in assessing MS disease activity, applied in combination with TSPO PET imaging.

Future implementations of the study might be beneficial in revealing associations between fiber connectivity and the spreading of smoldering lesions with activated microglia. Combination of complimentary techniques such as DTI and PET imaging might be used as a tool for predicting disease progression in MS patients.

7 ACKNOLEDGMENTS

This study was conducted in Turku PET Centre under the mentorship of Professor Dr. Laura Airas and Dr. Eero Rissanen. I would like to express my deepest gratitude to my supervisors for giving the opportunity to join the research group, for giving motivation and encouragement throughout the last year. Without their patient guidance, valuable support and assistance in keeping my progress on schedule it would not be possible to conduct this project.

I would like to thank my group members: Jouni Tuisku for providing the scripts, giving advices and helping with voxelwise analysis, and Markus Matilainen, who kindly assisted me with the statistical analysis. I would like also to mention other colleagues and thank Anna Vuorimaa, Marjo Nylund, Susanne Vainio, Heidi Högel, Imran Waggan, Eero Polvinen, Marcus Sucksdorff and Francisco Lopez Picon, with whom I have had a great pleasure to work and share a company at ECTRIMS congress in Berlin and other events outside Turku PET Centre.

I wish to acknowledge a friendship that began in Turku, and to say thanks to my friend Ciaran for helping not letting me give up, for all laughs and adventures we had.

I am also thankful to my best friends - Julia and Marina, who were always believing in me and encouraging to follow my dreams. I am forever thankful to Enzo for all love and support, positive mood, messages and phone calls, and for always being with me “in my pocket”, when we were separated by 2500 km distance.

Finally, I wish to thank my parents –Vladimir and Svetlana, who have always been an example of greatest love for me. I dedicate this thesis to my mother who left us 11.09.2004 after a long battle with MS.

Svetlana Bezukladova

September 2018, Turku

8 REFERENCES

Airas, L., M. Nylund, and E. Rissanen. 2018. Evaluation of microglial activation in multiple sclerosis patients using positron emission tomography. *Front. Neurol.* 9:1–10. doi:10.3389/fneur.2018.00181.

Alexander, A.L., J.E. Lee, M. Lazar, and A.S. Field. 2007. Diffusion tensor imaging of the brain. *Neurotherapeutics*. 4:316–29. doi:10.1016/j.nurt.2007.05.011.

Amit, B., F. Lama, F. Boli, D.P. J., R. Aja, G. Christine, C.P. A., W. Emmanuelle, H.S. L., Z. Jiameng, and S.C. H. 2010. Abnormal B-cell cytokine responses a trigger of T-cell–mediated disease in MS? *Ann. Neurol.* 67:452–461. doi:10.1002/ana.21939.

Assaf, Y., and P.J. Basser. 2005. Composite hindered and restricted model of diffusion (CHARMED) MR imaging of the human brain. *Neuroimage*. 27:48–58. doi:10.1016/j.neuroimage.2005.03.042.

Baecher-Allan, C., B.J. Kaskow, and H.L. Weiner. 2018. Multiple Sclerosis: Mechanisms and Immunotherapy. *Neuron*. 97:742–768. doi:10.1016/j.neuron.2018.01.021.

Banati, R.B. 2002. Visualising microglial activation in vivo. *Glia*. 40:206–217. doi:10.1002/glia.10144.

Baranzini, S.E., and J.R. Oksenberg. 2017. The Genetics of Multiple Sclerosis: From 0 to 200 in 50 Years. *Trends Genet.* 33:960–970. doi:10.1016/j.tig.2017.09.004.

Barbara, S., R. Barbara, M. Roberta, S. Egidio, and A. Francesca. 2006. Detection of Ectopic B-cell Follicles with Germinal Centers in the Meninges of Patients with Secondary Progressive Multiple Sclerosis. *Brain Pathol.* 14:164–174. doi:10.1111/j.1750-3639.2004.tb00049.x.

Bergamaschi, R. 2007. Prognostic Factors in Multiple Sclerosis. *Int. Rev. Neurobiol.* 79:423–447. doi:10.1016/S0074-7742(07)79019-0.

Le Bihan, D., J.F. Mangin, C. Poupon, C. a Clark, S. Pappata, N. Molko, and H. Chabriat. 2001. Diffusion tensor imaging: concepts and applications. *J. Magn. Reson. Imaging*. 13:534–46. doi:10.1002/jmri.1076.

Bloomgren, G., S. Richman, C. Hotermans, M. Subramanyam, S. Goelz, A. Natarajan, S. Lee, T. Plavina, J. V. Scanlon, A. Sandrock, and C. Bozic. 2012. Risk of Natalizumab-Associated Progressive Multifocal Leukoencephalopathy. *N. Engl. J. Med.* 366:1870–1880. doi:10.1056/NEJMoa1107829.

Boche, D., V.H. Perry, and J.A.R. Nicoll. 2013. Review: Activation patterns of microglia and their identification in the human brain. *Neuropathol. Appl. Neurobiol.* 39:3–18. doi:10.1111/nan.12011.

Bogie, J.F.J., P. Stinissen, and J.J.A. Hendriks. 2014. Macrophage subsets and microglia in multiple sclerosis. *Acta Neuropathol.* 128:191–213. doi:10.1007/s00401-014-1310-2.

Browne, P., D. Chandraratna, C. Angood, H. Tremlett, C. Baker, B. V. Taylor, and A.J. Thompson. 2014. Atlas of multiple sclerosis 2013: A growing global problem with widespread inequity. *Neurology*. 83:1022–1024. doi:10.1212/WNL.0000000000000768.

Bubb, E.J., C. Metzler-baddeley, and J.P. Aggleton. 2018. The cingulum bundle : Anatomy ,

function , and dysfunction. *Neurosci. Biobehav. Rev.* 92:104–127.

Cadavid, D., S. Jurgensen, and S. Lee. 2013. Impact of Natalizumab on Ambulatory Improvement in Secondary Progressive and Disabled Relapsing-Remitting Multiple Sclerosis. *PLoS One*. 8. doi:10.1371/journal.pone.0053297.

Castriota-Scanderbeg, A., F. Fasano, G. Hagberg, U. Nocentini, M. Filippi, and C. Caltagirone. 2003. Coefficient Dav is more sensitive than fractional anisotropy in monitoring progression of irreversible tissue damage in focal nonactive multiple sclerosis lesions. *Am. J. Neuroradiol.* 24:663–670.

Cerami, C., L. Iaccarino, and D. Perani. 2017. Molecular imaging of neuroinflammation in neurodegenerative dementias: The role of in vivo PET imaging. *Int. J. Mol. Sci.* 18. doi:10.3390/ijms18050993.

Chang, L.C., D.K. Jones, and C. Pierpaoli. 2005. RESTORE: Robust estimation of tensors by outlier rejection. *Magn. Reson. Med.* 53:1088–1095. doi:10.1002/mrm.20426.

Chen, M.-K., and T.R. Guilarte. 2006. Imaging the Peripheral Benzodiazepine Receptor Response in Central Nervous System Demyelination and Remyelination. *Toxicol. Sci.* 91:532–539. doi:10.1093/toxsci/kfj172.

Chun, J., and H.P. Hartung. 2010. Mechanism of action of oral fingolimod (FTY720) in multiple sclerosis. *Clin. Neuropharmacol.* 33:91–101. doi:10.1097/WNF.0b013e3181cbf825.

Ciccarelli, O., D.J. Werring, G.J. Barker, C.M. Griffin, C.A.M. Wheeler-Kingshott, D.H. Miller, and A.J. Thompson. 2003. A study of the mechanisms of normal-appearing white matter damage in multiple sclerosis using diffusion tensor imaging: Evidence of Wallerian degeneration. *J. Neurol.* 250:287–292. doi:10.1007/s00415-003-0992-5.

Ciccarelli, O., D.J. Werring, G.J. Barker, A.J. Thompson, and D.H. Miller. 2001. Investigation of MS normal-appearing brain using diffusion tensor MRI with clinical correlations. *Neurology*. 56:926–933.

De Coene, B., J. V. Hajnal, P. Gatehouse, D. Longmore, S.J. White, A. Oatridge, J.M. Pennock, ian R. Young, and G.M. Bydder. 1992. MR of the Brain Using Fluid-Attenuated Inversion Recovery (FLAIR) Pulse Sequences. *Am. J. Neuroradiol.* 13:1555–1564. doi:10.1007/BF00588360.

Colasanti, A., Q. Guo, N. Muhlert, P. Giannetti, M. Onega, R.D. Newbould, O. Ciccarelli, S. Rison, C. Thomas, R. Nicholas, P.A. Muraro, O. Malik, D.R. Owen, P. Piccini, R.N. Gunn, E.A. Rabiner, and P.M. Matthews. 2014. In Vivo Assessment of Brain White Matter Inflammation in Multiple Sclerosis with 18F-PBR111 PET. *J. Nucl. Med.* 55:1112–1118. doi:10.2967/jnumed.113.135129.

Correale, J. 2014. The role of microglial activation in disease progression. *Mult. Scler.* 20:1288–1295. doi:10.1177/1352458514533230.

Cosenza-nashat, M., M. Zhao, H. Suh, J. Morgan, S. Morgello, S.C. Lee, and A. Einstein. 2009. Expression of the TSPO of 18kDa by microglia, macrophages and astrocytes based on immunohistochemical localization in abnormal human brain. 35:306–328. doi:10.1111/j.1365-2990.2008.01006.x.Expression.

Costello, K., J. Halper, R. Kalb, L. Skutnik, and R. Rapp. 2014. The Use of Disease-Modifying Therapies in Multiple Sclerosis, Principles and Current Evidence: A Consensus Paper by

the Multiple Sclerosis Coalition. 72 pp.

Dal-Bianco, A., G. Grabner, C. Kronnerwetter, M. Weber, R. Höftberger, T. Berger, E. Auff, F. Leutmezer, S. Trattnig, H. Lassmann, F. Bagnato, and S. Hametner. 2017. Slow expansion of multiple sclerosis iron rim lesions: pathology and 7 T magnetic resonance imaging. *Acta Neuropathol.* 133:25–42. doi:10.1007/s00401-016-1636-z.

Debruyne, J.C., J. Versijpt, K.J. Van Laere, F. De Vos, J. Keppens, K. Strijckmans, E. Achten, G. Slegers, R.A. Dierckx, J. Korf, and J.L. De Reuck. 2003. Pet visualization of microglia in multiple sclerosis patients using [11C]PK11195. *Eur. J. Neurol.* 10:257–264. doi:10.1046/j.1468-1331.2003.00571.x.

Deppe, M., J. Krämer, J.G. Tenberge, J. Marinell, W. Schwindt, K. Deppe, S. Groppa, H. Wiendl, and S.G. Meuth. 2016. Early silent microstructural degeneration and atrophy of the thalamocortical network in multiple sclerosis. *Hum. Brain Mapp.* 37:1866–1879. doi:10.1002/hbm.23144.

Dev, K.K., F. Mullershausen, H. Mattes, R.R. Kuhn, G. Bilbe, D. Hoyer, and A. Mir. 2008. Brain sphingosine-1-phosphate receptors: Implication for FTY720 in the treatment of multiple sclerosis. *Pharmacol. Ther.* 117:77–93. doi:10.1016/j.pharmthera.2007.08.005.

Dillman, J.R., J.H. Ellis, R.H. Cohan, P.J. Strouse, and S.C. Jan. 2007. Frequency and severity of acute allergic-like reactions to gadolinium-containing IV contrast media in children and adults. *Am. J. Roentgenol.* 189:1533–1538. doi:10.2214/AJR.07.2554.

Dupont, A.-C., B. Largeau, M. Santiago Ribeiro, D. Guilloteau, C. Tronel, and N. Arlicot. 2017. Translocator Protein-18 kDa (TSPO) Positron Emission Tomography (PET) Imaging and Its Clinical Impact in Neurodegenerative Diseases. *Int. J. Mol. Sci.* 18:785. doi:10.3390/ijms18040785.

Filippi, M. 2000. Enhanced magnetic resonance imaging in multiple sclerosis. *Mult. Scler.* 6:320–326. doi:10.1177/135245850000600505.

Filippi, M., and M.A. Rocca. 2007. Conventional MRI in multiple sclerosis. *J. Neuroimaging*. 17:3–9. doi:10.1111/j.1552-6569.2007.00129.x.

Fox, R.J., T. Cronin, J. Lin, X. Wang, K. Sakaie, D. Ontaneda, S.Y. Mahmoud, M.J. Lowe, and M.D. Phillips. 2011. Measuring myelin repair and axonal loss with diffusion tensor imaging. *Am. J. Neuroradiol.* 32:85–91. doi:10.3174/ajnr.A2238.

Fragata, I., M. Alves, A.L. Papoila, A.P. Nunes, P. Ferreira, N. Canto-Moreira, and P. Canhaõ. 2017. Early Prediction of Delayed Ischemia and Functional Outcome in Acute Subarachnoid Hemorrhage: Role of Diffusion Tensor Imaging. *Stroke*. doi:10.1161/STROKEAHA.117.016811.

Friese, M.A., B. Schattling, and L. Fugger. 2014. Mechanisms of neurodegeneration and axonal dysfunction in multiple sclerosis. *Nat. Rev. Neurol.* 10:225–238. doi:10.1038/nrneurol.2014.37.

Frischer, J.M., S. Bramow, A. Dal-Bianco, C.F. Lucchinetti, H. Rauschka, M. Schmidbauer, H. Laursen, P.S. Sorensen, and H. Lassmann. 2009. The relation between inflammation and neurodegeneration in multiple sclerosis brains. *Brain*. 132:1175–1189. doi:10.1093/brain/awp070.

Frischer, J.M., S.D. Weigand, Y. Guo, N. Kale, J.E. Parisi, I. Pirko, J. Mandrekar, S. Bramow, M. Imke, W. Bruck, H. Lassmann, and C.F. Lucchinetti. 2015. Clinical and Pathological

Insights into the Dynamic Nature of the White Matter Multiple Sclerosis Plaque. *Ann Neurol*. 78:710–721. doi:doi:10.1002/ana.24497.

Gajofatto, A., M. Turatti, S. Monaco, and M.D. Benedetti. 2015. Clinical efficacy, safety, and tolerability of fingolimod for the treatment of relapsing-remitting multiple sclerosis. *Drug. Healthc. Patient Saf.* 7:157–167. doi:10.2147/DHPS.S69640.

Ge, Y., M. Law, G. Johnson, J. Herbert, J.S. Babb, L.J. Mannon, and R.I. Grossman. 2004. Preferential occult injury of corpus callosum in multiple sclerosis measured by diffusion tensor imaging. *J. Magn. Reson. Imaging*. 20:1–7. doi:10.1002/jmri.20083.

Giannetti, P., M. Politis, P. Su, F.E. Turkheimer, O. Malik, S. Keihaninejad, K. Wu, A. Waldman, R. Reynolds, R. Nicholas, and P. Piccini. 2015. Increased PK11195-PET binding in normal-appearing white matter in clinically isolated syndrome. *Brain*. 138:110–119. doi:10.1093/brain/awu331.

Gillen, K.M., M. Mubarak, T.D. Nguyen, and D. Pitt. 2018. Significance and In Vivo Detection of Iron-Laden Microglia in White Matter Multiple Sclerosis Lesions. *Front. Immunol.* 9:255. doi:10.3389/fimmu.2018.00255.

Goldenberg, M.M. 2012. Multiple sclerosis review. *P T*. 37:175–84. doi:https://www.ncbi.nlm.nih.gov/pmc/articles/PMC3351877/.

Gulyás, B., E. Pavlova, P. Kása, K. Gulya, L. Bakota, S. Várszegi, É. Keller, M.C. Horváth, S. Nag, I. Hermecz, K. Magyar, and C. Halldin. 2011. Activated MAO-B in the brain of alzheimer patients, demonstrated by [11C]-l-deprenyl using whole hemisphere autoradiography. *Neurochem. Int.* 58:60–68. doi:10.1016/j.neuint.2010.10.013.

Gunn, R.N., A.A. Lammertsma, and V.J. Cunningham. 1997. Parametric Imaging of Ligand-Receptor Binding in PET Using a Simplified Reference Region Model. *Neuroimage*. 6:279–287.

Gurevich, M., R. Waknin, E. Stone, and A. Achiron. 2018. Fingolimod-improved axonal and myelin integrity of white matter tracts associated with multiple sclerosis-related functional impairments. *CNS Neurosci. Ther.* 24:412–419. doi:10.1111/cns.12796.

Guy, C., and D. Ffytche. 2005. An introduction to the principles of medical imaging. Revised ed. D. ffytche, editor. Imperial College Press, London. 420 pp.

Hagmann, P., L. Jonasson, P. Maeder, J.-P. Thiran, V.J. Wedeen, and R. Meuli. 2006. Understanding Diffusion MR Imaging Techniques: From Scalar Diffusion-weighted Imaging to Diffusion Tensor Imaging and Beyond. *RadioGraphics*. 26:205–223. doi:10.1148/rg.26si065510.

Haider, L., C. Simeonidou, G. Steinberger, S. Hametner, N. Grigoriadis, G. Deretzi, G.G. Kovacs, A. Kutzelnigg, H. Lassmann, and J.M. Frischer. 2014. Multiple sclerosis deep grey matter: The relation between demyelination, neurodegeneration, inflammation and iron. *J. Neurol. Neurosurg. Psychiatry*. 85:1386–1395. doi:10.1136/jnnp-2014-307712.

Harrison, D.M., B. Caffo, N. Shiee, J. Farrell, P.-L. Bazin, S. Farrell, J. Ratchford, P. Calabresi, and D. Reich. 2011. Longitudinal changes in diffusion tensor – based quantitative MRI in multiple sclerosis. *Neurology*. 76:179–186. doi:http://dx.doi.org/10.1212/WNL.0b013e318206ca61.

Harrison, D.M., N. Shiee, P.-L. Bazin, S.D. Newsome, J.N. Ratchford, D. Pham, P.A. Calabresi, and D.S. Reich. 2013. Tract-specific quantitative MRI better correlates with disability than

conventional MRI in multiple sclerosis. *J. Neurol.* 260:397–406. doi:10.1007/s00415-012-6638-8.

Hartung, H.-P., D. Arnold, M. Freedman, E. Havrdova, D. Jeffery, R. Kapoor, A. Miller, F. Sellebjerg, H. Li, N. Lucas, D. Cadavid, N. Campbell, P.-R. Ho, and D. Steiner. 2017. ASCEND Phase 3 Trial Open-Label Extension Study Results: Natalizumab May Delay Disability Progression in Secondary Progressive Multiple Sclerosis (SPMS) (P5.330). *Neurology*. 88.

Hemmer, B., M. Kerschensteiner, and T. Korn. 2015. Role of the innate and adaptive immune responses in the course of multiple sclerosis. *Lancet Neurol.* 14:406–419. doi:10.1016/S1474-4422(14)70305-9.

Högel, H., E. Rissanen, A. Vuorimaa, and L. Airas. 2018. Positron emission tomography imaging in evaluation of MS pathology in vivo. 1–14. doi:10.1177/1352458518791680.

Housley, W.J., D. Pitt, and D.A. Hafler. 2015. Biomarkers in multiple sclerosis. *Clin. Immunol.* 161:51–58. doi:10.1016/j.clim.2015.06.015.

Howell, O.W., C.A. Reeves, R. Nicholas, D. Carassiti, B. Radotra, S.M. Gentleman, B. Serafini, F. Aloisi, F. Roncaroli, R. Magliozzi, and R. Reynolds. 2011. Meningeal inflammation is widespread and linked to cortical pathology in multiple sclerosis. *Brain*. 134:2755–2771. doi:10.1093/brain/awr182.

Hulkower, M.B., D.B. Poliak, S.B. Rosenbaum, M.E. Zimmerman, and M.L. Lipton. 2013. A decade of DTI in traumatic brain injury: 10 years and 100 articles later. *Am. J. Neuroradiol.* doi:10.3174/ajnr.A3395.

Janssen, B., D.J. Vugts, S.M. Wilkinson, D. Ory, S. Chalon, J.J.M. Hoozemans, R.C. Schuit, W. Beaino, E.J.M. Kooijman, J. Van Den Hoek, M. Chishty, A. Doméné, A. Van Der Perren, A. Villa, A. Maggi, G.T. Molenaar, U. Funke, R. V. Shevchenko, V. Baekelandt, G. Bormans, A.A. Lammertsma, M. Kassiou, and A.D. Windhorst. 2018. Identification of the allosteric P2X7receptor antagonist [11C]SMW139 as a PET tracer of microglial activation. *Sci. Rep.* 8:1–10. doi:10.1038/s41598-018-24814-0.

John F.Kurtzke. 1983. Rating neurologic impairment in multiple sclerosis: An expanded disability status scale(EDSS). *Neurology*. 33:1444. doi:10.1212/WNL.33.11.1444.

Jones, D.K. 2004. The Effect of Gradient Sampling Schemes on Measures Derived from Diffusion Tensor MRI: A Monte Carlo Study. *Magn. Reson. Med.* 51:807–815. doi:10.1002/mrm.20033.

Jones, D.K., T.R. Knösche, and R. Turner. 2013. White matter integrity, fiber count, and other fallacies: The do's and don'ts of diffusion MRI. *Neuroimage*. 73:239–254. doi:10.1016/j.neuroimage.2012.06.081.

Kannan, S., B. Balakrishnan, O. Muzik, R. Romero, and D. Chugani. 2009. Positron emission tomography imaging of neuroinflammation. *J Child Neurol*. 24:1190–1199. doi:10.1177/0883073809338063.

Kim, N.W., I.M. Chung, Y.S. Won, J. Lee, and J.G. Arnold. 2017. Diffusion tensor imaging of normal-appearing white matter in patients with neuromyelitis optica spectrum disorder and multiple sclerosis. *Eur. J. Neurol.* 24:1–55. doi:10.1111/ene.13321.

Klistorner, A., N. Vootakuru, C. Wang, C. Yiannikas, S.L. Graham, J. Parratt, R. Garrick, N. Levin, L. Masters, J. Lagopoulos, and M.H. Barnett. 2015. Decoding diffusivity in

multiple sclerosis: Analysis of optic radiation lesional and non-lesional white matter. *PLoS One*. 10:1–23. doi:10.1371/journal.pone.0122114.

Klistorner, A., C. Wang, V. Fofanova, M.H. Barnett, C. Yiannikas, J. Parratt, Y. You, and S.L. Graham. 2016. Diffusivity in multiple sclerosis lesions: At the cutting edge? *NeuroImage Clin.* 12:219–226. doi:10.1016/j.nicl.2016.07.003.

Kobayashi, M., T. Jiang, S. Telu, S.S. Zoghbi, R.N. Gunn, E.A. Rabiner, D.R. Owen, Q. Guo, V.W. Pike, R.B. Innis, and M. Fujita. 2018. 11C-DPA-713 has much greater specific binding to translocator protein 18 kDa (TSPO) in human brain than11C-(R)-PK11195. *J. Cereb. Blood Flow Metab.* 38:393–403. doi:10.1177/0271678X17699223.

Koch, M., E. Kingwell, P. Rieckmann, H. Tremlett, and U.M.C. UBC MS Clinic Neurologists. 2010. The natural history of secondary progressive multiple sclerosis. *J. Neurol. Neurosurg. Psychiatry*. 81:1039–43. doi:10.1136/jnnp.2010.208173.

Kočovská, E., F. Gaughran, A. Krivoy, and U.-C. Meier. 2017. Vitamin-D Deficiency As a Potential Environmental Risk Factor in Multiple Sclerosis, Schizophrenia, and Autism. *Front. psychiatry*. 8:47. doi:10.3389/fpsyt.2017.00047.

Kutzelnigg, A., C.F. Lucchinetti, C. Stadelmann, W. Brück, H. Rauschka, M. Bergmann, M. Schmidbauer, J.E. Parisi, and H. Lassmann. 2005. Cortical demyelination and diffuse white matter injury in multiple sclerosis. *Brain*. 128:2705–2712. doi:10.1093/brain/awh641.

Lassmann, H. 2018. Multiple sclerosis pathology. *Cold Spring Harb. Perspect. Med.* 8:1–16. doi:10.1101/cshperspect.a028936.

Lassmann, H., W. Brück, and C. Lucchinetti. 2001. Heterogeneity of multiple sclerosis pathogenesis: Implications for diagnosis and therapy. *Trends Mol. Med.* 7:115–121. doi:10.1016/S1471-4914(00)01909-2.

Lavisse, S., M. Guillermier, A.-S. Herard, F. Petit, M. Delahaye, N. Van Camp, L. Ben Haim, V. Lebon, P. Remy, F. Dolle, T. Delzescaux, G. Bonvento, P. Hantraye, and C. Escartin. 2012. Reactive Astrocytes Overexpress TSPO and Are Detected by TSPO Positron Emission Tomography Imaging. *J. Neurosci.* 32:10809–10818. doi:10.1523/JNEUROSCI.1487-12.2012.

Lebel, C., T. Benner, and C. Beaulieu. 2012. Six is enough? Comparison of diffusion parameters measured using six or more diffusion-encoding gradient directions with deterministic tractography. *Magn. Reson. Med.* 68:474–483. doi:10.1002/mrm.23254.

Leemans, A., and D.K. Jones. 2009. The B-matrix must be rotated when correcting for subject motion in DTI data. *Magn. Reson. Med.* 61:1336–1349. doi:10.1002/mrm.21890.

Leray, E., J. Yaouanq, E. Le Page, M. Coustans, D. Laplaud, J. Oger, and G. Edan. 2010. Evidence for a two-stage disability progression in multiple sclerosis. *Brain*. 133:1900–1913. doi:10.1093/brain/awq076.

Li, X., P.S. Morgan, J. Ashburner, J. Smith, and C. Rorden. 2016. The first step for neuroimaging data analysis: DICOM to NIfTI conversion. *J. Neurosci. Methods*. 264:47–56. doi:10.1016/j.jneumeth.2016.03.001.

Liu, G.J., R.J. Middleton, C.R. Hatty, W.W.Y. Kam, R. Chan, T. Pham, M. Harrison-Brown, E. Dodson, K. Veale, and R.B. Banati. 2014. The 18 kDa translocator protein, microglia and neuroinflammation. *Brain Pathol.* 24:631–653. doi:10.1111/bpa.12196.

Logan, J., J.S. Fowler, N.D. Volkow, A.P. Wolf, S.L. Dewey, D.J. Schlyer, R.R. Macgregor, R. Hitzemann, B. Bendriem, S.J. Gatley, and D.R. Christman. 1990. Graphical Analysis of Reversible Radioligand Binding from Time-Activity Measurements Applied to [N-11C-methyl]-(-)-Cocaine PET Studies in Human Subjects. *J. Cereb. Blood Flow Metab.* 10:740–747.

Logan, J., J.S. Fowler, G.-J. Wang, Y.-S. Ding, and D.L. Alexoff. 1996. Distribution Volume Ratios Without Blood Sampling from Graphical Analysis of PET Data. *J. Cereb. Blood Flow Metab.* 16:834–840.

Magliozzi, R., O. Howell, A. Vora, B. Serafini, R. Nicholas, M. Puopolo, R. Reynolds, and F. Aloisi. 2007. Meningeal B-cell follicles in secondary progressive multiple sclerosis associate with early onset of disease and severe cortical pathology. *Brain*. 130:1089–1104. doi:10.1093/brain/awm038.

Mazziotta, J., A. Toga, A. Evans, P. Fox, J. Lancaster, K. Zilles, R. Woods, T. Paus, G. Simpson, B. Pike, C. Holmes, L. Collins, P. Thompson, D. MacDonald, M. Iacoboni, T. Schormann, K. Amunts, N. Palomero-Gallagher, S. Geyer, L. Parsons, K. Narr, N. Kabani, G.L. Goualher, D. Boomsma, T. Cannon, R. Kawashima, and B. Mazoyer. 2001. A probabilistic atlas and reference system for the human brain: International Consortium for Brain Mapping (ICBM). *Philos. Trans. R. Soc. B Biol. Sci.* 356:1293–1322. doi:10.1098/rstb.2001.0915.

McCormack, P.L. 2013. Natalizumab: A review of its use in the management of relapsing-remitting multiple sclerosis. *Drugs*. 73:1463–1481. doi:10.1007/s40265-013-0102-7.

Mesaros, S., M.A. Rocca, E. Pagani, M.P. Sormani, M. Petrolini, G. Comi, and M. Filippi. 2011. Thalamic damage predicts the evolution of primary-progressive multiple sclerosis at 5 years. *Am. J. Neuroradiol.* 32:1016–1020. doi:10.3174/ajnr.A2430.

Mikita, J., N. Dubourdieu-Cassagno, M.S. Deloire, A. Vekris, M. Biran, G. Raffard, B. Brochet, M.H. Canron, J.M. Franconi, C. Boiziau, and K.G. Petry. 2011. Altered M1/M2 activation patterns of monocytes in severe relapsing experimental rat model of multiple sclerosis. Amelioration of clinical status by M2 activated monocyte administration. *Mult. Scler. J.* 17:2–15. doi:10.1177/1352458510379243.

Miller, D.H., D.T. Chard, and O. Ciccarelli. 2012. Clinically isolated syndromes. *Lancet. Neurol.* 11:157–69. doi:10.1016/S1474-4422(11)70274-5.

Miller, D.H., O.A. Khan, W.A. Sheremata, L.D. Blumhardt, G.P.A. Rice, M.A. Libonati, A.J. Willmer-Hulme, C.M. Dalton, K.A. Miszkiel, and P.W. O'Connor. 2003. A Controlled Trial of Natalizumab for Relapsing Multiple Sclerosis. *N. Engl. J. Med.* 348:15–23. doi:10.1056/NEJMoa020696.

Miller, P.W., N.J. Long, R. Vilar, and A.D. Gee. 2008. Imaging Methods Synthesis of 11 C , 18 F , 15 O , and 13 N Radiolabels for Positron Emission Tomography. *Angew. Chem. Int.* 47:8998–9033. doi:10.1002/anie.200800222.

Minagar, A., M.H. Barnett, R.H.B. Benedict, D. Pelletier, I. Pirko, M.A. Sahraian, E. Frohman, and R. Zivadinov. 2013. The thalamus and multiple sclerosis: Modern views on pathologic, imaging, and clinical aspects. *Neurology*. 80:210–219. doi:10.1212/WNL.0b013e31827b910b.

Moehle, M.S., and A.B. West. 2015. M1 and M2 immune activation in Parkinson's Disease: Foe and ally? *Neuroscience*. doi:10.1016/j.neuroscience.2014.11.018.

Moll, N.M., A.M. Rietsch, S. Thomas, A.J. Ransohoff, J.C. Lee, R. Fox, A. Chang, R.M. Ransohoff, and E. Fisher. 2011. Multiple sclerosis normal-appearing white matter: Pathology-imaging correlations. *Ann. Neurol.* 70:764–773. doi:10.1002/ana.22521.

Mori, S. 2007. Principle of diffusion tensor imaging. *In* Introduction to Diffusion Tensor Imaging. Elsevier B.V. 33–40.

Mosher, K.I., and T. Wyss-Coray. 2014. Microglial dysfunction in brain aging and Alzheimer's disease. *Biochem. Pharmacol.* doi:10.1016/j.bcp.2014.01.008.

Nandu, H., P. Y.Wen, and R. Y.Huang. 2018. Imaging in neuro-oncology. *Ther Adv Neurol Disord*. 11:1–19. doi:https://doi.org/10.1177/1756286.

Natarajan, R., S. Hagman, X. Wu, U. Hakulinen, M. Raunio, M. Helminen, M. Rossi, P. Dastidar, and I. Elovaara. 2013. Diffusion Tensor Imaging in NAWM and NADGM in MS and CIS: Association with Candidate Biomarkers in Sera. *Mult. Scler. Int.* doi:10.1155/2013/265259.

O'Gorman, C., R. Lucas, and B. Taylor. 2012. Environmental risk factors for multiple sclerosis: A review with a focus on molecular mechanisms. *Int. J. Mol. Sci.* 13:11718–11752. doi:10.3390/ijms130911718.

Oguz, I., M. Farzinfar, J. Matsui, F. Budin, Z. Liu, G. Gerig, H.J. Johnson, and M. Styner. 2014. DTIPrep: quality control of diffusion-weighted images. *Front. Neuroinform.* 8:1–11. doi:10.3389/fninf.2014.00004.

Olsson, T., L.F. Barcellos, and L. Alfredsson. 2016. Interactions between genetic, lifestyle and environmental risk factors for multiple sclerosis. *Nat. Rev. Neurol.* 13:26–36. doi:10.1038/nrneurol.2016.187.

Ontaneda, X.D., X.K. Sakaie, X.J. Lin, X.X.-F. Wang, X.M.J. Lowe, X.M.D. Phillips, and X.R.J. Fox. 2017. Measuring Brain Tissue Integrity during 4 Years Using Diffusion Tensor Imaging. *AJNR Am J Neuroradiol*. 38:31–38. doi:10.3174/ajnr.A4946.

Onu, M., A. Roceanu, U. Sboto-Frankenstein, R. Bendic, E. Tarta, F. Preoteasa, and O. Bajenaru. 2012. Diffusion abnormality maps in demyelinating disease: Correlations with clinical scores. *Eur. J. Radiol.* 81:e386–e391. doi:10.1016/j.ejrad.2011.12.014.

Pacheco, R., F. Contreras, and C. Prado. 2012. Cells, Molecules and Mechanisms Involved in the Neuro-Immune Interaction. *In* Cell Interaction. S.J.T. Gowder, editor. IntechOpen. 139–166.

Paling, D., B.S. Solanky, F. Riemer, D.J. Tozer, C.A.M. Wheeler-Kingshott, R. Kapoor, X. Golay, and D.H. Miller. 2013. Sodium accumulation is associated with disability and a progressive course in multiple sclerosis. *Brain*. 136:2305–2317. doi:10.1093/brain/awt149.

Papadopoulos, V., M. Baraldi, T.R. Guilarte, T.B. Knudsen, J.J. Lacapère, P. Lindemann, M.D. Norenberg, D. Nutt, A. Weizman, M.R. Zhang, and M. Gavish. 2006. Translocator protein (18 kDa): new nomenclature for the peripheral-type benzodiazepine receptor based on its structure and molecular function. *Trends Pharmacol. Sci.* 27:402–409. doi:10.1016/j.tips.2006.06.005.

Piehl, F., C. Holmén, J. Hillert, and T. Olsson. 2011. Swedish natalizumab (Tysabri) multiple sclerosis surveillance study. *Neurol. Sci.* 31:289–293. doi:10.1007/s10072-010-0345-y.

Politis, M., P. Giannetti, P. Su, F. Turkheimer, S. Keihaninejad, K. Wu, A. Waldman, O. Malik,

P.M. Matthews, R. Reynolds, R. Nicholas, and P. Piccini. 2012. Increased PK11195 PET binding in the cortex of patients with MS correlates with disability. *Neurology*. 79:523–530. doi:10.1212/WNL.0b013e3182635645.

Polman, C.H., P.W. O'Connor, E. Havrdova, H. Michael, K. Ludwig, D.H. Miller, PhillipsTheodore, Lublin, G. Giovannoni, Wajgt, Toal, Lynn, Panzara, and Sandrock Alfred. 2006. A Randomized, Placebo-controlled Trial of Natalizumab for Relapsing Mulltiple Sclerosis. *N. Engl. J. Med.* 354:899–910. doi:10.1056/NEJMoa044397.

Ponath, G., C. Park, and D. Pitt. 2018. The Role of Astrocytes in Multiple Sclerosis. *Front. Immunol.* 9:1–12. doi:10.3389/fimmu.2018.00217.

Popkin, B.M., and I.H. Rosenberg. 2011. Water, Hydration and Health. *Nutr Rev*. 68:439–458. doi:10.1111/j.1753-4887.2010.00304.x.Water.

Poutiainen, P., M. Jaronen, F.J. Quintana, and A.-L. Brownell. 2016. Precision Medicine in Multiple Sclerosis: Future of PET Imaging of Inflammation and Reactive Astrocytes. *Front. Mol. Neurosci.* 9:1–23. doi:10.3389/fnmol.2016.00085.

Pujol, S., W. Wells, C. Pierpaoli, C. Brun, J. Gee, G. Cheng, B. Vemuri, O. Commowick, S. Prima, A. Stamm, M. Goubran, A. Khan, T. Peters, P. Neher, K.H. Maier-Hein, Y. Shi, A. Tristan-Vega, G. Veni, R. Whitaker, M. Styner, C.-F. Westin, S. Gouttard, I. Norton, L. Chauvin, H. Mamata, G. Gerig, A. Nabavi, A. Golby, and R. Kikinis. 2015. The DTI Challenge: Toward Standardized Evaluation of Diffusion Tensor Imaging Tractography for Neurosurgery. *J. Neuroimaging*. 25:875–882. doi:10.1111/jon.12283.

Rashid, W., A. Hadjiprocopis, G. Davies, C. Griffin, D. Chard, M. Tiberio, D. Altmann, C. Wheeler-Kingshott, D. Tozer, A. Thompson, and D.H. Miller. 2008. Longitudinal evaluation of clinically early relapsing-remitting multiple sclerosis with diffusion tensor imaging. *J. Neurol.* 255:390–397. doi:10.1007/s00415-008-0678-0.

Rissanen, E. 2015. Imaging neuroinflammation in progressive multiple sclerosis.

Rissanen, E., J. Tuisku, J. Rokka, T. Paavilainen, R. Parkkola, J.O. Rinne, and L. Airas. 2014. In Vivo Detection of Diffuse Inflammation in Secondary Progressive Multiple Sclerosis Using PET Imaging and the Radioligand 11C-PK11195. *J. Nucl. Med.* 55:939–944. doi:10.2967/jnumed.113.131698.

Rissanen, E., J. Tuisku, T. Vahlberg, M. Sucksdorff, T. Paavilainen, R. Parkkola, J. Rokka, A. Gerhard, R. Hinz, P.S. Talbot, J.O. Rinne, and L. Airas. 2018. Microglial activation , white matter tract damage , and disability in MS. *Neurol Neuroimmunol Neuroinflamm*. 5:1–10. doi:10.1212/NXI.0000000000000443.

Romme Christensen, J., R. Ratzer, L. Börnsen, M. Lyksborg, E. Garde, T.B. Dyrby, H.R. Siebner, P.S. Sorensen, and F. Sellebjerg. 2014. Natalizumab in progressive MS. Results of an open-label, phase 2A, proof-of-concept trial. *Neurology*. 82:1499 LP-1507.

Roosendaal, S.D., J.J.G. Geurts, H. Vrenken, H.E. Hulst, K.S. Cover, J.A. Castelijns, P.J.W. Pouwels, and F. Barkhof. 2009. Regional DTI differences in multiple sclerosis patients. *Neuroimage*. 44:1397–1403. doi:10.1016/j.neuroimage.2008.10.026.

Rupprecht, R., V. Papadopoulos, G. Rammes, T.C. Baghai, J. Fan, N. Akula, G. Groyer, D. Adams, and M. Schumacher. 2010. Translocator protein (18 kDa) (TSPO) as a therapeutic target for neurological and psychiatric disorders. *Nat. Rev. Drug Discov.* 9:971–988. doi:10.1038/nrd3295.

Sahin, N., R. Selouan, C.E. Markowitz, E.R. Melhem, and M. Bilello. 2016. Limbic pathway lesions in patients with multiple sclerosis. *Acta radiol.* 57:341–347. doi:10.1177/0284185115578689.

Salat, D.H., D.N. Greve, J.L. Pacheco, B.T. Quinn, K. G.Helmer, R.L. Buckner, and B. Fischl. 2009. Regional White Matter Volume Differences in nondemented aging and Alzheimer's disease. *Neuroimage*. 44:1247–1258. doi:10.1016/j.neuroimage.2008.10.030.

Salata, B.M., and P. Singh. 2017. Role of Cardiac PET in Clinical Practice. *Curr. Treat. Options Cardiovasc. Med.* 19. doi:10.1007/s11936-017-0591-x.

Sayed, N., C. Liu, and J.C. Wu. 2016. Translation of Human-Induced Pluripotent Stem Cells from Clinical Trial in a Dish to Precision Medicine. *J. Am. Coll. Cardiol.* 67:2161–2176. doi:10.1016/j.jacc.2016.01.083.

Scanderbeg, A.C., F. Tomaiuolo, U. Sabatini, U. Nocentini, M.G. Grasso, and C. Caltagirone. 2000. Demyelinating plaques in relapsing-remitting and secondary-progressive multiple sclerosis: Assessment with diffusion MR imaging. *Am. J. Neuroradiol.* 21:862–868.

Schmidt, P., C. Gaser, M. Arsic, D. Buck, A. Förschler, A. Berthele, M. Hoshi, R. Ilg, V.J. Schmid, C. Zimmer, B. Hemmer, and M. Mühlau. 2012. An automated tool for detection of FLAIR-hyperintense white-matter lesions in Multiple Sclerosis. *Neuroimage*. 59:3774–3783. doi:10.1016/j.neuroimage.2011.11.032.

Seewann, A., H. Vrenken, P. Valk, E.L.A. Blezer, D.L. Knol, J.A. Castelijns, C.H. Polman, P.J.W. Pouwels, F. Barhhof, and J.J.G. Ceurts. 2009. Diffusely abnormal white matter in chronic multiple sclerosis. *Ann Neurol*. 66:601–609.

Sellebjerg, F., D. Cadavid, D. Steiner, L.M. Villar, R. Reynolds, and D. Mikol. 2016. Exploring potential mechanisms of action of natalizumab in secondary progressive multiple sclerosis. *Ther. Adv. Neurol. Disord.* 9:31–43. doi:10.1177/1756285615615257.

Senda, J., H. Watanabe, K. Endo, K. Yasui, Y. Hawsegawa, N. Yoneyama, T. Tsuboi, K. Hara, M. Ito, N. Atsuta, B. Epifanio, M. Katsuno, S. Naganawa, and G. Sobue. 2016. Active brain changes after initiating fingolimod therapy in multiple sclerosis patients using individual voxel-based analyses for diffusion tensor imaging. *Nagoya J Med Sci*. 78:455–463. doi:10.18999/nagjms.78.4.455.

Shah, F., S.P. Hume, V.W. Pike, S. Ashworth, and J. Mcdermott. 1994. Synthesis of the Enantiomers of [N-Methyl-C-11]Pk-11195 and Comparison of Their Behaviors as Radioligands for Pk Binding-Sites in Rats. *Nucl. Med. Biol.* 21:573–581. doi:Doi 10.1016/0969-8051(94)90022-1.

Simon, J., R. Kinkel, L. Jacobs, and L. Bub. 2000. A Wallerian degeneration pattern in patients at risk for MS. *Neurology*. 54:1155–1160.

Slifstein, M., and A. Abi-Dargham. 2017. Recent Developments in Molecular Brain Imaging of Neuropsychiatric Disorders. *Semin. Nucl. Med.* 47:54–63. doi:10.1053/j.semnuclmed.2016.09.002.

Smith, S.M., M. Jenkinson, H. Johansen-Berg, D. Rueckert, T.E. Nichols, C.E. Mackay, K.E. Watkins, O. Ciccarelli, M.Z. Cader, P.M. Matthews, and T.E.J. Behrens. 2006. Tract based spatial statistics: voxelwise analysis of multi-subjects diffusion data. *Neuroimage*. 31:1487–1505. doi:10.1016/j.neuroimage.2006.02.024.

Smith, S.M., and T.E. Nichols. 2009. Threshold-free cluster enhancement: Addressing problems

of smoothing, threshold dependence and localisation in cluster inference. *Neuroimage*. 44:83–98. doi:10.1016/j.neuroimage.2008.03.061.

Soares, J.M., P. Marques, V. Alves, and N. Sousa. 2013. A hitchhiker's guide to diffusion tensor imaging. *Front. Neurosci.* 7:1–14. doi:10.3389/fnins.2013.00031.

Soon, D., D.J. Tozer, D.R. Altmann, P.S. Tofts, and D.H. Miller. 2007. Quantification of subtle blood-brain barrier disruption in non-enhancing lesions in multiple sclerosis: A study of disease and lesion subtypes. *Mult. Scler.* 13:884–894. doi:10.1177/1352458507076970.

Stankoff, B., Y. Wang, M. Bottlaender, M.-S. Aigrot, F. Dolle, C. Wu, D. Feinstein, G.-F. Huang, F. Semah, C.A. Mathis, W. Klunk, R.M. Gould, C. Lubetzki, and B. Zalc. 2006. Imaging of CNS myelin by positron-emission tomography. *Proc. Natl. Acad. Sci.* 103:9304–9309. doi:10.1073/pnas.0600769103.

De Stefano, N., D.G. Silva, and M.H. Barnett. 2017. Effect of Fingolimod on Brain Volume Loss in Patients with Multiple Sclerosis. *CNS Drugs*. 31:289–305. doi:10.1007/s40263-017-0415-2.

De Stefano, N., D. Tomic, E.W. Radue, T. Sprenger, D.P. Meier, D. Häring, and M.P. Sormani. 2016. Effect of fingolimod on diffuse brain tissue damage in relapsing-remitting multiple sclerosis patients. *Mult. Scler. Relat. Disord.* 7:98–101. doi:10.1016/j.msard.2016.03.017.

Steven, A.J., J. Zhuo, and E.R. Melhem. 2014. Diffusion kurtosis imaging: An emerging technique for evaluating the microstructural environment of the brain. *Am. J. Roentgenol.* 202:26–33. doi:10.2214/AJR.13.11365.

Stüber, C., D. Pitt, and Y. Wang. 2016. Iron in multiple sclerosis and its noninvasive imaging with quantitative susceptibility mapping. *Int. J. Mol. Sci.* 17. doi:10.3390/ijms17010100.

Sucksdorff, M., E. Rissanen, J. Tuisku, S. Nuutinen, T. Paavilainen, J. Rokka, J. Rinne, and L. Airas. 2017. Evaluation of the Effect of Fingolimod Treatment on Microglial Activation Using Serial PET Imaging in Multiple Sclerosis. *J. Nucl. Med.* 58:1646–1651. doi:10.2967/jnumed.116.183020.

Symms, M., H.R. Jäger, K. Schmierer, and T.A. Yousry. 2004. A review of structural magnetic resonance neuroimaging. *J. Neurol. Neurosurg. Psychiatry*. 75:1235–1244. doi:10.1136/jnnp.2003.032714.

Takano, A., F. Piehl, J. Hillert, A. Varrone, S. Nag, B. Gulyas, P. Stenkrona, V.L. Villemagne, C.C. Rowe, R. Macdonell, N.A. Tawil, T. Kucinski, T. Zimmermann, M. Schultze-Mosgau, A. Thiele, A. Hoffmann, C. Halldin, N. Al Tawil, T. Kucinski, T. Zimmermann, M. Schultze-Mosgau, A. Thiele, A. Hoffmann, and C. Halldin. 2013. In vivo TSPO imaging in patients with multiple sclerosis: a brain PET study with [F-18]FEDAA1106. *Ejnmmi Res.* 3:30. doi:10.1186/2191-219X-3-30.

Thompson, A.J., B.L. Banwell, F. Barkhof, W.M. Carroll, T. Coetzee, G. Comi, J. Correale, F. Fazekas, M. Filippi, M.S. Freedman, K. Fujihara, S.L. Galetta, H.P. Hartung, L. Kappos, F.D. Lublin, R.A. Marrie, A.E. Miller, D.H. Miller, X. Montalban, E.M. Mowry, P.S. Sorensen, M. Tintoré, A.L. Traboulsee, M. Trojano, B.M.J. Uitdehaag, S. Vukusic, E. Waubant, B.G. Weinshenker, S.C. Reingold, and J.A. Cohen. 2018. Diagnosis of multiple sclerosis: 2017 revisions of the McDonald criteria. *Lancet Neurol.* 17:162–173. doi:10.1016/S1474-4422(17)30470-2.

Tremlett, H., and E. Waubant. 2017. The multiple sclerosis microbiome? *Ann. Transl. Med.* 5:53. doi:10.21037/atm.2017.01.63.

Tronel, C., B. Largeau, M.J.S. Ribeiro, D. Guilloteau, A.C. Dupont, and N. Arlicot. 2017. Molecular targets for PET imaging of activated microglia: The current situation and future expectations. *Int. J. Mol. Sci.* 18. doi:10.3390/ijms18040802.

Tuch, D.S. 2004. Q-ball imaging. *Magn. Reson. Med.* 52:1358–1372. doi:10.1002/mrm.20279.

Turkheimer, F.E., P. Edison, N. Pavese, F. Roncaroli, A.N. Anderson, A. Hammers, A. Gerhard, R. Hinz, Y.F. Tai, and D.J. Brooks. 2007. Reference and target region modeling of [11C]-(R)-PK11195 brain studies. *J. Nucl. Med.* 48:158–167. doi:48/1/158 [pii].

Turkheimer, F.E., G. Rizzo, P.S. Bloomfield, O. Howes, P. Zanotti-Fregonara, A. Bertoldo, and M. Veronese. 2015. The methodology of TSPO imaging with positron emission tomography. *Biochem. Soc. Trans.* 43:586–592. doi:10.1042/BST20150058.

Venneti, S., B. Loprestil, and C. Wiley. 2013. Molecular imaging of microglia / macrophages in the brain. *Glia*. 61:10–23. doi:10.1002/glia.22357.Molecular.

Vercellino, M., S. Masera, M. Lorenzatti, C. Condello, A. Merola, A. Mattioda, A. Tribolo, E. Capello, G.L. Mancardi, R. Mutani, M.T. Giordana, and P. Cavalla. 2009. Demyelination, inflammation, and neurodegeneration in multiple sclerosis deep gray matter. *J. Neuropathol. Exp. Neurol.* 68:489–502. doi:10.1097/NEN.0b013e3181a19a5a.

Vivash, L., and T.J. OBrien. 2016. Imaging Microglial Activation with TSPO PET: Lighting Up Neurologic Diseases? *J. Nucl. Med.* 57:165–168. doi:10.2967/jnumed.114.141713.

Vrenken, H., J.J.G. Geurts, D.L. Knol, C.H. Polman, J.A. Castelijns, P.J.W. Pouwels, and F. Barkhof. 2006. Normal-appearing white matter changes vary with distance to lesions in multiple sclerosis. *Am. J. Neuroradiol.* 27:2005–2011. doi:27/9/2005 [pii].

Wang, Y., C. Wu, A. V Caprariello, E. Somoza, W. Zhu, C. Wang, and R.H. Miller. 2009. In Vivo Quantification of Myelin Changes in the Vertebrate Nervous System. 29:14663–14669. doi:10.1523/JNEUROSCI.4082-08.2009.In.

Werring, D.J. 2000. The pathogenesis of lesions and normal-appearing white matter changes in multiple sclerosis: A serial diffusion MRI study. *Brain*. 123:1667–1676. doi:10.1093/brain/123.8.1667.

Werring, D.J., C.A. Clark, A.G. Droogan, G.J. Barker, D.H. Miller, and A.J. Thompson. 2001. Water diffusion in elevated in widespread regions of normal-appearing white matter in multiple sclerosis and correlates with diffusion in focal lesions. *Mult. Scler.* 7:83–89. doi:10.1191/135245801678227586.

Wheeler-Kingshott, C.A.M., and M. Cercignani. 2009. About "axial" and "radial" diffusivities. *Magn. Reson. Med.* 61:1255–1260. doi:10.1002/mrm.21965.

Wiebenga, O.T., M.M. Schoonheim, H.E. Hulst, G.J.A. Nagtegaal, E.M.M. Strijbis, M.D. Steenwijk, C.H. Polman, P.J.W. Pouwels, F. Barkhof, and J.J.G. Geurts. 2016. White matter diffusion changes during the first year of natalizumab treatment in relapsing-remitting multiple sclerosis. *Am. J. Neuroradiol.* 37:1030–1037. doi:10.3174/ajnr.A4690.

Winkler, A.M., G.R. Ridgway, M.A. Webster, S.M. Smith, and T.E. Nichols. 2014. Permutation inference for the general linear model. *Neuroimage*. 92:381–397. doi:10.1016/j.neuroimage.2014.01.060.

Winston, G.P. 2012. The physical and biological basis of quantitative parameters derived from diffusion MRI. *Quant. Imaging Med. Surg.* 2:254–65. doi:10.3978/j.issn.2223-

4292.2012.12.05.

Woo, C.W., A. Krishnan, and T.D. Wager. 2014. Cluster-extent based thresholding in fMRI analyses: Pitfalls and recommendations. *Neuroimage*. 91:412–419. doi:10.1016/j.neuroimage.2013.12.058.

Zanzonico, P. 2012. Principles of Nuclear Medicine Imaging : Planar , SPECT , PET , Multi-modality , and Autoradiography Systems Principles of Nuclear Medicine Imaging : Planar , SPECT , PET , Multi-modality , and Autoradiography Systems. *Radiat. Res.* 177:349–364. doi:10.1667/RR2577.1.

Zhang, H., T. Schneider, C.A. Wheeler-Kingshott, and D.C. Alexander. 2012. NODDI: Practical in vivo neurite orientation dispersion and density imaging of the human brain. *Neuroimage*. 61:1000–1016. doi:10.1016/j.neuroimage.2012.03.072.